Aus dem Institut

BIH-Centrum für Regenerative Therapien (BCRT)
Berlin Institut für Gesundheitsforschung und
Medizinische Fakultät Charité – Universitätsmedizin Berlin

DISSERTATION

CRISPR-Cas9 and T cells

CRISPR-Cas9 und T-Zellen

zur Erlangung des akademischen Grades

Medical Doctor - Doctor of Philosophy (MD/PhD)

vorgelegt der Medizinischen Fakultät
Charité – Universitätsmedizin Berlin

von

Dimitrios Laurin Wagner

aus Heidelberg

Datum der Promotion: 04.06.2021

Inhaltsverzeichnis

This thesis manuscript is a synopsis of the background, methods and key findings from the following three published studies, as well as discussion on their prospects in regard to clinical translation in regenerative medicine.

<u>**Co-authorships:**</u>

- **Highly Efficient Genome Editing of Murine and Human Hematopoietic Progenitor Cells by CRISPR/Cas9.**
Gundry MC, Brunetti L, Lin A, Mayle AE, Kitano A, <u>Wagner D</u>, Hsu JI, Hoegenauer KA, Rooney CM, Goodell MA, Nakada D.
published in Cell Reports 2016

- **CAR T-cells that target acute B-lineage leukemia irrespective of CD19 expression**
Fousek K, Watanabe J, Joseph SK, George A, An X, Byrd TT, Morris JS, Luong A, Martínez-Paniagua MA, Sanber K, Navai SA, Gad AZ, Salsman VS, Mathew PR, Kim HN, <u>Wagner DL</u>, Brunetti L, Jang A, Baker ML, Varadarajan N, Hegde M, Kim Y-M, Heisterkamp N, Abdel-Azim, Ahmed N.
published in Leukemia 2020

<u>**Primary authorship:**</u>

- **High prevalence of *Streptococcus pyogenes* Cas9-reactive T cells within the adult human population**
<u>Wagner DL</u>, Amini L, Wendering DJ, Burkhardt L-M, Akyüz L, Reinke P, Volk HD, Schmueck-Henneresse M.
published in Nature Medicine 2019

1. Abstracts (Zusammenfassung)

1.1. Zusammenfassung

Eine gezielte Modifikation des menschlichen Genoms ermöglicht die Entwicklung von neuartigen Therapien für vererbte und erworbene Erkrankungen. Seit der Entdeckung des programmierbaren Nukleasesystems in Bakterien avanciert die CRISPR-Cas9 Technologie zum meist angewendeten System für die gezielte Genmodifikation. Für therapeutische Ansätze müssen Protokolle entwickelt werden, die eine effiziente und präzise Veränderung der Zellen ermöglichen. Zusätzlich sollte eine sorgfältige Evaluation möglicher Sicherheitsrisiken der Technologie durchgeführt werden, um eine Risiko-Nutzen-Analyse zur klinischen Anwendung anzufertigen.

Die vorgelegten Arbeiten beschreiben eine neue virus-freie Methode zur Geneditierung mit CRISPR-Cas9. Elektroporation von CRISPR-Cas9 Ribonukleoproteinen ermöglicht eine hoch-effiziente Mutagenese von Genen in unterschiedlichen primären humanen hämatopoetischen Zellen bei geringer Toxizität. Das entwickelte Protokoll kann für unterschiedliche Zellarten adaptiert werden, die als schwer transfektierbar galten. Beispielsweise konnten primäre Leukämiezellen genetisch verändert werden, um Antigenverlust nach antigen-spezifischer Immuntherapie *in vitro* und mehreren Xenograft-Modellen zu simulieren.

Die hohe Effizienz und geringe Toxizität erlauben die Adaption des Protokolls für klinische Anwendungen. Im Hinblick auf den Einsatz der Technologie im Menschen wurde die Immunogenität des am häufigsten genutzten Cas9 Proteins aus dem Bakterium *Streptococcus pyogenes* (SpCas9) untersucht. SpCas9-reaktive T-Zellen wurden in 95% der Erwachsenen detektiert. Angereicherte SpCas9-reaktive Effektor T-Zellen eliminierten SpCas9-überexprimierende Zielzellen *in vitro*.

Zusammenfassend konnte eine Methode etabliert werden, um Gene in primären humanen Zellen – inklusive T-Zellen – hoch-effizient und spezifisch zu verändern. Die transiente Anwendung mittels Ribonukleoproteinkomplexen wurde als zusätzlicher Sicherheitsvorteil identifiziert, da die meisten Menschen über ein T-Zell-Gedächtnis mit Spezifität für Cas9 von *Streptococcus pyogenes* verfügen. Immunität könnte durch Kolonisierung und Infektionen durch fakultativ-pathogene Bakterien ausgelöst werden, aus denen das jeweilige CRISPR-Cas System hervorgeht. Die hohe Prävalenz von Cas9-spezifischen T-Zellen stellt ein vorher unerkanntes Sicherheitsheitsrisiko für die Anwendung von CRISPR-Cas9 in Menschen dar.

1.2. Abstract

Targeted editing of the human genome enables the development of novel treatment options for inherited and acquired diseases. Since the discovery of the programmable nuclease system in bacteria, the CRISPR-Cas9 technology has become the most commonly used tool for gene editing. Therapeutic application of the technology in human patients requires the development of protocols for its effective delivery into the cells of interest with minimal toxicity as well as a careful safety evaluation.

The works underlying this thesis describe a novel vector-free method for gene editing with CRISPR-Cas9. Electroporation of CRISPR-Cas9 ribonucleoproteins was used to achieve targeted mutagenesis in primary hemopoietic cells with high efficiency and little toxicity. The established protocol can be adapted for many cell types that were previously thought to be hard to transfect. Exemplary, CRISPR-Cas was used to modify primary human leukemia cells in order to then simulate antigen-escape after antigen-directed immunotherapies *in vitro* and in various xenograft models.

While high efficiency and minimal toxicity allow the adaption of the method for clinical applications, immunogenicity of Cas9 protein represents an unaddressed safety concern for its use in human patients. Therefore, T cell responses toward the most commonly used Cas9 nuclease protein from the bacterium *Streptococcus pyogenes* (SpCas9) were evaluated in healthy human adults. SpCas9-reactive T cells were detected in 95% of the healthy donors. Enriched SpCas9-reactive T cells lysed SpCas9-overexpressing target cells.

In summary, a method was established to specifically mutagenize genes in primary hematopoietic cells at unprecedented efficacy. Furthermore, transient delivery of CRISPR-Cas9 components was identified as an additional safety advantage, because most healthy human adults exhibit preexisting T cell memory against SpCas9. Immunity to Cas9 proteins could occur by colonization or infections with the commensal or facultative-pathogenic bacterial species from which they originated. The high prevalence of pre-existing Cas9-specific T cells highlights a previously unrecognized risk for CRISPR-Cas9 applications in humans.

1.3.   Graphical abstract

CRISPR-Cas9 genome editing

Translation & Basic science
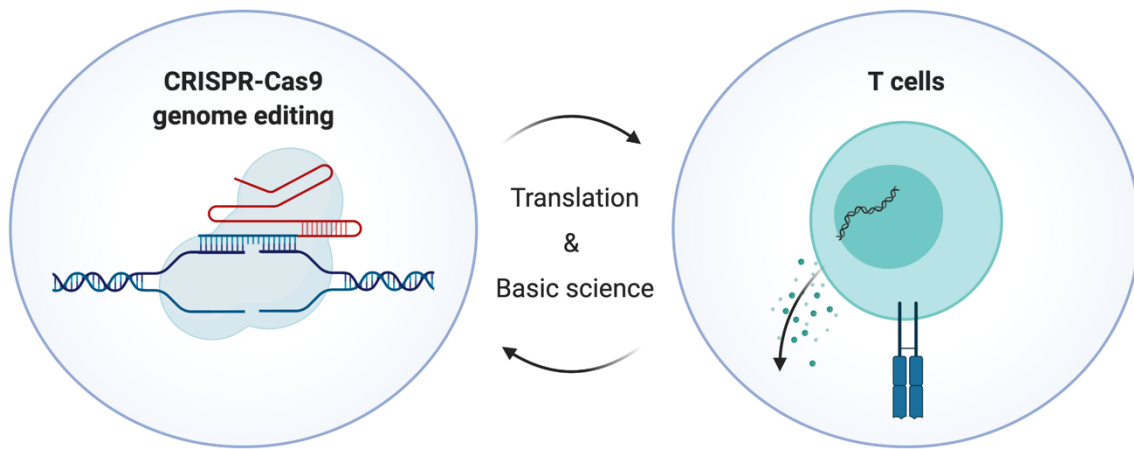
T cells

Gundry et al 2016 (Cell Reports)
Method for highly efficient genome editing through electroporation of sgRNA-Cas9 complexes into primary human cells

Gene KOs in T cells with high effciency and minimal toxicity
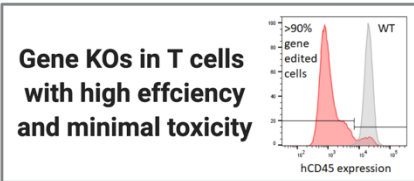
Fousek et al 2020 (Leukemia)
Example of CRISPR-Cas9 in T cell therapy development Efficient CD19 gene KO in primary leukemia cells to model tumor antigen escape

Modeling antigen escape to evaluate tri-specific chimeric antigen receptor (CAR) T cell therapy

Wagner et al 2019 (Nature Medicine)
1/2
Discovery of preexisting Cas9 specific T cells as important safety risk for CRISPR-Cas9 therapeutics in humans

Wagner et al 2019 (Nature Medicine)
2/2
Cas9 reactive regulatory T cell subset can suppress anti-Cas9 effector T cell responses in vitro

Graphical abstract was created with BioRender (www.biorender.com)
and flow cytometry data of Gundry et al. 2016

2. **Introduction and current state of research**

2.1.   Prospects and challenges of gene therapy

Gene therapy is becoming a cornerstone of regenerative medicine.(Anguela & High, 2019) Contrary to many regular pharmaceutical interventions, both *in vivo* and *ex vivo* gene therapies aim to introduce therapeutic genes into human cells for long-term expression and clinical benefit after a single application (Anguela & High, 2019). To this end, the gene of interest is usually transferred by a vector, most commonly an engineered non-replicative virus (Anguela & High, 2019). While under development since the 1990s, the field has been stalled because of genotoxicity and immunogenicity issues of the viral vectors. Infusions of *ex vivo* modified hematopoietic stem cells with randomly integrating lentiviral vectors led to the development of leukemia in some patients (Hacein-Bey-Abina et al., 2003). Furthermore, systemic high dose application of an adenovirus-based gene therapy induced an overwhelming immune response against the vector, killing 18 year old patient Jesse Gelsinger (Raper et al., 2002).

In the last two decades, the discovery of safer viral vectors has led to the slow reemergence of gene therapy with several successful clinical trials (Anguela & High, 2019). A few commercial products have been approved for inherited rare diseases including retinal dystrophy (Luxturna, Spark Therapeutics), severe combined immunodeficiency disorder (Strimvelis, GlaxoSmithKline) and spinal muscular atrophy (Zolgensma, Novartis). The vast majority of the ongoing and completed clinical trials until 2017 were performed in the cancer field (Anguela & High, 2019). A very prominent example of the gene therapy developments in oncology is the employment of *ex vivo* modified T cells that are redirected to recognize and kill leukemia cells by the introduction of so-called Chimeric Antigen Receptors (CAR) specific for the common B cell antigen CD19 (Maude et al., 2014).

Interestingly, the pioneers of gene therapy tested these approaches without full knowledge of the human genome. After the successful sequencing of >94% of the human genome in 2001, it was expected that this information could be used to identify errors that cause disease and ultimately rewrite the code of life for the eradication of inherited disease (International Human Genome Sequencing Consortium, 2001). However, precise and efficient modification of a specific disease-causing mutation in human cells was not achieved until 2005 (Urnov et al., 2005). In their seminal study, Urnov *et al.* demonstrated that the induction of DNA double strand breaks at a specific

location in the human genome and co-delivery of a homologous DNA donor template could be used to introduce a targeted change by exploiting the endogenous homologous recombination DNA repair pathway.

In the last decade, the new excitement about gene therapy was drastically amplified by the discovery that the bacterial defense system CRISPR-Cas could be harnessed to specifically cut DNA in 2012 (Jinek et al., 2012). While other site-specific nuclease systems such as zinc-finger nucleases had already been in development since 1996, the ease of target customization and generally high efficiency as well as moderate specificity make CRISPR-Cas the most popular gene editing tool today.

2.2. CRISPR-Cas9 technology for gene editing in T cells

The most frequently used CRISPR-Cas system was originally derived from *Streptococcus pyogenes* (SpCas9) (Jinek et al., 2012). In its essential format for genome editing, it consists of the Cas (CRISPR-associated) protein and the single guide RNA (sgRNA), which is typically 100 nucleotides long (Mali et al., 2013). A specific scaffold sequence, that was derived from the bacterial trans-activating RNA, enables binding of the sgRNA to the SpCas9 nuclease (Mali et al., 2013). Cas9-sgRNA complexes scan the DNA by three dimensional diffusion.(Sternberg et al., 2014) Once the SpCas9 protein binds to its protospacer-adjacent-motif (PAM, SpCas9: 5'-NGG-3'), its motion is halted (Sternberg et al., 2014). The protein's nuclease function becomes activated after successful Watson-Crick base-pairing of the 20 nucleotides "spacer" sequence of the sgRNA' to the target strand of the DNA (Mali et al., 2013). Altering the spacer sequence allows for targeting any 20 base pairs sequence in the genome with the only constraint being the presence of the PAM motif NGG (Jinek et al., 2012; Sternberg et al., 2014). PAM sequence, guide RNA format and spacer lengths vary between Cas nucleases from different species (Makarova et al., 2020).

Once introduced into the nucleus of human cells, the CRISPR-Cas technology results in fast and irreversible modification of the human genome (Cong et al., 2013). Through the efficient and repetitive induction of DNA double strand breaks at the target site in the genome, the cell's error prone non-homologous end joining leads to insertions and deletions during DNA repair (Porteus, 2019). This may create a frameshift in the coding sequence and premature stop codons, which abrogate the translation of functional or full-length proteins (Cong et al., 2013). Similar to other nuclease systems, co-delivery of DNA templates allows homology-directed repair to correct mutations or introduce

new sequences (Porteus, 2019).

For clinical application, the components need to be efficiently delivered into the cells (Porteus, 2019). Through artificially attached nuclear-localization sequences, the Cas proteins can be shuttled into the cell's nucleus (Cong et al., 2013). Most initial studies focused on the delivery via DNA plasmids (Cong et al., 2013; Mali et al., 2013; Mandal et al., 2014). Low efficiency and considerable toxicity prevented their widespread use for human T cell modification (Mandal et al., 2014). The delivery of Cas9-sgRNA ribonucleoprotein complex yielded increased efficiency with gene editing in up to 50% of the transfected T cells (Hendel et al., 2015; Schumann et al., 2015). The aforementioned studies lead to the hypothesis that application of preformed complexes of protein and sgRNA will achieve highly efficient gene disruption at the gene of interest without major reduction in the cells' viability. Additionally, "hit-and-run" approaches that deliver the active nuclease components for editing do not harbor the risk for insertional mutagenesis because they cannot be integrated and are quickly degraded in the cells (Porteus, 2019).

2.3. Safety risks of CRISPR-Cas gene editing

The safety of CRISPR-Cas gene editing must be carefully evaluated to create an informative and complete risk and benefit analysis. The major concern of CRISPR-Cas for clinical practice are unintended off-target effects of the nuclease activity (Porteus, 2019). Mutagenesis of tumor suppressors or protooncogenes could induce cancerous properties within the modified cells. For T cell therapeutics, the risk of such an event is considered to be low, because in over two decades of clinical experience with randomly inserting retroviral vectors no case of leukemic transformation has been reported (Scholler et al., 2012). Recently, one case has been described where the expression cassette of a CD19-specific chimeric antigen receptor integrated into the locus of the known protooncogene Tet2 (Fraietta et al., 2018). Surprisingly, the patient's leukemia was completely eradicated by CAR T cells derived from a single clone with the described Tet2 integration site, but the frequencies of Tet2-disrupted CAR T cells declined after successful tumor clearance and appeared not to pose a safety risk (Fraietta et al., 2018). Nevertheless, the lack of experience with the CRISPR-Cas technology warrants a stringent evaluation of unwanted gene editing events before clinical practice despite a relatively low risk of malignant transformation of terminally differentiated cell type like T cells.

While immunity was one of the major obstacles in early gene therapeutic trials, immunogenicity of the CRISPR-Cas system has only been addressed by few studies in humans (Charlesworth et al., 2019; Simhadri et al., 2018; Wagner et al., 2019). In 2015 and 2016, first studies in immunocompetent mice showed that the SpCas9 protein has the inherent capacity to induce an adaptive immune response via the production of antibodies as well as SpCas9-specific T cell responses (Chew et al., 2016; Wang et al., 2015). Long-lasting overexpression of the SpCas9 protein may therefore lead to the destruction of cells expressing the SpCas9 protein through Cas9-specific CD8+ T cells (Chew, 2018). However, preexisting T cell immunity could eliminate gene edited cell products that display Cas9 fragments on their cell surface. Preexisting neutralizing antibodies reportedly reduce the efficacy of viral gene therapies and patients with neutralizing antibodies are consistently excluded from clinical trials (Anguela & High, 2019). While only few applications aim to deliver SpCas9 systemically, antibodies could deplete free active nuclease prior to entering its target cells, thereby reducing its efficacy (Chew, 2018).

The bacteria from which the most popular Cas systems were adapted are well known human pathogens (Makarova et al., 2020). *Streptococcus pyogenes* as well as *Staphylococcus aureus* frequently colonize children and adults and are facultative pathogenic bacteria with a high incidence of infections, especially during childhood (Carapetis et al., 2005; Lowy, 1998). Therefore, the hypothesis was formulated that sensitization to Cas variants occurs in most human adults through exposure to the bacterial species from which they originate. To this end, a study was designed to evaluate and characterize memory T cell responses toward the most popular SpCas9 nuclease.

3. Methods

This section summarizes the key methodologies of the author's contributions to the works underlying this thesis. For a detailed account of all materials and methods, please refer to the corresponding sections of the enclosed publications.

3.1. Peripheral blood mononuclear cell (PBMC) isolation by density-gradient centrifugation

One milliliter peripheral venous blood of a healthy human adult contains between $0,25x10^6$ – $3x10^6$ T cells. To eliminate granulocytes, erythrocytes and most thrombocytes, density gradient centrifugation allows the separation of the so-called peripheral blood mononuclear cell (PBMC) fraction from whole blood. PBMCs consist mostly of T cells but also contain antigen-presenting cells like B cells and monocytes. Thus, this fraction is an optimal starting population for T cell stimulations and antigen-specific T cell expansion strategies. To isolate PBMC, heparinized venous blood is mixed 1:1 with phosphate buffered saline (PBS). The diluted blood is carefully layered on a high-molecular mass Ficoll polymer solution with high density. Centrifugation at 400 x g for twenty minutes at room temperature allows passing of granulocytes and erythrocytes through the polymer solution to the tubes bottom. Importantly, centrifugation is performed without break function to prevent disruption of the solution's layers. The white ring above the clear Ficoll solution layer are the cells of interest. Subsequent harvesting is carefully performed with a sterile Pasteur pipette without mixing the serum-PBS and the Ficoll phases. The harvested cells are transferred to a fresh 50-ml falcon tube and washed twice with PBS to remove residual Ficoll and some of the thrombocytes. Finally, the PBMCs are resuspended in T cell culture medium (Baylor College of Medicine: 45% CLICK's medium, 45% RPMI 1640 medium, 10% fetal calf serum; Charité: 90% RPMI 1640 medium, 10% fetal calf serum, supplemented with 1% Penicillin / Streptomycin antibiotics in all experiments without electroporation).

3.2. T cell culture

For optimal activation and expansion, T cells require all three signals: activation through ligation of their T cell receptor/CD3 complex, co-stimulation through co-receptors like CD28 and proliferation supporting cytokines. Therefore, polyclonal effector T cell culture is initiated by stimulation of PBMC with anti-CD3/anti-CD28-antibodies and cytokine-supplemented cell culture medium (effector T cells: 10 ng/ml

IL-7; 5 ng/ml IL-15 [both CellGenix]; regulatory T cells 500 IU/ml IL-2 [Proleukin, Novartis]).

To this end, antibodies can be immobilized on non-tissue-culture 24-well plates through overnight coating with 500 μl sterile water supplemented with 1 μg/ml anti-CD3 (clone OKT3) and 1 μg/ml anti-CD28 (clone CD28.2) at 4°C. Next day, the plates were washed once with PBS and a second time with complete cell culture medium (RPMI 1640, 10% fetal calf serum) before $1x10^6$ freshly isolated PBMCs are plated per well. Alternatively, anti-CD3/CD28 stimulus can be provided by antibody coated beads according to the manufacturer's recommendations (e.g. Dynabeads T cell Activator Kit [ThermoFisher] or T cell activation/expansion beads [Miltenyi Biotec]). Generally, activated T cells were counted and re-seeded at $0.5x10^6$ cells per ml every 2-3 days with cytokine-supplemented T cell culture medium.

3.3. sgRNA selection and synthesis

Design

SgRNAs were selected using the CRISPRscan web application.(Moreno-Mateos et al., 2015) The integration of CRISPRscan with the UCSC genome browser allowed the visual identification of sgRNAs high predicted efficiency (high score >70), minimal off-targets (green color) or both (light-green bars). SgRNAs within annotated exons were picked for gene disruption. The CRISPRscan algorithm provides a summary of several important pieces of information regarding every sgRNA, including a primer sequence for subsequent PCR-amplification.

Extension polymerase chain reaction (PCR)

Templates for *in vitro* transcription of single guide RNA (sgRNA) for Cas9 can be constructed by exchanging a given target-specific 5' "spacer" sequence through extension PCR with a synthetic DNA oligo primer. The 56 nucleotide-long DNA primers include a) the transcription start site for the T7-RNA-polymerase (prokaryotic TATA-box), b) the specific 20 nucleotide "spacer" sequence and c) a short overlapping sequence that anneals to the stem of the sgRNA scaffold sequence. To enhance binding of the primer to the sgRNA scaffold sequence on the px458 plasmid (Addgene Catalog#: 48138, gift from Dr. Feng Zhang, MIT), an additional 5'-ATAGC-3' sequence is added on the 3'-end of the primer sequence derived from CRISPRscan. For all sgRNA template PCRs a universal reverse primer can be used (5'-AGCACCGACTCGGTGCCACT-3'). The primer pair is designed to have an effective

annealing temperature of 60°C. The PCR is performed with a high-fidelity polymerase enzyme kit to reduce errors (KAPA HiFi Hot start Polymerase 2x Ready-mix, Roche). 20 µl reactions are set up with 1 µM of each the individual forward primer and the universal reverse primer and 2 ng of px458 plasmid DNA.

PCR purification

The PCR product is subsequently purified using MinElute DNA purification kit (Qiagen) and dissolved in 12 µl nuclease-free water. The amplification specificity is validated by 1% agarose gel electrophoresis and the concentration is measured by spectrophotometry on a NanoDrop2000 device (ThermoFisher). Typical concentrations are 50-80 ng/µl. PCR templates for *in vitro* RNA transcription can be used immediately or stored at -20°C.

in vitro transcription (IVT)

Purified DNA templates are kept or thawed on ice. For *in vitro* transcription, the HiScribe T7 High Yield RNA Synthesis Kit (NEB) was used. Briefly, 4 µl of DNA PCR template was mixed with ATP, CTP, GTP, UTP, 10x reaction buffer and T7 polymerase mix according to 50% of the manufacturers recommended volumes for a 10 µl reaction. *in vitro* transcription was subsequently performed in a PCR cell cycler at 37°C for 4-16 hours.

RNA purification

To isolate highly purified sgRNA, IVT reactions are diluted in a total volume of 50 µl nuclease free water and purified according to the manufacturer's manual (Zymo RNA Clean and concentrator 25 Kit; Zymo Research). Purified RNA is eluted from the columns with 25 µl nuclease-free water. RNA concentrations are determined by spectrophotometry and RNA volume is adjusted to a final concentration of 1 µg/µl. To prevent multiple freeze-and-thaw cycles, sgRNA is aliquoted at small volume (e.g. 4 µl) prior to storage at -80°C. Importantly, workplace and pipettes should be treated with decontaminating agents to remove RNAse (e.g. RNAseZAP; ThermoFisher). Only sterile and nuclease-free filter tips and tubes are used to reduce the risk of RNA decay.

3.4.   Cell electroporation

Cell electroporation requires careful preparation of all needed reagents. Cells of interest are seeded one or two days prior to transfection in an antibiotic-free medium and at optimal seeding ratio. Depending on the cell type of interest, 100.000 – 250.000 cells are used in a 10 µl transfection using the Neon Transfection System

(ThermoFisher). For T cells, as well as immortalized or cancerous lymphatic cell lines, 250.000 cells are used per 10 µl transfection volume. At the day of transfection, the cells are harvested and washed twice in sterile PBS to remove all residual medium components that could contain DNA/RNA nucleases. A second wash step is performed in a 1.5 ml tube to allow the complete removal of residual liquid. Then, the cells are resuspended in electroporation buffer ("T": T cells, "R": cell lines; both part of Neon Transfection Kit; ThermoFisher). Just prior to electroporation, the cell suspension is mixed with the CRISPR-Cas RNPs or the DNA plasmid. Transfection of lymphatic cells (T cells, Lymphoblastoid Cell Lines, B-ALL lines) is performed at 1600 Volt for 10 milliseconds and 3 pulses. Immediately after electroporation, the cells are added into pre-warmed medium (supplemented with cytokines in case of T cells) and rested for at least 24 hours.

Formulation of CRISPR-Cas9 ribonucleoprotein (RNP) complexes

RNPs are formulated by mixing 1 µg of sgRNA with 1 µg of recombinant Cas9 Protein (PNAbio or Integrated DNA Technologies) per 10 µl transfection. The high sgRNA to Cas9 molar ratio (5:1) ensures saturation of Cas9 with sgRNA after 10-15 minutes of incubation at room temperature in a nuclease free tube.

Plasmids (LCLs)

Ultra-pure plasmids were isolated with the ZymoPURE Midi Prep Kit (Zymo Research). To model a gene therapeutic scenario, B-LCLs were transfected with 500 ng of plasmid DNA. The px458 plasmid leads to the expression of a green fluorescent protein reporter gene, a Cas9 protein and a sgRNA targeting the human AAVS1 safe harbor locus.(Mali et al., 2013)

3.5. Flow cytometry

Labeling of both intracellular and extracellular proteins on cells with fluorochrome-linked antibodies allows high-dimensional profiling of cell populations. Here it was used to characterize the outcome of gene disruption, characterize antigen-specific T cells after specific stimulation as well as analyze cell proliferation survival after cell culture. For gene editing experiments, analysis is performed at least 3 days after transfection to allow for sufficient protein turnover.(Fousek et al., 2020; Gomes-Silva et al., 2017; Gundry et al., 2016) At the time of the respective readout, cells were harvested and aliquoted into 5 ml polystyrene round bottom tubes (Falcon). After centrifugation at 400g for 5 minutes, supernatants are discarded, and cells are resuspended in 100 µl

PBS. Antibodies for surface staining and live/dead discrimination dyes are added first. Intracellular staining requires fixation and permeabilization of cells. Unless otherwise stated, Foxp3 Transcription Factor Staining Kit (eBioscience, now ThermoFisher) is used according to the manufacturer's recommendations. In case of intracellular staining, only fixation resistant fluorochromes like APC and live-dead staining are used during surface staining. Further, after fixation and permeabilization, all washing and staining steps are performed in saponin containing permeabilization buffers to allow antibodies to penetrate the cell membrane. After a final wash, cells are analysed on flow cytometer (e.g. Navios; Beckman Coulter(Gomes-Silva et al., 2017) or LSRII Fortessa, BD(Wagner et al., 2019)). Data analysis is performed with FlowJo Version 10 (BD Bioscience).

3.6. Antigen-specific T cell stimulation

To detect antigen-specific T cell responses, PBMCs were incubated overnight in the presence of recombinant Cas proteins (SpCas9 [PNAbio], *Staphylococcus aureus* SaCas9 [Applied Biological Materials Inc], *Acidaminococcus species* Cas12a/Cpf1 [Integrated DNA Technologies]). As a control for a common recall antigen, stimulations with a peptide mix derived of cytomegalovirus antigen pp65 (CMV PepMix pp65, JPT) are included in seropositive healthy human adults. Additionally, staphylococcal enterotoxin B (Sigma) is included as a separate positive control. To evaluate whether T cell activation is MHC dependent, blocking antibodies for major histocompatibility complexes (MHC class 1 or 2) are added during the incubations in some experiments. For whole protein stimulations, 1.5 (SaCas9) / 2.5 µg recombinant Cas protein (SpCas9, Cpf1) is added to at least 5×10^6 PBMCs in complete medium in a small volume (100 µl) for 15 minutes at 37°C to allow for efficient uptake of the protein into the antigen presenting cells. Then, the volume is adjusted to 500 µl with complete medium and the cells are rested for 6 hours to ensure sufficient protein processing and loading on major histocompatibility complexes of antigen presenting cells. Subsequently, brefeldin A is added to the samples to block the Golgi apparatus in cells and thereby prevent cytokine secretion. For all other stimulants, brefeldin A is supplemented one hour after the beginning of stimulation.

After a total of 16 hours, intracellular staining (as described above) allows the identification of activated T cells through activation markers as well as unreleased cytokines. Unstimulated PBMCs served as negative control to measure background

activation. For cell sorting experiments, the PBMCs are dosed with Cas9 proteins as described above, but no Brefeldin A is added to retain long-term viability. CD40-blocking antibody is added to the medium to prevent downregulation of CD154 (also known as CD40 Ligand) on the T cells' surfaces after ligation to its receptor. For a full list of antibodies used, please refer to the method sections of the enclosed manuscripts.

3.7. Fluorescence-activated cell sorting

Cell sorting allows the enrichment of target populations. To this end, cells are stained with fluorochrome linked antibodies as described earlier. Prior to sorting, the stained cells are resuspended in cold PBS and filtered with a 0.45 mm cell strainer to create a single cell suspension. Within the cell sorter, a continuous stream of droplets containing mostly single cells is created in a buffered saline solution and analysed by flow cytometry. The cells of interest are selected based on fluorescence intensity of multiple markers using logic gating strategies. This enables to identification of target populations that are negative for marker A (e.g. CD19), but positive for marker B (e.g. green fluorescent protein). If a cell of interest is detected by the flow cytometer, the droplet containing the cell is diverted via a charge created by two metal plates adjacent to the flow stream. The droplets containing single cells with the defined fluorescence characteristics are collected in sterile collection tubes containing a small volume of complete medium. After completion of the sort, the cell purity is confirmed by flow cytometry. The sorted cells are washed and counted. Depending on the downstream application, the cells can either be used directly or resuspended in the respective culture medium (e.g. cytokine containing T cell medium) for cell expansion. As the cell sorting requires intensive cell handling, the medium is supplemented with antibiotics to prevent an outgrowth of bacterial contaminations in subsequent cultures.

3.8. Flow cytometry-based cytotoxicity assay

A fundamental function of T cells is the elimination of cells that express their target antigens on MHC molecules. In Wagner *et al.*, a flow cytometry-based cytotoxicity assay was used to evaluate whether enriched SpCas9-reactive effector T cells lyse autologous cells that endogenously expressed SpCas9 in a dose dependent manner. As target cells, established B lymphoblastoid cells (B-LCL) are transfected with DNA plasmids to force the expression of SpCas9 and a green fluorescent protein (px458, details above) or green florescent protein only (pMAX-GFP, Lonza Ltd, Cologne). To

exclude unspecific killing of target cells, unmodified autologous B-LCL stained with the red fluorescent dye (DDAO phosphate, Molecular Probes, ThermoFisher) are included as internal controls in each co-culture. For the setup of the assay, control B-LCLs (red dye) were mixed with GFP-transfected target LCLs, and co-cultures were set up with different T cells to target LCL ratios (1:10, 1:1, 10:1). After 16 hours of incubation in 96-Well-U-Bottom-Plates (Corning), the remaining cells are harvested, washed with PBS and stained with Life/Dead Fixable Blue Dead Cell Stain Kit (ThermoFisher) to demark apoptotic cells during the flow cytometric readout. The ratio between alive control B-LCLs and alive GFP positive target LCLs is used to normalize for unspecific lysis. In order to calculate the mean survival, the relative amount of alive GFP positive LCLs is compared to the condition without T cells.

3.9. Effector T cell suppression assays

Regulatory T (Treg) cells modulate immune responses with suppressive signals. A key function of Treg cells is the inhibition and reduction of effector T cell activation and proliferation. In co-culture experiments, SpCas9-reactive or polyclonal Treg cells are mixed with SpCas9-activated effector cells and their expansion and cytokine secretion is monitored. To evaluate proliferation, SpCas9-reactive or polyclonal CD4$^+$/CD8$^+$ effector cells are enriched with and stained with CellTrace CFSE dye (ThermoFisher) according to the manufacturer's recommendations. For antigen-specific effector T cells, the initial activation was enough to promote cell expansion. In contrast, polyclonal effector T cells are stimulated by adding anti-CD3/CD28-coated microbeads (Treg suppression inspector; Miltenyi Biotec) at 1:1 ratio. Subsequently, effector T cells are plated in 96-Well-U-Bottom-Plates (Corning) alone or with different amounts of Treg cells. The incorporation of CFSE dye in protein-containing organelles leads to a high green-fluorescent signal after stimulation with a 488 nm blue laser during flow cytometry. As T cells proliferate, the CFSE signal is diluted in each cell division. Therefore, proliferation can be monitored by quantifying T cells with low CFSE signal in flow cytometry multiple days later. Unlabeled Treg cells are excluded from the analysis based on CFSE negativity and percentage of proliferating effector T cells is quantified and compared. The supernatants from the same experiments are harvested for measurements of TNF-α, IFN-γ, IL-2 and IL-10 using a multiplex ELISA (Proinflammatory cytokine kit, Mesoscale Discovery platform, Mesoscale Diagnostics). In these experiments, no recombinant cytokine is added to the culture medium to

specifically determine the cytokine concentrations secreted by T cells. For the accurate quantification of the respective cytokines, the run included a standard curve for calibration and internal blank controls for background subtraction.

3.10. T cell receptor beta chain sequencing

Every conventional T cell expresses a T cell receptor (TCR) heterodimer consisting of an alpha chain and a beta chain. Due to genetic recombination, variable portions of the alpha and beta chains are highly diverse between naïve T cell clones. Sequencing the TCR repertoire allows to distinguish between highly diverse T cell populations (naïve polyclonal) and oligoclonal (antigen-specific memory) T cell populations. Additionally, T cell populations that share high percentages TCR sequences likely arise from the same T cell clones. An accurate determination of the TCR repertoire can be performed by targeted sequencing of the respective variable complementary-determining regions of their TCR alpha or beta chain. In Wagner *et al.*, the commercial TCR beta chain repertoire "immunoSEQ platform" by Adaptive Biotechnologies is used. To this end, genomic DNA is isolated from freshly sorted T cells with the Quick-DNA Miniprep Plus Kit (Zymo Research). The different activated T cell subsets are sorted based on expression of activation markers CD137 and CD154 as well as the respective T cell phenotype: Treg ($CD25^{high}CD127^{low}$) or Teff ($CD25^{low}CD127^{high}$) respectively. To determine whether SpCas9-reactive regulatory and effector T cells originate from same original clones, only CD4 positive T cells are sorted for this analysis. Subsequently, clonal diversity and TCR repertoire overlaps between different T cell subsets are analyzed with immunoSEQ Analyzer 3.0 (Adaptive Biotechnologies).

3.11. Serological analysis of *Streptococcus pyogenes* exposure

The formulated hypothesis on sensitization to SpCas9 is based on the assumption, that most human adults are exposed to the bacterium. To confirm prior exposure, antibody titers against two intracellular proteins of *Streptococcus pyogenes* (Streptolysin O; streptococcal DNAse B) are measured in the qualified clinical laboratory of Labor Berlin GmbH. For these analyses, venous blood is collected from 20 healthy human donors from our cohort in a tube without anticoagulants, centrifuged at 1.000 g for 10 minutes and aliquoted in sterile containers, transferred at room temperature or stored at -20°C until analysis.

4. Essential Results

4.1.   Highly efficient gene disruption in activated human T cells

The electroporation of ribonucleoproteins achieves a high frequency of gene disruption while retaining a high viability of hematopoietic cell types like primary human T cells (Gundry et al., 2016). Cell culture conditions before manipulation were the key for high efficiency of the genetic modification (Gundry et al., 2016). Polyclonally activated T cells that strongly proliferated after four days of culture in the presence of T-cell promoting cytokines (IL-7 and IL-15) could be efficiently edited, but unstimulated and non-dividing cells could not be genetically modified through electroporation (Figure 3A, (Gundry et al., 2016) and data not shown in manuscript). Similarly, activation of CD34 enriched hematopoietic progenitor cells with a cytokine cocktail over up to three days increased the efficiency of gene disruption, while preserving their progenitor potential as indicated through the generation of multiple hematopoietic lineages in immunocompromised mice (Figure 3B, (Gundry et al., 2016)) Importantly, our protocol yielded significantly higher editing compared to reports of a plasmid-based editing approach in hematopoietic stem and progenitor cells (Mandal et al., 2014; Xu et al., 2019) and even compared to prior studies that employed RNPs in T cells (Schumann et al., 2015).

We characterized off-target events in primary human T cells edited with the RNPs containing the hCD45 sgRNA and discovered up to 1.7% small insertions or deletions at one of three top predicted off-target sites (Figure 4B, (Gundry et al., 2016)). During initial sgRNA design, the sgRNA were selected for the highest on-target efficiency score with the CRISPRscan algorithm (Moreno-Mateos et al., 2015). Off-target events present a serious concern for the clinical translation of the CRISPR-Cas technology. Therefore, for all subsequent studies our sgRNA design protocols were adjusted to put more emphasis on lowering the probability for off-target events through an additional screening of designed sgRNA with the COSMID algorithm (Cradick et al., 2014; Lee et al., 2016).

4.2.   Modeling antigen-escape in primary leukemia cells with CRISPR-Cas9

A common problem that limits the success of immunotherapy is antigen escape that has been observed after treatment with checkpoint blockade and CAR-T cell therapy (Majzner & Mackall, 2018; Zaretsky et al., 2016). Downregulation of CD19 on leukemic cells is observed in 7-25% of acute lymphoblastic leukemia patients and disease

relapse after CD19-specific CAR T cell therapy (Majzner & Mackall, 2018). In an effort to model antigen escape, the established technique from Gundry *et al.* was used to disrupt the CD19 gene. To this end, RNPs with three sgRNA targeting the CD19 gene were electroporated into a B-cell cancer cell line (Raji) as well as primary tumor cells of patients with acute B-cell leukemia (Fousek et al., 2020). Loss of the CD19 protein was confirmed by flow cytometry and CD19 negative cells were sorted through fluorescence-activated cell sorting. Interestingly, CD19-edited cancer cells partially downregulated CD20, another common B-cell antigen. Subsequently, different CAR T-cells were challenged with the CD19 negative cell lines. In contrast to single CD19-specific CAR T cells, T cells transduced with a tri-cistronic retroviral vector expressing a CD19-specific, a CD20-specific as well as a CD22-specific CAR were able to efficiently eradicate both the CD19 positive as well as the CD19 negative cancer cell lines *in vitro* and in multiple xenograft mouse models (Fousek et al., 2020).

4.3.   T cell immunity towards *Streptococcus pyogen*es Cas9 protein in healthy human adults

In preparation to moving CRISPR-Cas9 edited T cell products into clinical studies, the immunogenicity of Cas9 proteins in humans must be evaluated.(Chew, 2018) Cellular immune responses toward CAR-equipped T cells that target the solid tumor antigen TAG72 lead to CAR T cell elimination, reduced CAR T cell persistence and poor outcome (Hege et al., 2017). Similarly, preexisting Cas9-directed T cell responses could reduce the persistence of Cas9 gene-edited cells *in vivo*.

Cas9-specific memory T cells in peripheral blood were evaluated through short-term stimulation experiments. Isolated peripheral blood mononuclear cells (PBMC) contain both T cells as well as professional antigen-presenting cells like monocytes and B cells. Incubation of PBMC with recombinant Cas9 protein allows uptake, protein processing and presentation of Cas9-fragments on major histocompatibility complexes (MHC). Subsequently, T cell responses were recorded with multi-parameter flow cytometry. Low frequencies of SpCas9-reactive T cells were detected in 46 of 48 of our healthy human donors. As expected with a bacterial-specific T cell response, more cytokine-producing cells were found in CD4+ than in the CD8+ compartment. Nevertheless, an upregulation of the activation marker CD137 in CD8 T cells was noted in 80% of the donors. In accordance with the observed T cell responses, 85% of the analyzed donors displayed serological evidence of exposure, measured by detectable titers of

antibodies with specificity for the two intracellular proteins from *Streptococcus pyogenes*, DNAse B or Streptolysin O. Therefore, sensitization to the SpCas9 protein and potentially other commonly used variants could occur either by colonization or repeated infections with the facultative pathogenic bacteria in which the gene editing tools were discovered. Notably, other Cas9 homologs from *Staphylococcus aureus* and the Cas12a nuclease, a CRISPR-Cas type 2 nuclease system from *Acidaminococcus sp. BV3L6*, elicited a comparable T cell immune response in six of six tested healthy human donors of the cohort.

More importantly, enriched SpCas9-reactive effector T cells lysed autologous lymphoblastoid cells that endogenously express SpCas9 after plasmid transfection in a dose dependent manner. GFP-expressing lymphoblastoid cells were not killed by our SpCas9-specific effector T cells suggesting an antigen-specific effect. These results clearly indicate that preexisting SpCas9-specific T cells could eliminate gene-edited cells which constitutively overexpress the SpCas9 protein.

Repeated exposure and colonization with commensal microbiota at the body's surfaces can induce regulatory T cells (Lathrop et al., 2011). This immunosuppressive T cell subset is essential for immunological tolerance at mucosal barriers and it enables a symbiosis with the microbiome. As human adults experience repeated infections or are colonized with *Streptococcus pyogenes*, the hypothesis was formulated that regulatory T cells (Treg) contribute to the CD4+ T cell response against SpCas9 and potentially other homologs. To this end, markers for the identification of Treg cells were integrated in the flow cytometry readout panel. Strikingly, varying percentages of CD4+ T cells expressed a canonical regulatory phenotype CD25+ Foxp3+ within the activated CD137+ T cell fraction after Cas9-exposure. The Treg identity was confirmed through different classical markers for Treg (low expression of CD127, high expression of CTLA-4), their lack of inflammatory cytokine production as well as epigenetic analysis of the Treg-specific demethylation region (TSDR). Functionally, flow cytometrically enriched SpCas9-specific Treg were able to suppress the proliferation and cytokine production by SpCas9-reactive effector T cells *in vitro*. Killing of SpCas9-expressing targets could not be significantly reduced by addition of SpCas9-reactive Treg cells. Interestingly, only a minimal overlap (< 5%) existed between the T cell receptor repertoire of Cas9-activated CD4+ T cells with and without Treg phenotype. Therefore, conventional and immunosuppressive T cells may recognize different parts of Cas9, offering the possibility for engineered Cas9 variants which are recognized by

Treg but invisible to pro-inflammatory T cells.

"[The presented] results shed light on T cell-mediated immunity toward CRISPR-associated nucleases and offer a possible solution to overcome the problem of preexisting immunity." (Wagner et al., 2019)

5. Clinical applications and outlook

5.1. Facilitating progress in basic and translational research

CRISPR-Cas9 gene editing with ribonucleoproteins allows the highly efficient and moderately specific modification of the DNA of hematopoietic cells including T-lymphocytes. We established a stable protocol for rapid gene knockout experiments for enabling preclinical research that is currently adapted for a clinical trial with a genetically modified T cell product.

In the gene editing experiments described in this thesis, sgRNAs were transcribed *in vitro* and purified as described above. While we achieved remarkably efficient gene editing with only low toxicity, the electroporated RNA could induce innate immune responses in some cell types (Chew, 2018). Certain chemical modifications at the ends of the sgRNAs, e.g. the incorporation of 2′-O-methyl 3′phosphorothioate linkages, can reduce toxicity and increase nuclease-resistance (Hendel et al., 2015). Modified synthetic sgRNAs increase efficacy of gene editing across multiple primary cell types (Hendel et al., 2015). Additionally, synthetic sgRNAs are preferable for clinical trials due to their enhanced stability and the lack of commercially available GMP-compatible *in vitro* transcription enzyme kits.

The results detailed herein demonstrate that electroporation of CRISPR-Cas ribonucleoprotein complexes can be used to perform previously difficult experiments such as modeling antigen escape in primary human leukemia lines as exemplified in the study from Fousek and colleagues (Fousek et al., 2020). Previously, this could only have been achieved by the transfection of small inhibitory RNAs to knock down gene expression. However, transient transfection of siRNAs is not suitable for *in vivo* experiments where continuous suppression of the antigen is needed. Using the RNP-enabled "hit-and-run" approach obviates the need for time-consuming production of plasmids and retro- or lentiviral vectors that would be required for long-term knockdown with siRNA technology.

5.2. Minimizing off-target activity of CRISPR-Cas9 for clinical applications

The high efficiency and mild toxicity of this approach warranted its application for other clinically relevant genetic interventions. The off-target activity of the CRISPR-Cas9 system is an important safety concern for its clinical translation. Comparisons indicate that transient delivery of RNP induces less off-targets than plasmid overexpression or even mRNA delivery (Vakulskas et al., 2018). Nevertheless, we detected up to 1.7% edited alleles in genetic sequences with two mismatches to the sgRNA sequence after electroporation of CD45 specific RNPs into human T cells. To my knowledge, this was the first time significant off-target cutting has been observed in human T cells after electroporation of CRISPR-Cas9 ribonucleoprotein complexes. Therefore, off-target editing can occur with RNP delivery and must be carefully investigated in preparation of clinical trials.

In a subsequent study, a novel T cell immunotherapeutic agent was established that could selectively recognize and kill cancer cells expressing the CD7 antigen (Gomes-Silva et al., 2017). The sgRNAs were selected for higher specificity and fewer unintended off-target events. The specificity of the approach was subsequently tested by both an unbiased cell-based approach for off-target identification (GUIDE-seq (Tsai et al., 2015)) and amplification of *in silico* predicted off-target sites in CD7-edited T cells. GUIDE-seq for the CD7 sgRNA did not identify any off-target sites that were not predicted *in silico* (Gomes-Silva et al., 2017). Deep sequencing of the potential off-target sites showed no small insertions or deletions above the limit of detection (0.1%). In summary, careful sgRNA selection in this study allowed a genetic intervention with no detectable off-targets in the predicted sites (Lee et al., 2016).

Nevertheless, this analysis does not rule out that off-target editing occurs at a level below the detection limit of the next-generation sequencing approach or at other sites unidentified by *in silico* mechanisms. Lessard *et al.* reported that interindividual genetic variability could lead to off-target events unpredicted by *in silico* algorithms dependent on the reference genome (Lessard et al., 2017). To further reduce the risk for off-target editing in clinical cell products, Cas enzymes with improved fidelity could be applied (Vakulskas et al., 2018). Currently, the clinical efficacy of edited CD7-specific CAR T cells in patients with aggressive T-cell leukemia or lymphoma awaits clinical investigation in a phase 1/2a trial at Baylor College of Medicine, USA. (ClinicalTrials.gov Identifier NCT03690011)

5.3. Preexisting immunity to Cas9 proteins creates challenges for *in vivo* applications

The detection of pre-existing T cell memory against commonly used Cas9 nucleases highlights a previously unrecognized risk of applying the CRISPR-Cas9 system in humans. Importantly, our finding of pre-existing T cell immunity toward SpCas9 and *Staphylococcus aureus* Cas9 (SaCas9) were independently reproduced by different groups (Charlesworth et al., 2019; Ferdosi et al., 2019; Stadtmauer et al., 2020). Charlesworth *et al.* evaluated the Cas-directed T cell responses concluding 67% of adults showed a response to SpCas9 and a slightly higher percentage of adults showed a response to SaCas9 (Charlesworth et al., 2019). Their assays focused on IFN-gamma producing lymphocytes, thereby potentially underestimating the rate of sensitization in their cohort. Ferdosi *et al.* evaluated the reactivity of HLA-A2 positive donors regarding their reactivity to 35-different *in silico* predicted peptides with the highest probability of binding to HLA-A*02:01 (Ferdosi et al., 2019). In line with the presented results of this thesis, they found CD8+ T cell responses in 83% of the tested donors (Ferdosi et al., 2019; Wagner et al., 2019). Nevertheless, most clinical trials deliver Cas9-RNP directly into rapidly dividing cell cultures *ex vivo*. In these circumstances, Cas9 is rapidly degraded and diluted, which reduces the likelihood of Cas9-directed cellular immune responses upon infusion (Stadtmauer et al., 2020). In fact, first results of a clinical trial with CRISPR-Cas9 edited and TCR-redirected T cell products reported the persistence of modified cells despite confirmed preexisting immunity in the patients (Stadtmauer et al., 2020).

Preexisting immunity in humans could compromise the safety and efficacy of the therapeutic intervention in human adults through Cas9-specific effector T cell responses (Charlesworth et al., 2019; Ferdosi et al., 2019; Wagner et al., 2019). Classical animal models to evaluate gene therapies do not reflect the human situation as mice are held under sterile environments or the species are not colonized with *Streptococcus pyogenes* or *Staphylococcus aureus*. This creates the need for models that take into account diverse Cas9-directed immunization. In a first attempt for a better model, Li *et al.* evaluated a SaCas9-based *in vivo* gene therapy approach, comparing regular mice and mice that were immunized with small amounts of SaCas9 one week prior to the application of low immunogenic adenovirus-associated virus with liver tropism (Li et al., 2020). Sensitization of mice to SaCas9 lead to a substantial reduction

in transgene expression and marked liver damage that coincided with an increased detection of activated CD8+ T cells in the liver and complete loss of gene edited cells 12 weeks post treatment (Li et al., 2020). They could also detect elevated frequencies of CD4+ regulatory T cells in the blood of mice after immunization, although their specificity was not determined (Li et al., 2020).

This highlights that Cas9 based *in vivo* gene therapies could be at a higher risk of immune complications. The first clinical trial with an AAV-based CRISPR-Cas9 *in vivo* strategy for RPE65-mutated retinal dystrophy which causes blindness started enrollment in 2020 (ClinicalTrials.gov Identifier: NCT03872479). The trial is a unique opportunity to understand the extent and clinical relevance of Cas9-directed immune responses in humans. In depth monitoring of Cas9-directed T cell responses may enable to guide treatment decision making regarding immunosuppressive co-treatments and reveal whether endogenous Cas9-specific CD4+ Treg can blunt hazardous immune responses *in vivo*.

5.4. Summary and outlook

CRISPR-Cas genome engineering applications build on the previous experiences in the gene therapy field (Porteus, 2019). Prior shortcomings of viral gene therapies in respect to genotoxicity and immunogenicity informed the early safety investigations for this new technology (Anguela & High, 2019; Hacein-Bey-Abina et al., 2003; Porteus, 2019; Raper et al., 2002). The remarkable efficacy of RNP-mediated gene editing as well as the problems associated with Cas9-directed immunity imply that gene editing components should be used transiently (Charlesworth et al., 2019; Ferdosi et al., 2019; Gundry et al., 2016; Hendel et al., 2015; Wagner et al., 2019). For *ex vivo* modified cell products this can be performed through electroporation as exemplified in some of the works underlying this thesis. (Gundry et al., 2016) The technique outlined in Gomes-Silva *et al.* represents a novel treatment option for patients with T cell malignancies refractory to standard treatments that was enabled by gene editing. (Gomes-Silva et al., 2017) This emphasizes that the CRISPR-Cas gene editing technology is becoming a powerful asset in the toolbox for gene-modified cell therapies in regenerative medicine (Anguela & High, 2019; Porteus, 2019).

Some genetic diseases are caused by mutations in genes that are expressed in tissues and cell types that either cannot be cultured or do not engraft to form functional organs after infusion. Restricting expression time after delivery should reduce the time of Cas9

fragment presentation on major histocompatibility complexes and limit the priming of immunity. Changes introduced by CRISPR-Cas gene editing persist long-term and therefore do not require the constitutive presence of the nuclease. Ultimately, the next frontier within the CRISPR-Cas gene editing field will focus on establishing safe and effective technologies for time-restricted and cell-type specific *in vivo* delivery of the gene editing machinery. Alternatively, methods to induce tolerance to gene therapeutic vectors and cargo could be envisioned. This may be achieved by exploiting and promoting Cas9-specific Treg. Future studies should elucidate whether Cas9-specific Treg can induce long-lasting tolerance in a vector-independent fashion without compromising anti-bacterial immunity globally.

6. References

Anguela, X. M., & High, K. A. (2019). Entering the Modern Era of Gene Therapy. *Annual Review of Medicine*, *70*(1), 273–288. https://doi.org/10.1146/annurev-med-012017-043332

Carapetis, J. R., Steer, A. C., Mulholland, E. K., & Weber, M. (2005). The global burden of group A streptococcal diseases. *The Lancet Infectious Diseases*, *5*(11), 685–694. https://doi.org/10.1016/S1473-3099(05)70267-X

Charlesworth, C. T., Deshpande, P. S., Dever, D. P., Camarena, J., Lemgart, V. T., Cromer, M. K., Vakulskas, C. A., Collingwood, M. A., Zhang, L., Bode, N. M., Behlke, M. A., Dejene, B., Cieniewicz, B., Romano, R., Lesch, B. J., Gomez-Ospina, N., Mantri, S., Pavel-Dinu, M., Weinberg, K. I., & Porteus, M. H. (2019). Identification of preexisting adaptive immunity to Cas9 proteins in humans. *Nature Medicine*, *25*(2), 249–254. https://doi.org/10.1038/s41591-018-0326-x

Chew, W. L. (2018). Immunity to CRISPR Cas9 and Cas12a therapeutics: Immunity to CRISPR Cas9 and Cas12a therapeutics. *Wiley Interdisciplinary Reviews: Systems Biology and Medicine*, *10*(1), e1408. https://doi.org/10.1002/wsbm.1408

Chew, W. L., Tabebordbar, M., Cheng, J. K. W., Mali, P., Wu, E. Y., Ng, A. H. M., Zhu, K., Wagers, A. J., & Church, G. M. (2016). A multifunctional AAV–CRISPR–Cas9 and its host response. *Nature Methods*, *13*(10), 868–874. https://doi.org/10.1038/nmeth.3993

Cong, L., Ran, F. A., Cox, D., Lin, S., Barretto, R., Habib, N., Hsu, P. D., Wu, X., Jiang, W., Marraffini, L. A., & Zhang, F. (2013). Multiplex Genome Engineering Using CRISPR/Cas Systems. *Science (New York, N.Y.)*, *339*(6121), 819–823. https://doi.org/10.1126/science.1231143

Cradick, T. J., Qiu, P., Lee, C. M., Fine, E. J., & Bao, G. (2014). COSMID: A Web-based Tool for Identifying and Validating CRISPR/Cas Off-target Sites. *Molecular Therapy. Nucleic Acids*, *3*(12), e214. https://doi.org/10.1038/mtna.2014.64

Ferdosi, S. R., Ewaisha, R., Moghadam, F., Krishna, S., Park, J. G., Ebrahimkhani, M. R., Kiani, S., & Anderson, K. S. (2019). Multifunctional CRISPR-Cas9 with engineered immunosilenced human T cell epitopes. *Nature Communications*, *10*(1), 1842. https://doi.org/10.1038/s41467-019-09693-x

Fousek, K., Watanabe, J., Joseph, S. K., George, A., An, X., Byrd, T. T., Morris, J. S., Luong, A., Martínez-Paniagua, M. A., Sanber, K., Navai, S. A., Gad, A. Z., Salsman, V. S., Mathew, P. R., Kim, H. N., Wagner, D. L., Brunetti, L., Jang, A., Baker, M. L., … Ahmed, N. (2020). CAR T-cells that target acute B-lineage leukemia irrespective of CD19 expression. *Leukemia*, 1–15. https://doi.org/10.1038/s41375-020-0792-2

Fraietta, J. A., Nobles, C. L., Sammons, M. A., Lundh, S., Carty, S. A., Reich, T. J., Cogdill,

A. P., Morrissette, J. J. D., DeNizio, J. E., Reddy, S., Hwang, Y., Gohil, M., Kulikovskaya, I., Nazimuddin, F., Gupta, M., Chen, F., Everett, J. K., Alexander, K. A., Lin-Shiao, E., … Melenhorst, J. J. (2018). Disruption of TET2 promotes the therapeutic efficacy of CD19-targeted T cells. *Nature*, *558*(7709), 307–312. https://doi.org/10.1038/s41586-018-0178-z

Gomes-Silva, D., Srinivasan, M., Sharma, S., Lee, C. M., Wagner, D. L., Davis, T. H., Rouce, R. H., Bao, G., Brenner, M. K., & Mamonkin, M. (2017). CD7-edited T cells expressing a CD7-specific CAR for the therapy of T-cell malignancies. *Blood*, *130*(3), 285–296. https://doi.org/10.1182/blood-2017-01-761320

Gundry, M. C., Brunetti, L., Lin, A., Mayle, A. E., Kitano, A., Wagner, D., Hsu, J. I., Hoegenauer, K. A., Rooney, C. M., Goodell, M. A., & Nakada, D. (2016). Highly Efficient Genome Editing of Murine and Human Hematopoietic Progenitor Cells by CRISPR/Cas9. *Cell Reports*, *17*(5), 1453–1461. https://doi.org/10.1016/j.celrep.2016.09.092

Hacein-Bey-Abina, S., von Kalle, C., Schmidt, M., Le Deist, F., Wulffraat, N., McIntyre, E., Radford, I., Villeval, J.-L., Fraser, C. C., Cavazzana-Calvo, M., & Fischer, A. (2003). A serious adverse event after successful gene therapy for X-linked severe combined immunodeficiency. *The New England Journal of Medicine*, *348*(3), 255–256. https://doi.org/10.1056/NEJM200301163480314

Hege, K. M., Bergsland, E. K., Fisher, G. A., Nemunaitis, J. J., Warren, R. S., McArthur, J. G., Lin, A. A., Schlom, J., June, C. H., & Sherwin, S. A. (2017). Safety, tumor trafficking and immunogenicity of chimeric antigen receptor (CAR)-T cells specific for TAG-72 in colorectal cancer. *Journal for ImmunoTherapy of Cancer*, *5*(1), 22. https://doi.org/10.1186/s40425-017-0222-9

Hendel, A., Bak, R. O., Clark, J. T., Kennedy, A. B., Ryan, D. E., Roy, S., Steinfeld, I., Lunstad, B. D., Kaiser, R. J., Wilkens, A. B., Bacchetta, R., Tsalenko, A., Dellinger, D., Bruhn, L., & Porteus, M. H. (2015). Chemically modified guide RNAs enhance CRISPR-Cas genome editing in human primary cells. *Nature Biotechnology*, *33*(9), 985–989. https://doi.org/10.1038/nbt.3290

International Human Genome Sequencing Consortium. (2001). Initial sequencing and analysis of the human genome. *Nature*, *409*(6822), 860–921. https://doi.org/10.1038/35057062

Jinek, M., Chylinski, K., Fonfara, I., Hauer, M., Doudna, J. A., & Charpentier, E. (2012). A programmable dual-RNA-guided DNA endonuclease in adaptive bacterial immunity. *Science (New York, N.Y.)*, *337*(6096), 816–821. https://doi.org/10.1126/science.1225829

Lathrop, S. K., Bloom, S. M., Rao, S. M., Nutsch, K., Lio, C.-W., Santacruz, N., Peterson, D.

A., Stappenbeck, T. S., & Hsieh, C.-S. (2011). Peripheral education of the immune system by colonic commensal microbiota. *Nature*, *478*(7368), 250–254. https://doi.org/10.1038/nature10434

Lee, C. M., Cradick, T. J., Fine, E. J., & Bao, G. (2016). Nuclease Target Site Selection for Maximizing On-target Activity and Minimizing Off-target Effects in Genome Editing. *Molecular Therapy*, *24*(3), 475–487. https://doi.org/10.1038/mt.2016.1

Lessard, S., Francioli, L., Alfoldi, J., Tardif, J.-C., Ellinor, P. T., MacArthur, D. G., Lettre, G., Orkin, S. H., & Canver, M. C. (2017). Human genetic variation alters CRISPR-Cas9 on- and off-targeting specificity at therapeutically implicated loci. *Proceedings of the National Academy of Sciences*, *114*(52), E11257–E11266. https://doi.org/10.1073/pnas.1714640114

Li, A., Tanner, M. R., Lee, C. M., Hurley, A. E., De Giorgi, M., Jarrett, K. E., Davis, T. H., Doerfler, A. M., Bao, G., Beeton, C., & Lagor, W. R. (2020). AAV-CRISPR gene editing is negated by pre-existing immunity to Cas9. *Molecular Therapy*, S1525001620301982. https://doi.org/10.1016/j.ymthe.2020.04.017

Lowy, F. D. (1998). Staphylococcus aureus Infections. *New England Journal of Medicine*, *339*(8), 520–532. https://doi.org/10.1056/NEJM199808203390806

Majzner, R. G., & Mackall, C. L. (2018). Tumor Antigen Escape from CAR T-cell Therapy. *Cancer Discovery*, *8*(10), 1219–1226. https://doi.org/10.1158/2159-8290.CD-18-0442

Makarova, K. S., Wolf, Y. I., Iranzo, J., Shmakov, S. A., Alkhnbashi, O. S., Brouns, S. J. J., Charpentier, E., Cheng, D., Haft, D. H., Horvath, P., Moineau, S., Mojica, F. J. M., Scott, D., Shah, S. A., Siksnys, V., Terns, M. P., Venclovas, Č., White, M. F., Yakunin, A. F., … Koonin, E. V. (2020). Evolutionary classification of CRISPR–Cas systems: A burst of class 2 and derived variants. *Nature Reviews Microbiology*, *18*(2), 67–83. https://doi.org/10.1038/s41579-019-0299-x

Mali, P., Yang, L., Esvelt, K. M., Aach, J., Guell, M., DiCarlo, J. E., Norville, J. E., & Church, G. M. (2013). RNA-guided human genome engineering via Cas9. *Science (New York, N.Y.)*, *339*(6121), 823–826. https://doi.org/10.1126/science.1232033

Mandal, P. K., Ferreira, L. M. R., Collins, R., Meissner, T. B., Boutwell, C. L., Friesen, M., Vrbanac, V., Garrison, B. S., Stortchevoi, A., Bryder, D., Musunuru, K., Brand, H., Tager, A. M., Allen, T. M., Talkowski, M. E., Rossi, D. J., & Cowan, C. A. (2014). Efficient ablation of genes in human hematopoietic stem and effector cells using CRISPR/Cas9. *Cell Stem Cell*, *15*(5), 643–652. https://doi.org/10.1016/j.stem.2014.10.004

Maude, S. L., Frey, N., Shaw, P. A., Aplenc, R., Barrett, D. M., Bunin, N. J., Chew, A., Gonzalez, V. E., Zheng, Z., Lacey, S. F., Mahnke, Y. D., Melenhorst, J. J., Rheingold, S. R., Shen, A., Teachey, D. T., Levine, B. L., June, C. H., Porter, D. L., & Grupp, S.

A. (2014). Chimeric antigen receptor T cells for sustained remissions in leukemia. *The New England Journal of Medicine*, *371*(16), 1507–1517. https://doi.org/10.1056/NEJMoa1407222

Moreno-Mateos, M. A., Vejnar, C. E., Beaudoin, J.-D., Fernandez, J. P., Mis, E. K., Khokha, M. K., & Giraldez, A. J. (2015). CRISPRscan: Designing highly efficient sgRNAs for CRISPR-Cas9 targeting in vivo. *Nature Methods*, *12*(10), 982–988. https://doi.org/10.1038/nmeth.3543

Porteus, M. H. (2019). A New Class of Medicines through DNA Editing. *The New England Journal of Medicine*, *380*(10), 947–959. https://doi.org/10.1056/NEJMra1800729

Raper, S. E., Yudkoff, M., Chirmule, N., Gao, G.-P., Nunes, F., Haskal, Z. J., Furth, E. E., Propert, K. J., Robinson, M. B., Magosin, S., Simoes, H., Speicher, L., Hughes, J., Tazelaar, J., Wivel, N. A., Wilson, J. M., & Batshaw, M. L. (2002). A Pilot Study of In Vivo Liver-Directed Gene Transfer with an Adenoviral Vector in Partial Ornithine Transcarbamylase Deficiency. *Human Gene Therapy*, *13*(1), 163–175. https://doi.org/10.1089/10430340152712719

Scholler, J., Brady, T. L., Binder-Scholl, G., Hwang, W.-T., Plesa, G., Hege, K. M., Vogel, A. N., Kalos, M., Riley, J. L., Deeks, S. G., Mitsuyasu, R. T., Bernstein, W. B., Aronson, N. E., Levine, B. L., Bushman, F. D., & June, C. H. (2012). Decade-Long Safety and Function of Retroviral-Modified Chimeric Antigen Receptor T Cells. *Science Translational Medicine*, *4*(132), 132ra53-132ra53. https://doi.org/10.1126/scitranslmed.3003761

Schumann, K., Lin, S., Boyer, E., Simeonov, D. R., Subramaniam, M., Gate, R. E., Haliburton, G. E., Ye, C. J., Bluestone, J. A., Doudna, J. A., & Marson, A. (2015). Generation of knock-in primary human T cells using Cas9 ribonucleoproteins. *Proceedings of the National Academy of Sciences*, *112*(33), 10437–10442. https://doi.org/10.1073/pnas.1512503112

Simhadri, V. L., McGill, J., McMahon, S., Wang, J., Jiang, H., & Sauna, Z. E. (2018). Prevalence of Pre-existing Antibodies to CRISPR-Associated Nuclease Cas9 in the USA Population. *Molecular Therapy. Methods & Clinical Development*, *10*, 105–112. https://doi.org/10.1016/j.omtm.2018.06.006

Stadtmauer, E. A., Fraietta, J. A., Davis, M. M., Cohen, A. D., Weber, K. L., Lancaster, E., Mangan, P. A., Kulikovskaya, I., Gupta, M., Chen, F., Tian, L., Gonzalez, V. E., Xu, J., Jung, I., Melenhorst, J. J., Plesa, G., Shea, J., Matlawski, T., Cervini, A., … June, C. H. (2020). CRISPR-engineered T cells in patients with refractory cancer. *Science*, *367*(6481), eaba7365. https://doi.org/10.1126/science.aba7365

Sternberg, S. H., Redding, S., Jinek, M., Greene, E. C., & Doudna, J. A. (2014). DNA interrogation by the CRISPR RNA-guided endonuclease Cas9. *Nature*, *507*(7490),

62–67. https://doi.org/10.1038/nature13011

Tsai, S. Q., Zheng, Z., Nguyen, N. T., Liebers, M., Topkar, V. V., Thapar, V., Wyvekens, N., Khayter, C., Iafrate, A. J., Le, L. P., Aryee, M. J., & Joung, J. K. (2015). GUIDE-seq enables genome-wide profiling of off-target cleavage by CRISPR-Cas nucleases. *Nature Biotechnology*, *33*(2), 187–197. https://doi.org/10.1038/nbt.3117

Urnov, F. D., Miller, J. C., Lee, Y.-L., Beausejour, C. M., Rock, J. M., Augustus, S., Jamieson, A. C., Porteus, M. H., Gregory, P. D., & Holmes, M. C. (2005). Highly efficient endogenous human gene correction using designed zinc-finger nucleases. *Nature*, *435*(7042), 646–651. https://doi.org/10.1038/nature03556

Vakulskas, C. A., Dever, D. P., Rettig, G. R., Turk, R., Jacobi, A. M., Collingwood, M. A., Bode, N. M., McNeill, M. S., Yan, S., Camarena, J., Lee, C. M., Park, S. H., Wiebking, V., Bak, R. O., Gomez-Ospina, N., Pavel-Dinu, M., Sun, W., Bao, G., Porteus, M. H., & Behlke, M. A. (2018). A high-fidelity Cas9 mutant delivered as a ribonucleoprotein complex enables efficient gene editing in human hematopoietic stem and progenitor cells. *Nature Medicine*, *24*(8), 1216–1224. https://doi.org/10.1038/s41591-018-0137-0

Wagner, D. L., Amini, L., Wendering, D. J., Burkhardt, L.-M., Akyüz, L., Reinke, P., Volk, H.-D., & Schmueck-Henneresse, M. (2019). High prevalence of Streptococcus pyogenes Cas9-reactive T cells within the adult human population. *Nature Medicine*, *25*(2), 242–248. https://doi.org/10.1038/s41591-018-0204-6

Wang, D., Mou, H., Li, S., Li, Y., Hough, S., Tran, K., Li, J., Yin, H., Anderson, D. G., Sontheimer, E. J., Weng, Z., Gao, G., & Xue, W. (2015). Adenovirus-Mediated Somatic Genome Editing of Pten by CRISPR/Cas9 in Mouse Liver in Spite of Cas9-Specific Immune Responses. *Human Gene Therapy*, *26*(7), 432–442. https://doi.org/10.1089/hum.2015.087

Xu, L., Wang, J., Liu, Y., Xie, L., Su, B., Mou, D., Wang, L., Liu, T., Wang, X., Zhang, B., Zhao, L., Hu, L., Ning, H., Zhang, Y., Deng, K., Liu, L., Lu, X., Zhang, T., Xu, J., … Chen, H. (2019). CRISPR-Edited Stem Cells in a Patient with HIV and Acute Lymphocytic Leukemia. *New England Journal of Medicine*, *381*(13), 1240–1247. https://doi.org/10.1056/NEJMoa1817426

Zaretsky, J. M., Garcia-Diaz, A., Shin, D. S., Escuin-Ordinas, H., Hugo, W., Hu-Lieskovan, S., Torrejon, D. Y., Abril-Rodriguez, G., Sandoval, S., Barthly, L., Saco, J., Homet Moreno, B., Mezzadra, R., Chmielowski, B., Ruchalski, K., Shintaku, I. P., Sanchez, P. J., Puig-Saus, C., Cherry, G., … Ribas, A. (2016). Mutations Associated with Acquired Resistance to PD-1 Blockade in Melanoma. *The New England Journal of Medicine*, *375*(9), 819–829. https://doi.org/10.1056/NEJMoa1604958

7. Anteilserklärung an den erfolgten Publikationen

Dimitrios Laurin Wagner hatte folgenden Anteil an den folgenden Publikationen:

Publikation 1: Michael C. Gundry, Lorenzo Brunetti, Angelique Lin, Allison E. Mayle, Ayumi Kitano, Dimitrios Wagner, Joanne I. Hsu, Kevin A. Hoegenauer, Cliona Rooney, Margaret A. Goodell, and Daisuke Nakada;
Highly efficient genome editing of murine and human hematopoietic progenitor cells by CRISPR/Cas9
Cell Reports, 2016
Beitrag im Einzelnen: Durchführung der Experimente mit humanen T-Zellen, im Besonderen: die Isolation, Aktivierung, Zellkultur, Elektroporation und durchflusszytometrische Analyse von primären humanen T-Zellen, die in den Graphiken 3A, S3B, S3C gezeigt sind. Anfertigung des Methodenteils „Human cell culture and transfection" im Manuskript zu den T-Zellkulturen. Kritische Revision des gesamten Manuskripts.

Publikation 2: Dimitrios L Wagner, Leila Amini, Desiree J Wendering, Lisa-Marie Burkhardt, Levent Akyüz, Petra Reinke, Hans-Dieter Volk, Michael Schmueck-Henneresse
High Prevalence of Streptococcus Pyogenes Cas9-reactive T Cells Within the Adult Human Population
Nature Medicine, 2019
Beitrag im Einzelnen: Entwicklung der Hypothese sowie Durchführung der Stimulationsexperimente, durchflusszytometrischen Analysen, Zellsortierung, T-Zellkulturen, Elektroporation und VITAL-Assay und die Anfertigung des Manuskriptes. Wie im Manuskript geschrieben wurde die T-Zell-Rezeptor-Sequenzierung von Adaptive Biotechnologies durchgeführt. Bioinformatische Analysen der TZR-Datensätze wurde von L. Amini und M. Schmück-Henneresse angefertigt. Die Zytokinmessungen wurden von Ko-Autor Levent Akyüz durchgeführt. TSDR Analyse wurde von D. Jacqueline Wendering erledigt. Serologische Untersuchungen auf DNAse B und Streptolysin O wurden bei Labor Berlin in Auftrag gegeben. Im Rahmen der Revisionsexperimente wurde die Anzahl an gesunden Spendern für die Studie verdoppelt, hierbei wurde ein Teil der Experimente von Ko-Autorinnen Lisa-Marie Burkhardt, Desirée Jacqueline Wendering und Leila Amini durchgeführt.

Publikation 3: Kristen Fousek, Junji Watanabe, Sujith K. Joseph, Ann George, Xingyue An, Tiara T. Byrd, Jessica S. Morris, Annie Luong, Melisa A. Martínez-Paniagua, Khaled Sanber, Shoba A. Navai, Ahmed Z. Gad, Vita S. Salsman, Pretty R. Mathew, Hye Na Kim, Dimitrios L. Wagner, Lorenzo Brunetti, Albert Jang, Matthew L. Baker, Navin Varadarajan, Meenakshi Hegde, Yong-Mi Kim, Nora Heisterkamp, Hisham Abdel-Azim and Nabil Ahmed
CAR T-cells that target acute B-lineage leukemia irrespective of CD19 expression
Leukemia, 2020
Beitrag im Einzelnen: Herstellung der CD19 sgRNAs sowie Durchführung CD19-Knockout in Raji Zelllinie und primären B-ALL-Linie UPN02 und anschließende Zellsortierung zur Erstellung der CD19-KO Raji Linie und und CD19-KOUPN02-Linie. Dies führte zu den Graphiken 1E und die Zellen wurden genutzt für die Experimente der Abbildungen 4A, 4D, 4E, 4F, 4G, 5. Außerdem wurden der relevante Methodikteil verfasst und das finale Manuskript kritisch revidiert.

_____
Unterschrift, Datum und Stempel des/der erstbetreuenden Hochschullehrers/in

_____
Unterschrift des Doktoranden/der Doktorandin

8. Eidesstattliche Versicherung

„Ich, Dimitrios Laurin Wagner, versichere an Eides statt durch meine eigenhändige Unterschrift, dass ich die vorgelegte Dissertation mit dem Thema: „CRISPR-Cas9 und T-Zellen"/"CRISPR-Cas9 and T-cells" selbstständig und ohne nicht offengelegte Hilfe Dritter verfasst und keine anderen als die angegebenen Quellen und Hilfsmittel genutzt habe.
Alle Stellen, die wörtlich oder dem Sinne nach auf Publikationen oder Vorträgen anderer Autoren/innen beruhen, sind als solche in korrekter Zitierung kenntlich gemacht. Die Abschnitte zu Methodik (insbesondere praktische Arbeiten, Laborbestimmungen, statistische Aufarbeitung) und Resultaten (insbesondere Abbildungen, Graphiken und Tabellen) werden von mir verantwortet.

Ich versichere ferner, dass ich die in Zusammenarbeit mit anderen Personen generierten Daten, Datenauswertungen und Schlussfolgerungen korrekt gekennzeichnet und meinen eigenen Beitrag sowie die Beiträge anderer Personen korrekt kenntlich gemacht habe (siehe Anteilserklärung). Texte oder Textteile, die gemeinsam mit anderen erstellt oder verwendet wurden, habe ich korrekt kenntlich gemacht.

Meine Anteile an etwaigen Publikationen zu dieser Dissertation entsprechen denen, die in der untenstehenden gemeinsamen Erklärung mit dem/der Erstbetreuer/in, angegeben sind. Für sämtliche im Rahmen der Dissertation entstandenen Publikationen wurden die Richtlinien des ICMJE (International Committee of Medical Journal Editors) zur Autorenschaft eingehalten. Ich erkläre ferner, dass ich mich zur Einhaltung der Satzung der Charité – Universitätsmedizin Berlin zur Sicherung Guter Wissenschaftlicher Praxis verpflichte.

Weiterhin versichere ich, dass ich diese Dissertation weder in gleicher noch in ähnlicher Form bereits an einer anderen Fakultät eingereicht habe.

Die Bedeutung dieser eidesstattlichen Versicherung und die strafrechtlichen Folgen einer unwahren eidesstattlichen Versicherung (§§156, 161 des Strafgesetzbuches) sind mir bekannt und bewusst."

Datum 28.Juli 2020   Unterschrift

9. Publikationen

1. Auszug Journal Summary List für Zeitschrift „Cell Reports"

InCites Journal Citation Reports   Clarivate Analytics

Journal Data Filtered By: Selected JCR Year: 2014 Selected Editions: SCIE Selected Categories: 'CELL BIOLOGY' Selected Category Scheme: WoS

Rank	Full Journal Title	Total Cites	Journal Impact Factor	Eigenfactor Score
1	NATURE REVIEWS MOLECULAR CELL BIOLOGY	35,928	37.806	0.112420
2	CELL	201,108	32.242	0.577030
3	NATURE MEDICINE	62,572	28.223	0.162900
4	CANCER CELL	27,283	23.523	0.106800
5	Cell Stem Cell	17,720	22.268	0.102450
6	NATURE CELL BIOLOGY	35,734	19.679	0.125310
7	Cell Metabolism	18,502	17.565	0.079190
8	Advances in Anatomy Embryology and Cell Biology	424	17.000	0.000440
9	Annual Review of Cell and Developmental Biology	9,301	16.660	0.023560
10	Science Translational Medicine	13,031	15.843	0.091690
11	MOLECULAR CELL	53,786	14.018	0.200630
12	NATURE STRUCTURAL & MOLECULAR BIOLOGY	26,673	13.309	0.114740
13	CELL RESEARCH	9,195	12.413	0.034820
14	TRENDS IN CELL BIOLOGY	11,481	12.007	0.034740
15	Autophagy	9,457	11.753	0.032890
16	GENES & DEVELOPMENT	59,511	10.798	0.128000
17	EMBO JOURNAL	72,583	10.434	0.128000
18	JOURNAL OF CELL BIOLOGY	71,695	9.834	0.130140
19	DEVELOPMENTAL CELL	23,646	9.708	0.090600
20	CURRENT BIOLOGY	48,575	9.571	0.144060
21	TRENDS IN MOLECULAR MEDICINE	7,186	9.453	0.019460
22	PLANT CELL	46,901	9.338	0.080800
23	EMBO REPORTS	11,419	9.055	0.035720

24	Cold Spring Harbor Perspectives in Biology	7,817	8.679	0.057770
25	CURRENT OPINION IN CELL BIOLOGY	13,844	8.467	0.038410
26	ONCOGENE	64,071	8.459	0.103620
27	**Cell Reports**	**6,886**	**8.358**	**0.056460**
28	CELL DEATH AND DIFFERENTIATION	16,082	8.184	0.040700
29	CURRENT OPINION IN GENETICS & DEVELOPMENT	8,084	7.574	0.026580
30	CURRENT OPINION IN STRUCTURAL BIOLOGY	10,897	7.201	0.030910
31	Journal of Molecular Cell Biology	1,141	6.870	0.005730
32	AGEING RESEARCH REVIEWS	2,986	6.634	0.008790
33	STEM CELLS	20,143	6.523	0.048880
34	Aging-US	2,583	6.432	0.012550
35	Oncotarget	3,908	6.359	0.014340
36	AGING CELL	5,793	6.340	0.019120
37	Science Signaling	7,211	6.279	0.047140
38	SEMINARS IN CELL & DEVELOPMENTAL BIOLOGY	6,404	6.265	0.022440
39	Wiley Interdisciplinary Reviews-RNA	1,305	6.019	0.008860
40	CELLULAR AND MOLECULAR LIFE SCIENCES	19,985	5.808	0.049040
41	STRUCTURE	13,533	5.618	0.043490
42	JOURNAL OF CELL SCIENCE	42,808	5.432	0.094680
43	Stem Cell Reports	461	5.365	0.002560
44	CYTOKINE & GROWTH FACTOR REVIEWS	4,708	5.357	0.008870
45	Journal of Tissue Engineering and Regenerative Medicine	2,634	5.199	0.007490
46	BIOCHIMICA ET BIOPHYSICA ACTA-MOLECULAR AND CELL BIOLOGY OF LIPIDS	7,312	5.162	0.020620
47	MATRIX BIOLOGY	3,721	5.074	0.005240
48	FASEB JOURNAL	41,076	5.043	0.069200
49	BIOCHIMICA ET BIOPHYSICA ACTA-MOLECULAR CELL RESEARCH	11,055	5.019	0.033670
50	Cell Death & Disease	5,309	5.014	0.023420

2. Publikation: Gundry et al. 2016 Cell Reports

Cell Reports

Highly Efficient Genome Editing of Murine and Human Hematopoietic Progenitor Cells by CRISPR/Cas9

Graphical Abstract
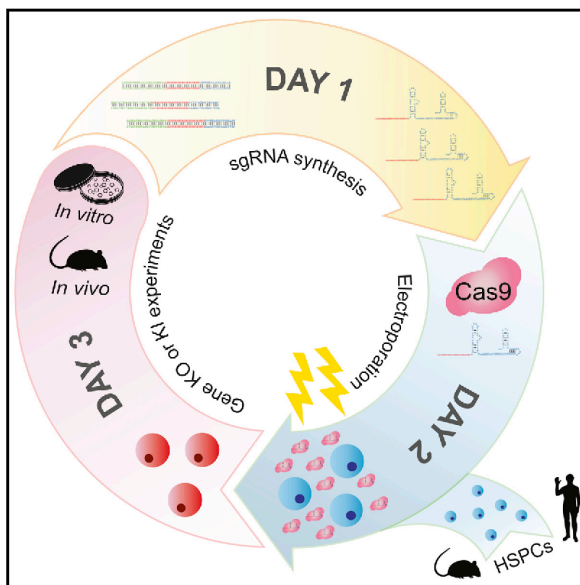
Authors

Michael C. Gundry, Lorenzo Brunetti, Angelique Lin, ..., Cliona M. Rooney, Margaret A. Goodell, Daisuke Nakada

Correspondence

goodell@bcm.edu (M.A.G.), nakada@bcm.edu (D.N.)

In Brief

Gundry et al. develop an efficient and simple method implementing CRISPR/Cas9-mediated gene disruption and HDR in murine and human HSPCs. This method enables quick evaluation of the function of genes by performing in vitro or transplantation assays using the modified HSPCs.

Highlights

- Gene knockout of primary murine HSPCs with efficiencies routinely higher than 60%

- Gene knockout of primary human HSPCs and T cells from 75% to 90%

- CRISPR/Cas9 homology-directed repair in >20% of primary human HSPCs

CellPress

Highly Efficient Genome Editing of Murine and Human Hematopoietic Progenitor Cells by CRISPR/Cas9

Michael C. Gundry,[1,2,5,10] Lorenzo Brunetti,[2,5,7,10] Angelique Lin,[1,3,10] Allison E. Mayle,[1,2,5] Ayumi Kitano,[1]
Dimitrios Wagner,[5,8,9] Joanne I. Hsu,[2,4,5] Kevin A. Hoegenauer,[1] Cliona M. Rooney,[5,6,8] Margaret A. Goodell,[1,2,5,6,8,*]
and Daisuke Nakada[1,2,5,11,*]

[1]Department of Molecular and Human Genetics
[2]Stem Cells and Regenerative Medicine Center
[3]Integrative Molecular and Biomedical Sciences Program
[4]Translational Biology and Molecular Medicine Program
[5]Center for Cell and Gene Therapy
[6]Department of Pediatrics
Baylor College of Medicine, Houston, TX 77030, USA
[7]Centro di Ricerca Emato-Oncologica (CREO), University of Perugia, 06156 Perugia, Italy
[8]Texas Children's Hospital and Houston Methodist Hospital, Houston, TX 77030, USA
[9]Institute for Medical Immunology, Charité University Medicine Berlin, 13353 Berlin, Germany
[10]Co-first author
[11]Lead Contact
*Correspondence: goodell@bcm.edu (M.A.G.), nakada@bcm.edu (D.N.)
http://dx.doi.org/10.1016/j.celrep.2016.09.092

SUMMARY

Our understanding of the mechanisms that regulate hematopoietic stem/progenitor cells (HSPCs) has been advanced by the ability to genetically manipulate mice; however, germline modification is time consuming and expensive. Here, we describe fast, efficient, and cost-effective methods to directly modify the genomes of mouse and human HSPCs using the CRISPR/Cas9 system. Using plasmid and virus-free delivery of guide RNAs alone into Cas9-expressing HSPCs or Cas9-guide RNA ribonucleoprotein (RNP) complexes into wild-type cells, we have achieved extremely efficient gene disruption in primary HSPCs from mouse (>60%) and human ($\sim$75%). These techniques enabled rapid evaluation of the functional effects of gene loss of *Eed*, *Suz12*, and *DNMT3A*. We also achieved homology-directed repair in primary human HSPCs (>20%). These methods will significantly expand applications for CRISPR/Cas9 technologies for studying normal and malignant hematopoiesis.

INTRODUCTION

The ability to genetically manipulate the genomes of animal models or isolated cells has driven hematopoietic stem cell (HSC) research, revealing key mechanisms that control HSC self-renewal and differentiation. Numerous genetically engineered mouse models have contributed to our understanding of the pathways that control HSC maintenance and regeneration in physiological settings (Rossi et al., 2012). Although this approach produces invaluable insights and still remains a gold standard in studying HSC biology, large time and cost commitments are required to generate new mouse models, and the approach is generally not amenable to high-throughput studies. On the other hand, somatic engineering of hematopoietic stem/progenitor cell (HSPC) genomes has been achieved, in large, using retroviral vectors to either overexpress or knock down the expression of genes of interest (Rivière et al., 2012). This approach has been used to screen for both positive and negative regulators of HSC function from up to 100 candidate genes (Deneault et al., 2009; Hope et al., 2010). Although this approach allows investigators to quickly assess the function of multiple genes, retroviral transduction negatively impacts HSC function during in vitro culture, and retroviral genome integration is a serious concern when these engineered cells are used clinically (Hacein-Bey-Abina et al., 2003). A new method to edit the genomes of HSPCs should not only accelerate gene discovery research but also open up new clinical opportunities in using engineered HSPCs for gene therapy.

Among the several engineered nucleases enabling site-specific genome editing, the CRISPR-Cas9 system (Jinek et al., 2012) stands out since it does not require cumbersome engineering of nucleases for each target and only requires a 20-nt RNA sequence contained within a chimeric single-guide RNA (sgRNA) to drive the endonuclease Cas9 to its target sequence. Thus, CRISPR/Cas9 provides a versatile, modular, and cost-effective means to edit the genomes of multiple model systems (Hsu et al., 2014; Sternberg and Doudna, 2015). Several delivery methods have been used to perform CRISPR/Cas9-mediated gene editing of HSPCs, including lentiviral transduction (Heckl et al., 2014), plasmid DNA transfection (Mandal et al., 2014), or chemically modified RNA (Hendel et al., 2015), achieving up to

48% gene disruption in human HSPCs. While these studies have shown the enormous potential of HSPC gene editing by CRISPR/Cas9, a method that is highly efficient and simple, without the need for any cloning and nucleotide modifications, and that addresses clinical concerns of retroviral genome insertion is still lacking. We sought to develop simple strategies to perform CRISPR/Cas9-mediated gene editing in HSPCs with minimal manipulations and while avoiding viral integration into the HSPC genome. Here we describe fast, efficient, and cost-effective methods of CRISPR/Cas9-mediated gene editing in primary murine and human HSPCs, and we demonstrate that this method can be used to directly examine gene function.

RESULTS

Efficient Gene Disruption in Mouse HSPCs

We reasoned that transfecting HSPCs isolated from Cas9-expressing mice (Platt et al., 2014) with sgRNA would be an efficient method to edit the genome of HSPCs, since only the small RNA molecules would need to be introduced. To test this idea, we designed small guide RNAs to target the GFP gene (GFP-sg1) co-expressed in the Cas9-expressing mice. When we electroporated c-kit⁺ HSPCs with in vitro-transcribed GFP-sg1, we observed highly efficient loss of GFP expression by flow cytometry, compared to cells electroporated with sgRNA against *Rosa26* (R26-sg) (Figure 1A). Although electroporation reduced the survival of HSPCs ~20% immediately after electroporation, cells maintained at least 80% viability throughout the experiment for up to 96 hr post-electroporation (Figure 1B). In this condition maintaining high viability, we found that 67% ± 4% of HSPCs lost GFP expression upon electroporation of GFP-sg1 (Figures S1A and S1B), demonstrating efficient gene editing with high cell viability. The frequency of GFP ablation exhibited a sgRNA dose-dependent increase, plateauing at 1 μg GFP-sg1 for 10⁵ HSPCs per transfection (Figure 1C).

Because retroviral transduction is enhanced by culturing with cytokines to stimulate the cell cycle of quiescent HSPCs, we also tested whether brief in vitro exposure to cytokines in culture before sgRNA electroporation increased GFP gene editing. We electroporated Cas9-expressing HSPCs after varying the duration of culture. We found that a brief culture (1–3 hr) increased the frequency of GFP-negative cells from around 60% in fresh progenitors to a maximum of 85% ± 1% after 3 hr, without further increase after 12 hr (Figure 1D). In the context of this gene-editing strategy, incorporation of an optimized scaffold sequence previously shown to improve Cas9-mediated imaging (Chen et al., 2013) did not significantly increase the frequencies of gene disruption further (Figure S1C).

Because the c-kit⁺ population contains various progenitors besides HSCs, we tested whether HSCs themselves undergo successful gene disruption upon transfection of sgRNAs. After electroporation of Cas9-expressing c-kit⁺ cells with GFP-sg1, we sorted CD150⁺CD48 lineage Sca-1⁺ cells (c-kit expression was attenuated within 1 hr of pre-culture before electroporation, Figure S1D) into semi-solid media, and we monitored colonies arising from these single HSCs for GFP ablation. Flow cytometry of individual colonies revealed that most HSC-derived colonies (40 of 48: 83%) lost GFP expression (representative three col-

onies shown in Figure 1E), whereas electroporation with or without sgRNA did not affect the clonality of HSCs compared to cultured, un-electroporated cells (Figure S1E). Thus, our method efficiently ablates genes in HSCs with minimum impact on HSC survival.

With the optimized sgRNA delivery method in hand, we next considered whether Cas9 protein pre-complexed with sgRNA to generate a ribonucleoprotein (RNP) particle (Kim et al., 2014; Lin et al., 2014; Schumann et al., 2015) also could be used to edit genes in murine HSPCs. Different amounts of GFP-sg1 were mixed with Cas9 protein, and the RNP complex was electroporated into HSPCs isolated from a mouse strain that ubiquitously expresses GFP (Schaefer et al., 2001). As shown in Figures 1F and 1G, ~70% of HSPCs lost GFP expression upon co-delivery of Cas9 protein and GFP-sg1. Two other sgRNAs against GFP also attenuated GFP expression in significant fractions of HSPCs (Figure S1G). Under this condition, HSPCs electroporated with Cas9 RNP maintained viability of >80% for up to 96 hr after electroporation (Figure S1F). Since loss of GFP expression is an indirect measure of genome editing, we directly examined insertion or deletion (indel) frequencies at the genomic level. First, we performed T7 endonuclease I (T7E1) assays and found that a significant fraction of HSPCs accrued indels (Figure 1H). We note that the T7E1 assay often underestimates the rate of indel formation, potentially due to self-hybridization of the alleles that carry the indel, incomplete duplex melting, and inefficient cleavage of single nucleotide indels (Schumann et al., 2015). To accurately determine the nature of the indels, we next performed high-throughput sequencing, which revealed that ~60% of HSPCs accrued small indels (Figure S1H; Table S2). These genomic analyses corroborated the flow cytometry data demonstrating that GFP alleles were mutated by the Cas9 RNP approach. Thus, this strategy allows us to study gene function directly in HSPCs in any genetic background.

Functional Assessment of Gene Disruption in Mouse HSPCs

We then tested whether targeted gene editing in HSPCs by CRISPR/Cas9 could be used to alter HSPC function. We chose to disrupt two polycomb-repressive complex 2 (PRC2) components *Eed* and *Suz12*, which are both found mutated in human leukemias (Shih et al., 2012). It has been shown that monoallelic loss, but not biallelic loss, of *Eed* or *Suz12* confers proliferative advantages to HSPCs (Lee et al., 2015; Xie et al., 2014). We transfected wild-type HSPCs with Cas9-RNP complexes against *Rosa26*, *Eed*, or *Suz12*; plated them on semi-solid media; and serially replated the cells. Whereas most *Rosa26*-targeted HSPCs lost proliferative capacity upon the fourth replating, *Eed*- and *Suz12*-targeted HSPCs exhibited extensive proliferative capacity at the fourth passage (Figure 2A). T7E1 assays performed on HSPC cultures shortly (48 hr) after electroporation revealed that a substantial fraction of cells accrued indels in *Eed* and *Suz12* (Figure 2B). Sanger sequencing and tracking of indels by decomposition (TIDE) analysis (Brinkman et al., 2014) revealed that ~50% of the sequence reads accrued small indels between 4-bp deletion and 2-bp insertion (Figures S2A and S2B).
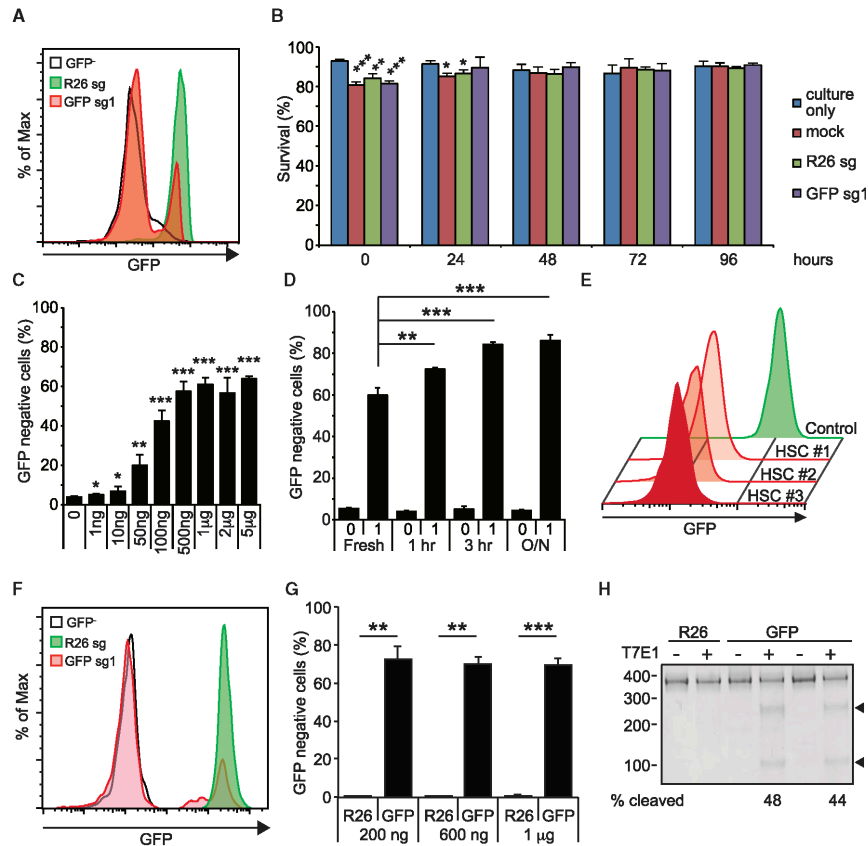
Figure 1. Gene Editing in Murine HSPCs

(A) A representative flow cytometry histogram showing efficient ablation of GFP by electroporating GFP-sg1 into Cas9-expressing HSPCs. Black histogram represents GFP⁻ HSPCs, and green and red histograms represent *Rosa26* (R26)- and GFP-disrupted HSPCs, respectively (n = 3).

(B) Survival of HSPCs was determined by trypan blue staining of cells cultured without electroporation, cells mock electroporated without sgRNA, and cells electroporated with R26 or GFP sgRNA. 1 μg of sgRNA was used to electroporate 10^5 cells (n = 3).

(C) Deletion efficiencies of GFP exhibiting sgRNA dose-dependent response. A plateau in gene-editing efficiency was reached by 1 μg sgRNA/10^5 cells (n = 3).

(D) A brief culture of murine HSPCs for 1–3 hr increased gene-editing frequency, while overnight (O/N) culture did not further increase gene editing (n = 3).

(E) After electroporating c-kit⁺ HSPCs with GFP-sg1, HSCs were sorted clonally into methylcellulose media. Most (40 of 48) HSC colonies exhibited loss of GFP expression, as shown by the representative flow cytometry histograms for three HSC-derived colonies from one donor mouse (n = 3 independent experiments).

(F) A representative histogram demonstrates efficient ablation of GFP expression by electroporating Cas9/GFP-sg1 RNP into GFP-expressing HSPCs (n = 3).

(G) Quantification of results in (F). Even as little as 200 ng GFP-sg1 efficiently ablated GFP upon delivery with Cas9 protein (1 μg).

(H) T7E1 assays performed with GFP amplicon derived from R26- or GFP-disrupted HSPCs. PCR amplicons were either treated (+) or untreated (−) with T7E1. Arrowheads indicate the bands with expected size assuming small indels, based on the Cas9 cleavage site. 1 μg of sgRNA was used to electroporate 10^5 Cas9-expressing cells unless otherwise noted. All data represent mean ± SD (*p < 0.05, **p < 0.01, and ***p < 0.001 by Student's t test). See also Figure S1.

We also cloned individual colonies at later passages and examined the editing status. T7E1 assay revealed that *Eed*- and *Suz12*-edited colonies acquired indels, and sequencing verified that they all acquired monoallelic loss of *Eed* or *Suz12* (Figures 2C–2F), consistent with the haploinsufficient function of *Eed* and Suz12 (Lee et al., 2015; Xie et al., 2014). These results establish that Cas9 RNPs can be used to perform gene editing in primary murine HSPCs regardless of genetic background, resulting in clear loss-of-function phenotypes.
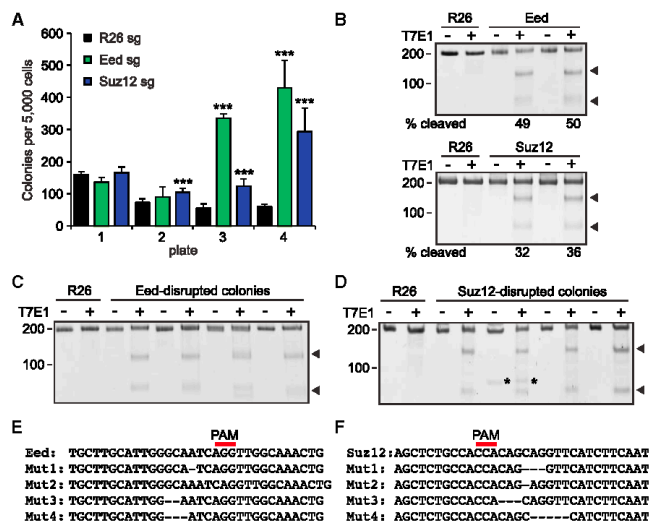
Figure 2. Editing Endogenous Genes in Murine HSPCs

(A) Gene editing of *Eed* or *Suz12* using Cas9-sgRNA RNP increased the ability of murine HSPCs to serially replate in culture; 1 μg Cas9 protein and 1 μg sgRNA were used (n = 4).

(B) T7E1 assays performed with *Eed* (top) or *Suz12* (bottom) amplicon derived from *Rosa26*- (R26), *Eed*-, or *Suz12*-disrupted HSPCs 48 hr after electroporation. The numbers below the gel image represent the cleavage efficiency determined by densitometric analysis (n = 3).

(C and D) T7E1 assays performed with *Eed* (C) or *Suz12* (D) amplicons derived from *Rosa26*- (R26), *Eed*-, or *Suz12*-disrupted colonies, with (+) or without (−) the nuclease (n = 4). Arrowheads indicate the bands with expected size based on the Cas9 cleavage site, whereas asterisks indicate nonspecific bands.

(E and F) Sequencing results of representative four clones each (of 12) after electroporating with Eed (E) or Suz12 (F) sgRNA. All colonies analyzed (Eed, 12/12; Suz12, 12/12) acquired indels. Red line represents the position of the protospacer adjacent motif (PAM) sequence. All data represent mean ± SD (***p < 0.001 by Student's t test). See also Figure S2.

Efficient Gene Disruption in Human HSPCs

Encouraged by the results obtained in mice, we assessed the feasibility and efficiency of our protocol in human hematopoietic cells. We first sought to target human CD45 (hCD45) in HL-60 cells, a human acute myeloid leukemia (AML) cell line. We electroporated HL-60 cells with Cas9/hCD45-sg RNPs testing three different CD45 guides. Strikingly, all three guides displayed very high efficiencies of disrupting CD45 expression (sg1, 98%; sg2, 91%; and sg3, 74%), as assessed by flow cytometry (Figure S3A). Two additional AML cell lines, OCI-AML2 and Kasumi, exhibited similar editing efficiencies (Figure 3A).

We also tested whether our protocol was capable of editing peripheral blood mononuclear cell (PBMC)-derived primary T lymphocytes. While resting T cells were resistant to CD45 editing (data not shown), activated T cells targeted with hCD45-sg1 exhibited efficient (86% ± 2%; n = 3) loss of CD45 (Figure 3A), with some residual CD45bright and CD45mid cells (Figure S3B). We performed high-throughput sequencing of unfractionated T cells as well as cells sorted based on CD45 expression (CD45bright, CD45mid, CD45dim, and CD45neg cells), and we discovered that, while the unfractionated cells had an indel frequency of 83%, more than 95% of alleles in CD45neg and CD45dim cells and 40% of alleles in CD45mid cells had acquired indels (Figure S3B). Interestingly, CD45dim cells harbored 51% in-frame and 49% out-of-frame indels (Figure S3C), which may explain the residual CD45 expression (Figure S3C). Importantly, low indel frequencies (0.2%, 1.7%, and 0.4%; read depth: 924, 301, and 527) were observed at the top three predicted off-target (OT) sites (Figure 4B; Supplemental Experimental Procedures).

We then tested whether primary human CD34+ HSPCs could be gene edited. To search for the optimal conditions, we first electroporated primary CD34+ cells derived from umbilical

cord blood with Cas9/hCD45-sg1 RNP using nine different electroporation parameters, and we performed flow cytometry 96 hr later to measure CD45 expression levels together with cell viability (Figure S3D). The optimized electroporation parameter (condition 9) was used for all further experiments. Since short-term ex vivo expansion is routinely exploited to increase transfection and transduction efficiency, we explored the impact of short cytokine exposure on transfection and gene disruption efficiency. We electroporated CD34+ cells from single donors (n = 5) with mRNA encoding for GFP-fused Nucleophosmin 1 (GFP-NPM1) immediately after isolation, or after 24 or 48 hr of cytokine exposure, and we analyzed GFP expression 24 hr later. While fresh cells showed only 28% ± 13% GFP positivity, cells cultured for either 24 or 48 hr displayed transfection efficiencies higher than 75% (24 hr, 81% ± 12%; 48 hr, 78% ± 10%) (Figure S3E).

To assess whether CRISPR-mediated gene disruption efficiency was influenced by exposure to cytokines, we performed a similar experiment electroporating CD34+ from single donors (n = 8) with Cas9/hCD45-sg1 RNP again at 0, 24, and 48 hr of culture, and we analyzed CD45 expression 4 days later. As expected, freshly isolated CD34+ cells not exposed to cytokines exhibited limited loss of CD45 cell surface expression (8% ± 4%). However, gene disruption efficiency was significantly higher in cells cultured for 48 hr compared to 24 hr (73% ± 16% versus 41% ± 12%, p = 0.003) (Figure 3B), implying that the efficiency of gene disruption is dependent upon more than transfection efficiency. Importantly, CD34 expression remained unchanged even following efficient CD45 knockout (Figure 3C).

We also determined the impact of CRISPR-Cas9 delivery on human HSPC viability. CD34+ cells from single donors were electroporated with Cas9 only or Cas9/hCD45-sg1 RNP or left
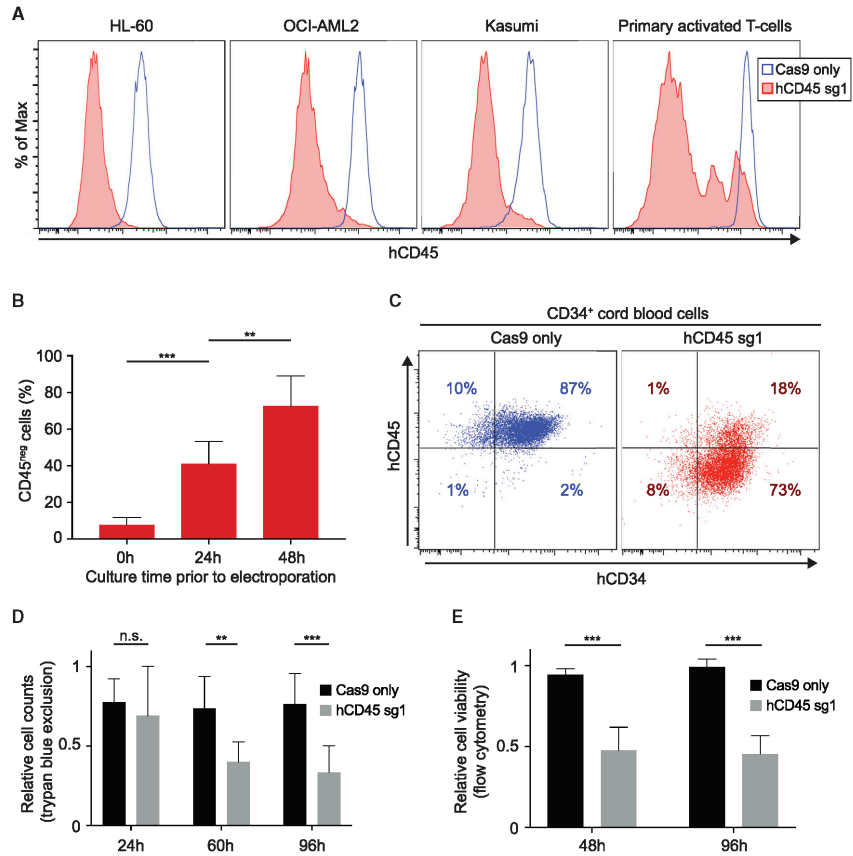
Figure 3. Efficient CD45 Knockout in Human Hematopoietic Cells

(A) Flow cytometry analysis of hCD45 expression in three AML cell lines and activated primary T cells 96 hr following electroporation with Cas9 only (blue) or Cas9/hCD45-sg1 RNP (red) is shown.

(B) Effects of pre-culture before electroporation on gene disruption efficiency. hCD45 loss was examined in CD34+ cells cultured for 0, 24, and 48 hr in the presence of cytokines before electroporation with Cas9/hCD45-sg1 RNP. hCD45 expression was evaluated 4 days after electroporation. Each experiment (n = 8) was performed on CD34+ cells isolated from single donors.

(C) Flow cytometry analysis of CD45 and CD34 expression in CD34+ cells 96 hr following electroporation with Cas9 only (left) or Cas9/hCD45-sg1 RNP (right) is shown.

(D and E) Cell viability examined by trypan blue staining (D, n = 8) or flow cytometry (E, n = 6) of CD34+ cells electroporated either with Cas9 only (black) or with Cas9/hCD45-sg1 RNP (gray) relative to non-electroporated cells at the indicated time points. The cell counts (D) or viability (E) of Cas9 only- and Cas9/hCD45-sg1-transfected cells was compared to the viable cell counts of non-electroporated cells.

All data represent mean ± SD; *p < 0.05, **p < 0.01, and ***p < 0.001 by non-parametric tests.

untreated in culture, and viable cell counts were recorded by trypan blue staining at 24, 60, and 96 hr after electroporation. Non-electroporated cells expanded in vitro, reaching 2.1×10^5 cells, 5×10^5 cells, and 1.1×10^6 cells at 24, 60, and 96 hr of culture, respectively, starting with 10^5 cells. Electroporated cells exhibited significant but acceptable cell loss in Cas9/hCD45-sg1 RNP-treated cells compared to non-electroporated cells (24 hr, 69% ± 31%; 60 hr, 40% ± 13%; 96 hr, 34% ± 17%; n = 8) (Figure 3D). Cell viability assessed by flow cytometry at 48 and 96 hr corroborated these results (48 hr, 48% ± 18%; 96 hr, 45% ± 11%; n = 6) (Figure 3E). These results are consistent with those reported by others using electroporation of
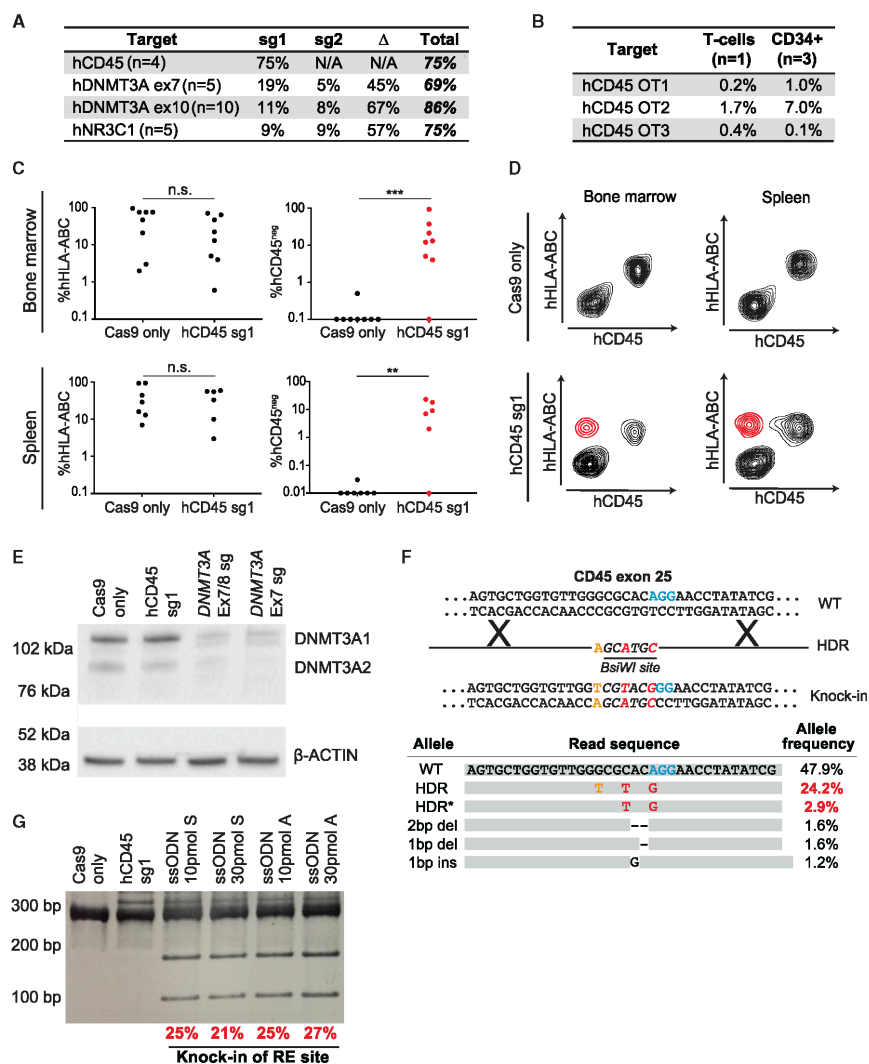
Figure 4. CRISPR-Cas9-Mediated Gene Disruption and HDR in Human HSPCs

(A) Indel frequencies at targeted loci. When multiple sgRNAs were used in the same experiment, sg1 indicates alleles with disruption of sg1 only, sg2 indicates alleles with disruption of sg2 only, and a triangle indicates alleles with a deletion between sg1 and sg2. Raw allele counts for each indel/deletion are found in Table S2.

(B) Indel frequencies at three predicted hCD45-sg1 OT sites. OT sites (OT1–3) were predicted using CRISPRscan (Moreno-Mateos et al., 2015).

(C) Plots showing percentages of human cells (left) in the bone marrow and the spleen of 16 NSG recipient mice (eight Cas9 only and eight Cas9/hCD45-sg1 RNP) and the fraction of engrafted human cells that have lost hCD45 (right) in Cas9 only (black) and Cas9/hCD45-sg1 RNP (red). Human CD34+ cells from individual cord blood donors were electroporated with Cas9 only and Cas9/hCD45-sg1 RNP, and they were transplanted into sublethally irradiated NSG mice. Engraftment was analyzed 8 weeks post-transplant.

(legend continued on next page)

site-directed nucleases (De Ravin et al., 2016; Genovese et al., 2014).

CD45 knockout efficiency measured by flow cytometry (73% ± 16%) was confirmed by high-throughput sequencing of the hCD45 locus (75% ± 10%) (Figure 4A; Table S2). As in T cells, CD34$^+$ cells electroporated with Cas9/hCD45-sg1 (n = 3) displayed minimal OT cleavage (1.0%, 7.0%, and 0.1%; average read depth: 5,319, 5,164, and 5,089 at OT1, OT2, and OT3, respectively) (Figure 4B). To verify that the edited CD34$^+$ HSPCs maintained engraftment and multilineage differentiation capacity, we transplanted Cas9-only (n = 8) and Cas9/hCD45-sg1 RNP-edited cells (n = 8) into sub-lethally irradiated NOD scid gamma (NSG) mice. To avoid possible donor-dependent bias, each experimental pair (i.e., one Cas9-only replicate and one Cas9/hCD45-sg1 RNP-treated replicate) was performed on cells derived from a single cord blood. Bone marrow of 16/16 recipients and spleens of 13/16 recipients were successfully engrafted with human cells (Figure 4C). Importantly, we observed significant levels of engraftment by hCD45^{neg} cells in the bone marrow of 7/8 mice and in the spleen of 5/8 mice transplanted with Cas9/hCD45-sg1 RNP-edited cells (Figures 4C, 4D, and S4A). Sequencing of the amplified human CD45 locus from bone marrow cells confirmed the presence of indels with frequencies consistent with flow cytometry data (Figure S4B). As expected for this time point (Goyama et al., 2015; McDermott et al., 2010), engrafted human HSPCs gave rise mainly to B and myeloid cells in the bone marrow in both Cas9 only- and Cas9/hCD45-sg1 RNP-engrafted mice, with no differences between these two groups (Figure S4C). The Cas9/hCD45-sg1 RNP-edited samples displayed no significant difference in CD45 gene disruption between B and myeloid cells (Figure S4D).

We also analyzed human CD34$^+$ HSPCs in one bone marrow sample in which 37% of engrafted human cells were CD45 negative. CD45 loss was evident in 40% of CD34$^+$ cells (Figure S4E) and 36% of the CD34$^+$CD38$^-$ population, which contained the most immature progenitor cells. These results establish that our method allows for efficient gene disruption of human CD34$^+$ HSPCs while retaining multilineage reconstitution capacity and the ability of these cells to engraft and expand in recipient mice. Given the known limitations of NSG mice to support robust generation of cells from all human hematopoietic lineages, such as T cells and erythroid cells, further assessment in additional models and longer time points will reveal whether the most long-term HSCs are successfully modified and viable after these treatments.

Multiple Guide Approach Allows for Rapid Deletion of Genes of Interest

To ensure functional ablation of a target gene and to facilitate rapid assessment of gene editing by PCR, larger deletions are often desirable. Thus, we synthesized guide RNA pairs targeting exons 7–14 of *DNMT3A*. We tested combinations of up to four guides per electroporation in HL-60 cells, assessing the frequency and spectra of deletions after 12 hr and the level of DNMT3A protein after 96 hr. All tested combinations of guides demonstrated efficient deletions and significantly diminished DNMT3A protein (Figure S4G).

We then targeted *DNMT3A* in primary CD34$^+$ cord blood cells. Guides targeting exons 7 and 8 were tested and the expected deletions were observed by PCR (Figure S4F). Importantly, the DNMT3A protein was nearly absent 96 hr after disruption of exon 7 or exons 7+8 (Figure 4E). To verify this result, *DNMT3A* exon 7 was targeted in CD34$^+$ cells enriched from an additional five cord blood samples, and high-throughput sequencing confirmed a gene disruption frequency of 69% ± 4% (Figure 4A; Table S2), suggesting that most cells likely experience loss of at least one allele, whereas many cells lose both alleles. To further validate the flexibility and efficiency of our approach, we targeted exon 10 of *DNMT3A* (n = 10) and exon 3 of *NR3C1* (n = 5) in CD34$^+$ cells, and high-throughput sequencing showed allelic disruption frequencies of 86% ± 14% and 75% ± 6%, respectively (Figures 4A and S4H; Table S2).

Efficient HDR-Mediated Gene Editing in Human HSPCs

Finally, we considered whether these editing strategies could be used to introduce specific point mutations into primary human HSPCs using Cas9-mediated homology-directed repair (HDR). HDR would enable specific lesions to be introduced in HSPCs, potentially correcting deleterious mutations or mimicking cancer-associated mutations. Single-stranded oligonucleotide HDR templates (ssODNs) were designed with symmetric or asymmetric homology arms (Richardson et al., 2016) to introduce three base pair changes, two of which resulted in the generation of a BsiWI site near the hCD45-sg1 spacer sequence (Figure 4F). After 48 hr of culture with cytokines, CD34$^+$ HSPCs were electroporated with the Cas9/hCD45-sg1 RNP along with either 10 or 30 pmol ssODNs. The addition of 10 or 30 pmol ssODNs did not significantly affect the viability (Figures S3F and S3G), although a trend toward lower viability after electroporation with a higher dose of ssODN was observed. Following BsiWI digestion of genomic DNA 24 hr after transfection, all samples with a donor template displayed a digested band, indicating

---

(D) Flow cytometry analysis of two engrafted NSG mice. Top panels show the engraftment of normal human cells (CD45^{pos}HLA-ABC^{pos}). Bottom panels show the presence of hCD45 knockout cells (highlighted in red) both in the bone marrow and the spleen.

(E) Western blot analysis of DNMT3A expression in CD34$^+$ cord blood cells 96 hr after electroporation with Cas9 only, Cas9/hCD45-sg1 RNP, Cas9/*DNMT3A* exon 7/8-sg (four sgRNAs) RNP, or Cas9/*DNMT3A* exon 7-sg (two sgRNAs) RNP is shown.

(F) Schematic representation of the CRISPR-mediated knockin (top). Three single-nucleotide changes, two of which (red) resulted in the formation of a BsiWI restriction site (italics), were introduced into hCD45 exon 25. The most commonly observed alleles from a representative sample (bottom), which included both precise (HDR; all three single-nucleotide changes) and imprecise (HDR*; two of three nucleotide changes) knockin events, were assessed by high-throughput sequencing, and their allele frequencies are displayed. The numbers in red represent frequencies of reads containing the BsiWI restriction site.

(G) A gel image of BsiWI-digested PCR amplicon prepared from CD34$^+$ cord blood cells targeted with Cas9/hCD45-sg1 (1 μg each) RNP and different single-stranded DNA oligonucleotides (ssODN) containing BsiWI sites. Both symmetric (S) and asymmetric (A) homology arms were tested. BsiWI digests the 282-bp amplicon with HDR editing into 172-bp and 110-bp fragments. The numbers below the gel represent efficiency of restriction site knockin (HDR+HDR*) as determined by high-throughput sequencing.

successful HDR (Figure 4G). High-throughput sequencing performed on these samples revealed efficient precise knockin (22%; range: 19%–25%) of the mutant allele (Figure 4F; Table S2). Additionally, many reads (1%–2%) displayed imprecise or partial knockin of the mutant allele (one of three or two of three bases) (Figure 4F; Table S2). Samples electroporated with only the donor template displayed no detectable mutant allele by high-throughput sequencing (data not shown). Thus, our method allows homology-directed gene editing at a substantial frequency in human HSPCs. Additional testing in multiple mouse and other animal models will be required to establish whether the most long-term HSCs are successfully edited.

DISCUSSION

The strategies we describe herein enable efficient gene editing, particularly loss-of-function studies, in both murine and human HSPCs directly. With the RNP-based methods, it is possible to generate gene-edited HSPCs within a week starting with conception of the study, including downtime for oligonucleotide synthesis. This is substantially shorter than editing HSPCs using lentiviral transduction, which requires cloning sgRNAs into lentiviral vectors, generation and quality control of lentiviral particles, and results in variable HSPC transduction efficiencies and risks of lentiviral integration in undesirable sites. Furthermore, electroporation of RNPs is a transient hit-and-run approach that obviates the need for a special mouse strain expressing Cas9, and it reduces concerns of constitutive Cas9 expression and OT cleavage. The costs of generating gene-edited HSPCs with these methods are substantially lower than those with lentiviral methods. Although commercially available Cas9 protein makes gene ablation with RNPs feasible, we also envision this strategy could be used for other Cas9 derivatives where transient effects may be desirable, such as CRISPR interference (Konermann et al., 2015; Qi et al., 2013).

One limitation of our protocol is that it lacks the ability to mark the cells that were successfully electroporated, unlike lentiviral transduction methods in which transduced cells can be marked by fluorescent proteins or by antibiotic resistance. However, with a gene-editing efficiency approaching 90% as we show for some targets, our method makes it possible to examine the molecular or phenotypic changes without selection for transfected cells. We have shown that deletion of *DNMT3A* from primary human CD34+ cells leads to a precipitous reduction in DNMT3A protein levels in the population within 96 hr after electroporation.

We have observed that gene-editing efficiency is slightly more efficient in human than murine HSPCs. It is possible that this difference reflects developmental states, since the human cells are derived from cord blood rather than bone marrow. Additional optimization using murine HSPCs from the fetal liver or after mobilization may further increase the gene-editing efficiency.

Perhaps the most significant finding we observed was efficient HDR in human HSPCs. The ability to introduce specific mutations in HSPCs will enable the expanded study of cancer-driver mutations in AML and other hematologic diseases. More importantly, the repair of inherited mutations in both common and rare blood disorders using CRISPR may now be feasible without integration of viral vectors or delivery of plasmid DNA, represent-

ing a major stepping-stone toward therapeutic gene editing. We have not yet achieved detectable HDR frequencies in mouse HSPCs, and it is possible that a longer culture time prior to electroporation is necessary to activate this repair process in murine cells.

These remarkable knockout and HDR efficiencies in human HSPCs may suggest the possibility of broad and immediate utility. However, most ex vivo manipulations ultimately have been shown to impact function of the most long-term HSCs (Genovese et al., 2014; Hoban et al., 2015), and all of the available assays have limitations in their ability to assess bona fide HSC function. Therefore, caution in application of these strategies is still warranted.

In conclusion, we describe a fast, efficient, and cost-effective method to edit the genomes of both murine and human HSPCs based on the CRISPR/Cas9 system. The ability to quickly and efficiently edit primary HSPCs makes it possible to test the function of genetic variants identified in association with hematologic diseases, such as leukemia or bone marrow failure. Moreover, the high efficiency offers the possibility to perform large-scale combinatorial gene editing in HSPCs to model complex mutational landscapes.

EXPERIMENTAL PROCEDURES

Production of sgRNA and Electroporation
Protospacer sequences for each target gene were identified using the CRISPRscan algorithm (http://www.crisprscan.org) (Moreno-Mateos et al., 2015). DNA templates for sgRNAs were made using the protocol described by Li et al. (2013) using primers listed in Table S1. The sgRNA (1 μg) was electroporated into 1×10^5 Cas9-expressing c-kit+ murine HSPCs after 1–3 hr of culture. The optimized electroporation condition for murine HSPCs was 1,700 V, 20 ms, and one pulse, using a Neon transfection system (Thermo Fisher Scientific). To electroporate Cas9-sgRNA RNPs, 200 ng to 1 μg sgRNA was incubated with 1 μg Cas9 protein (PNA Bio) for 10–15 min at room temperature and electroporated as above. Human CD34+ cells were isolated by AutoMACS (Miltenyi Biotec) using CD34 microbeads, and they were electroporated as described for murine cells except the optimized electroporation condition was 1,600 V, 10 ms, and three pulses. See the Supplemental Experimental Procedures for details.

Statistical Analysis
For comparisons involving two groups, unpaired Student's t tests (two-tailed) or non-parametric tests were used. See the figure legends for details.

ACCESSION NUMBERS

The accession number for the data reported in this paper is NCBI Sequence Read Archive: PRJNA339433.

SUPPLEMENTAL INFORMATION

Supplemental Information includes Supplemental Experimental Procedures, four figures, and two tables and can be found with this article online at http://dx.doi.org/10.1016/j.celrep.2016.09.092.

AUTHOR CONTRIBUTIONS

OPEN
ACCESS
CellPress

REFERENCES

Brinkman, E.K., Chen, T., Amendola, M., and van Steensel, B. (2014). Easy quantitative assessment of genome editing by sequence trace decomposition. Nucleic Acids Res. 42, e168.

Chen, B., Gilbert, L.A., Cimini, B.A., Schnitzbauer, J., Zhang, W., Li, G.W., Park, J., Blackburn, E.H., Weissman, J.S., Qi, L.S., and Huang, B. (2013). Dynamic imaging of genomic loci in living human cells by an optimized CRISPR/Cas system. Cell 155, 1479–1491.

De Ravin, S.S., Reik, A., Liu, P.Q., Li, L., Wu, X., Su, L., Raley, C., Theobald, N., Choi, U., Song, A.H., et al. (2016). Targeted gene addition in human CD34(+) hematopoietic cells for correction of X-linked chronic granulomatous disease. Nat. Biotechnol. 34, 424–429.

Deneault, E., Cellot, S., Faubert, A., Laverdure, J.P., Fréchette, M., Chagraoui, J., Mayotte, N., Sauvageau, M., Ting, S.B., and Sauvageau, G. (2009). A functional screen to identify novel effectors of hematopoietic stem cell activity. Cell 137, 369–379.

Genovese, P., Schiroli, G., Escobar, G., Di Tomaso, T., Firrito, C., Calabria, A., Moi, D., Mazzieri, R., Bonini, C., Holmes, M.C., et al. (2014). Targeted genome editing in human repopulating haematopoietic stem cells. Nature 510, 235–240.

Goyama, S., Wunderlich, M., and Mulloy, J.C. (2015). Xenograft models for normal and malignant stem cells. Blood 125, 2630–2640.

Hacein-Bey-Abina, S., Von Kalle, C., Schmidt, M., McCormack, M.P., Wulffraat, N., Leboulch, P., Lim, A., Osborne, C.S., Pawliuk, R., Morillon, E., et al. (2003). LMO2-associated clonal T cell proliferation in two patients after gene therapy for SCID-X1. Science 302, 415–419.

Heckl, D., Kowalczyk, M.S., Yudovich, D., Belizaire, R., Puram, R.V., McConkey, M.E., Thielke, A., Aster, J.C., Regev, A., and Ebert, B.L. (2014). Generation of mouse models of myeloid malignancy with combinatorial genetic lesions using CRISPR-Cas9 genome editing. Nat. Biotechnol. 32, 941–946.

Hendel, A., Bak, R.O., Clark, J.T., Kennedy, A.B., Ryan, D.E., Roy, S., Steinfeld, I., Lunstad, B.D., Kaiser, R.J., Wilkens, A.B., et al. (2015). Chemically modified guide RNAs enhance CRISPR-Cas genome editing in human primary cells. Nat. Biotechnol. 33, 985–989.

Hoban, M.D., Cost, G.J., Mendel, M.C., Romero, Z., Kaufman, M.L., Joglekar, A.V., Ho, M., Lumaquin, D., Gray, D., Lill, G.R., et al. (2015). Correction of the sickle cell disease mutation in human hematopoietic stem/progenitor cells. Blood 125, 2597–2604.

Hope, K.J., Cellot, S., Ting, S.B., MacRae, T., Mayotte, N., Iscove, N.N., and Sauvageau, G. (2010). An RNAi screen identifies Msi2 and Prox1 as having opposite roles in the regulation of hematopoietic stem cell activity. Cell Stem Cell 7, 101–113.

Hsu, P.D., Lander, E.S., and Zhang, F. (2014). Development and applications of CRISPR-Cas9 for genome engineering. Cell 157, 1262–1278.

Jinek, M., Chylinski, K., Fonfara, I., Hauer, M., Doudna, J.A., and Charpentier, E. (2012). A programmable dual-RNA-guided DNA endonuclease in adaptive bacterial immunity. Science 337, 816–821.

Kim, S., Kim, D., Cho, S.W., Kim, J., and Kim, J.S. (2014). Highly efficient RNA-guided genome editing in human cells via delivery of purified Cas9 ribonucleoproteins. Genome Res. 24, 1012–1019.

Konermann, S., Brigham, M.D., Trevino, A.E., Joung, J., Abudayyeh, O.O., Barcena, C., Hsu, P.D., Habib, N., Gootenberg, J.S., Nishimasu, H., et al. (2015). Genome-scale transcriptional activation by an engineered CRISPR-Cas9 complex. Nature 517, 583–588.

Lee, S.C., Miller, S., Hyland, C., Kauppi, M., Lebois, M., Di Rago, L., Metcalf, D., Kinkel, S.A., Josefsson, E.C., Blewitt, M.E., et al. (2015). Polycomb repressive complex 2 component Suz12 is required for hematopoietic stem cell function and lymphopoiesis. Blood 126, 167–175.

Li, D., Qiu, Z., Shao, Y., Chen, Y., Guan, Y., Liu, M., Li, Y., Gao, N., Wang, L., Lu, X., et al. (2013). Heritable gene targeting in the mouse and rat using a CRISPR-Cas system. Nat. Biotechnol. 31, 681–683.

Lin, S., Staahl, B.T., Alla, R.K., and Doudna, J.A. (2014). Enhanced homology-directed human genome engineering by controlled timing of CRISPR/Cas9 delivery. eLife 3, e04766.

Mandal, P.K., Ferreira, L.M., Collins, R., Meissner, T.B., Boutwell, C.L., Friesen, M., Vrbanac, V., Garrison, B.S., Stortchevoi, A., Bryder, D., et al. (2014). Efficient ablation of genes in human hematopoietic stem and effector cells using CRISPR/Cas9. Cell Stem Cell 15, 643–652.

McDermott, S.P., Eppert, K., Lechman, E.R., Doedens, M., and Dick, J.E. (2010). Comparison of human cord blood engraftment between immunocompromised mouse strains. Blood 116, 193–200.

Moreno-Mateos, M.A., Vejnar, C.E., Beaudoin, J.D., Fernandez, J.P., Mis, E.K., Khokha, M.K., and Giraldez, A.J. (2015). CRISPRscan: designing highly efficient sgRNAs for CRISPR-Cas9 targeting in vivo. Nat. Methods 12, 982–988.

Platt, R.J., Chen, S., Zhou, Y., Yim, M.J., Swiech, L., Kempton, H.R., Dahlman, J.E., Parnas, O., Eisenhaure, T.M., Jovanovic, M., et al. (2014). CRISPR-Cas9 knockin mice for genome editing and cancer modeling. Cell 159, 440–455.

Qi, L.S., Larson, M.H., Gilbert, L.A., Doudna, J.A., Weissman, J.S., Arkin, A.P., and Lim, W.A. (2013). Repurposing CRISPR as an RNA-guided platform for sequence-specific control of gene expression. Cell 152, 1173–1183.

Richardson, C.D., Ray, G.J., DeWitt, M.A., Curie, G.L., and Corn, J.E. (2016). Enhancing homology-directed genome editing by catalytically active and inactive CRISPR-Cas9 using asymmetric donor DNA. Nat. Biotechnol. 34, 339–344.

Rivière, I., Dunbar, C.E., and Sadelain, M. (2012). Hematopoietic stem cell engineering at a crossroads. Blood 119, 1107–1116.

Rossi, L., Lin, K.K., Boles, N.C., Yang, L., King, K.Y., Jeong, M., Mayle, A., and Goodell, M.A. (2012). Less is more: unveiling the functional core of hematopoietic stem cells through knockout mice. Cell Stem Cell 11, 302–317.

Schaefer, B.C., Schaefer, M.L., Kappler, J.W., Marrack, P., and Kedl, R.M. (2001). Observation of antigen-dependent CD8+ T-cell/ dendritic cell interactions in vivo. Cell. Immunol. 214, 110–122.

Schumann, K., Lin, S., Boyer, E., Simeonov, D.R., Subramaniam, M., Gate, R.E., Haliburton, G.E., Ye, C.J., Bluestone, J.A., Doudna, J.A., and Marson, A. (2015). Generation of knock-in primary human T cells using Cas9 ribonucleoproteins. Proc. Natl. Acad. Sci. USA 112, 10437–10442.

Shih, A.H., Abdel-Wahab, O., Patel, J.P., and Levine, R.L. (2012). The role of mutations in epigenetic regulators in myeloid malignancies. Nat. Rev. Cancer 12, 599–612.

Sternberg, S.H., and Doudna, J.A. (2015). Expanding the biologist's toolkit with CRISPR-Cas9. Mol. Cell 58, 568–574.

Xie, H., Xu, J., Hsu, J.H., Nguyen, M., Fujiwara, Y., Peng, C., and Orkin, S.H. (2014). Polycomb repressive complex 2 regulates normal hematopoietic stem cell function in a developmental-stage-specific manner. Cell Stem Cell 14, 68–80.

Supplemental Information

Highly Efficient Genome Editing

of Murine and Human Hematopoietic

Progenitor Cells by CRISPR/Cas9

Michael C. Gundry, Lorenzo Brunetti, Angelique Lin, Allison E. Mayle, Ayumi Kitano, Dimitrios Wagner, Joanne I. Hsu, Kevin A. Hoegenauer, Cliona M. Rooney, Margaret A. Goodell, and Daisuke Nakada

Supplemental Figures

A

GFP negative cells (%)

control
1200V/30ms/2p
1300V/20ms/2p
1400V/30ms/1p
1550V/10ms/3p
1650V/10ms/3p
1700V/20ms/1p
2000V/20ms/1p

B

Survival (%)

24 48 | control
24 48 | 1200V/30ms/2p
24 48 | 1300V/20ms/2p
24 48 | 1400V/30ms/1p
24 48 | 1550V/10ms/3p
24 48 | 1650V/10ms/3p
24 48 | 1700V/20ms/1p
24 48 | 2000V/20ms/1p

C

control
GFP sg1
GFP sg1(i)

GFP cells (%)

Fresh   1 hr

D

Fresh
Cultured
Cultured, then electroporated

c-kit

E

Colony formation (%)

culture only
mock electroporation
R26 sg
GFP sg1
Cas9 protein
Cas9 + R26 sg
Cas9 + GFP sg1

F

Survival (%)

0hr   24hr   48hr   72hr   96hr

G

Counts

0.7±0.5%   R26 sg
71.7±5%   GFP sg1
52.5±9%   GFP sg2
48±9%   GFP sg3

GFP

H

PAM

WT GTGAGCAAGGGCGAGGAGCTGTTCACCGGGGTGGTGCCCATCCTGGTCGA

% indel

GTGAGCAAGGGCGAGGAGCTGTTCAACCGGGGTGGTGCCCATCCTGGTCGA
GTGAGCAAGGGCGAGGAGCTGTT--CCGGGGTGGTGCCCATCCTGGTCGA
#1 GTGAGCAAGGGCGAGGAGCTGT---CCGGGGTGGTGCCCATCCTGGTCGA   62%
GTGAGCAAGGGCGAGGAGCTG---ACCGGGGTGGTGCCCATCCTGGTCGA
GTGAGCAAGGGCGAGGAGC-------CCGGGGTGGTGCCCATCCTGGTCGA

GTGAGCAAGGGCGAGGAGCTGTTCAACCGGGGTGGTGCCCATCCTGGTCGA
GTGAGCAAGGGCGAGGAGCTGT--ACCGGGGTGGTGCCCATCCTGGTCGA
#2 GTGAGCAAGGGCGAGGAGCTGTTCA-----GGTGGTGCCCATCCTGGTCGA   61%
GTGAGCAAGGGCGAGGAGC-----ACCGGGGTGGTGCCCATCCTGGTCGA
GTGAGCAAGGGCGAGGAGCTG---ACCGGGGTGGTGCCCATCCTGGTCGA

GTGAGCAAGGGCGAGGAGCTGTTCAACCGGGGTGGTGCCCATCCTGGTCGA
GTGAGCAAGGGCGAGGAGCTGTTCA—GGGGTGGTGCCCATCCTGGTCGA
#3 GTGAGCAAGGGCGAGGAGC-----ACCGGGGTGGTGCCCATCCTGGTCGA   65%
GTGAGCAAGGGCGAGGAGCTG---ACCGGGGTGGTGCCCATCCTGGTCGA
GTGAGCAAGGGCGAGGAGCTGTTC---GGGGTGGTGCCCATCCTGGTCGA

Supplemental Materials   1

Figure S1. Gene editing in murine HSPCs (related to Figure 1). (**A-B**) Optimization of electroporation conditions. 10^5 c-kit$^+$ cells

from Cas9-expressing mice were electroporated with 1 μg of GFP-sg1 using the parameters as indicated. Cells were analyzed for GFP

expression at 24 hours after electroporation (**A**) and survival by trypan blue staining at 24 and 48 hours after electroporation (**B**). One

pulse at 1700 V, 20 ms had the highest GFP-ablation efficiency with minimum loss of viability (see also Figure 1B), and this

condition was used throughout for murine experiments. Comparisons in (**B**) were done with the control at each time points. (**C**) 10^5

c-kit$^+$ cells from Cas9-expressing mice, either freshly isolated or after 1 hour pre-culture, were electroporated with 1 μg of GFP-sg1

with the standard scaffold (GFP-sg) or with the improved scaffold described previously (GFP-sg(i), (Chen et al., 2013)). We did not

observe significant increase in GFP ablation efficiency by incorporating the improved scaffold. (**D**) Bone marrow cells enriched for

c-kit$^+$ cells were either analyzed freshly, or after 1 hour of pre-culture without electroporation, or after 1 hour of pre-culture with

electroporation. 1 hour of pre-culture significantly attenuated c-kit expression. (**E**) We pre-cultured c-kit$^+$ HSPCs for 1 hour and then

performed either mock electroporation without sgRNA, electroporated with R26-sg or GFP-sg, or electroporated with Cas9-sgRNA

RNP as indicated. Cell were then stained for HSCs and clonally sorted into semi-solid media. HSC pre-cultured and sorted without

electroporation had somewhat lower cloning efficiency, but the clonality was not affected by electroporation of sgRNA with or

without Cas9 protein. (**F**) Cell survival determined by trypan blue staining at the indicated time points. GFP-expressing HSPCs were

either pre-cultured only or electroporated with the sgRNA, Cas9 protein, or Cas9-sgRNA RNP, as indicated in the legend in (**E**). (**G**)

Three different sgRNA targeting GFP were electroporated into c-kit$^+$ cells with Cas9 protein. GFP expression was efficiently ablated

GFP expression by GFP-sg1, making 71.7±0.5% of cells GFP$^-$, while GFP-sg2 and GFP-sg3 had slightly lower efficiencies. (**H**)

High-throughput sequencing of GFP after editing with Cas9-sgRNA RNP. Shown are top 5 GFP-edited sequences discovered by

sequencing of 3 samples, and the overall indel frequencies. All data represent mean ± standard deviation; *, $p<0.05$;   **, $p<0.01$; and

***, $p<0.001$ by Student's t-test.

Figure S2. Editing of murine Eed and Suz12 (related to Figure 2).
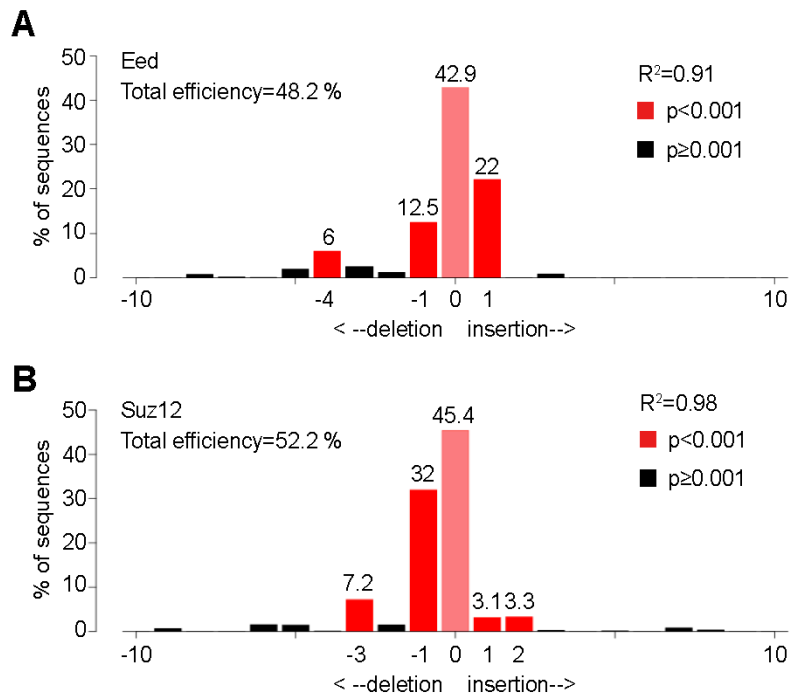
TIDE assay (Brinkman et al., 2014) was performed 48 hours after electroporation for Eed **(A)** and Suz12 **(B)** (n=3). PCR amplicons spanning the Cas9 cleavage site were subjected to Sanger sequencing and the resulting trace files were analyzed by TIDE. Approximately 50% of the cells at this early time point after electroporation exhibited small indels (n=3).

A

HL-60

sg1 98%

sg2 91%

sg3 74%

% of Max

hCD45

Ctrl
CD45 sgRNA

B

Primary activated T-cells

SSC

98% neg

98% dim

Indel frequency

40% mid

10% bright

hCD45

C A G T G C T G G T G T T G G G C G C A C A G G A A C C T A T A T C G

hCD45 sg1   PAM

C

hCD45neg

Read count

Indel length

Insertion
Deletion

hCD45dim

Read count

Indel length

Insertion
Deletion

D

Efficiency and viability (%)

Viability
CD45neg

Electroporation condition

1 2 3 4 5 6 7 8 9†

E

GFP positive (%)

Culture time prior to electroporation

0h   24h   48h

F

Relative cell count (trypan blue exclusion)

n.s.   n.s.   n.s.

24h   60h   96h

hCD45 sg1
hCD45 sg1+10pmol HDR
hCD45 sg1+30pmol HDR

G

Relative cell viability (flow cytometry)

n.s.   n.s.

48h   96h

hCD45 sg1
hCD45 sg1+10pmol HDR
hCD45 sg1+30pmol HDR

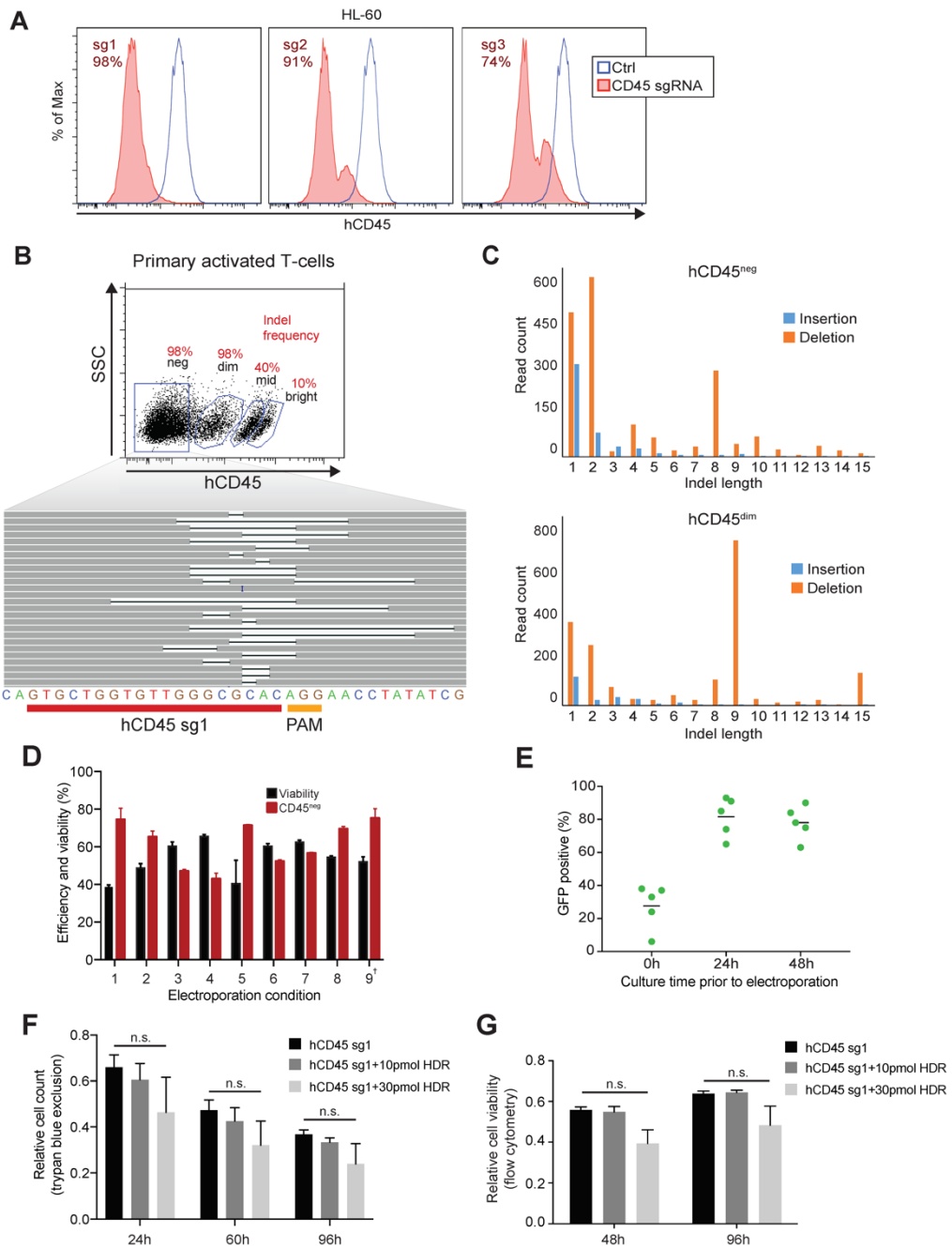Supplemental Materials   4

Figure S3. Gene editing in human hematopoietic cells (related to Figure 3).

(**A**) Flow cytometry analysis of hCD45 expression in the HL-60 cell line 96hrs following electroporation with Cas9 only (blue) or Cas9 and sgRNAs targeting different CD45 exons (red). (**B**) Dot-plot showing four distinct populations of T-lymphocytes based on hCD45 expression levels (above). Sequencing of the targeted CD45 locus in the sorted CD45^{neg} population displayed in an IGV diagram (below). Each horizontal grey bar represents a sequencing read (allele). Deletions are depicted by thin horizontal black lines and insertions are depicted by vertical lines. (**C**) Indel spectra within CD45^{neg} (top panel) and CD45^{dim} (bottom panel) sorted T-lymphocyte populations. (**D**) Optimization of electroporation parameters in human HSPCs: CD34^{+} cells were electroporated with Cas9/hCD45-sg1 RNP using different electroporation parameters. CD45 expression along with viability was measured 96 hours following electroporation. 9 different conditions were tested: 1) 1700V, 20ms, 1pulse; 2) 1400V, 30ms, 1pulse; 3) 1200V, 40ms, 1pulse; 4) 1200V, 20ms, 2pulses; 5) 1400V, 20ms, 2pulses; 6) 1150V, 30ms, 2pulses; 7) 1400V, 10ms, 3pulses; 8) 1500V, 10ms, 3pulses; 9) 1600V, 10ms, 3pulses. Condition 9 (highlighted with †) was used for all further experiments. (**E**) GFP positivity following electroporation of GFP-NPM1 construct in CD34^{+} cells. Cells were cultured for 0, 24 and 48 hours in presence of cytokines (SCF, FLT3L and TPO) and electroporated with GFP-NPM1 mRNA. GFP positivity was measured 24 hours post-electroporation. (**F**) Total viable cell counts examined by trypan blue staining (n=3) of CD34+ cells electroporated either with Cas9/hCD45-sg1 RNP (black), RNP + 10pmol ssODN (dark grey) or RNP + 30pmol ssODN (light grey), relative to non-electroporated cells (n=8). (**G**) Cell viability measured by flow cytometry (n=3) 48 and 96 hours following electroporation with either Cas9/hCD45-sg1 RNP (black), RNP + 10pmol ssODN (dark grey) or RNP + 30pmol ssODN (light grey). The percentages of viable cells (based on scatter plot and PI staining) of Cas9/hCD45-sg1 RNP and RNP + ssODN transfected cells were normalized to the percentage of viable cells of non-electroporated cells. The differences were not statistically significant based on a non-parametric test.

A

Cas9 only   hCD45 sg1

B

Sample	hCD45^{neg}	Indel %
Cas9 only 2.1	0%	<1%
hCD45 sg1 2.2	12%	14%
hCD45 sg1 2.3	13%	24%
hCD45 sg1 3.2	92%	87%
hCD45 sg1 3.4	37%	44%

C

D
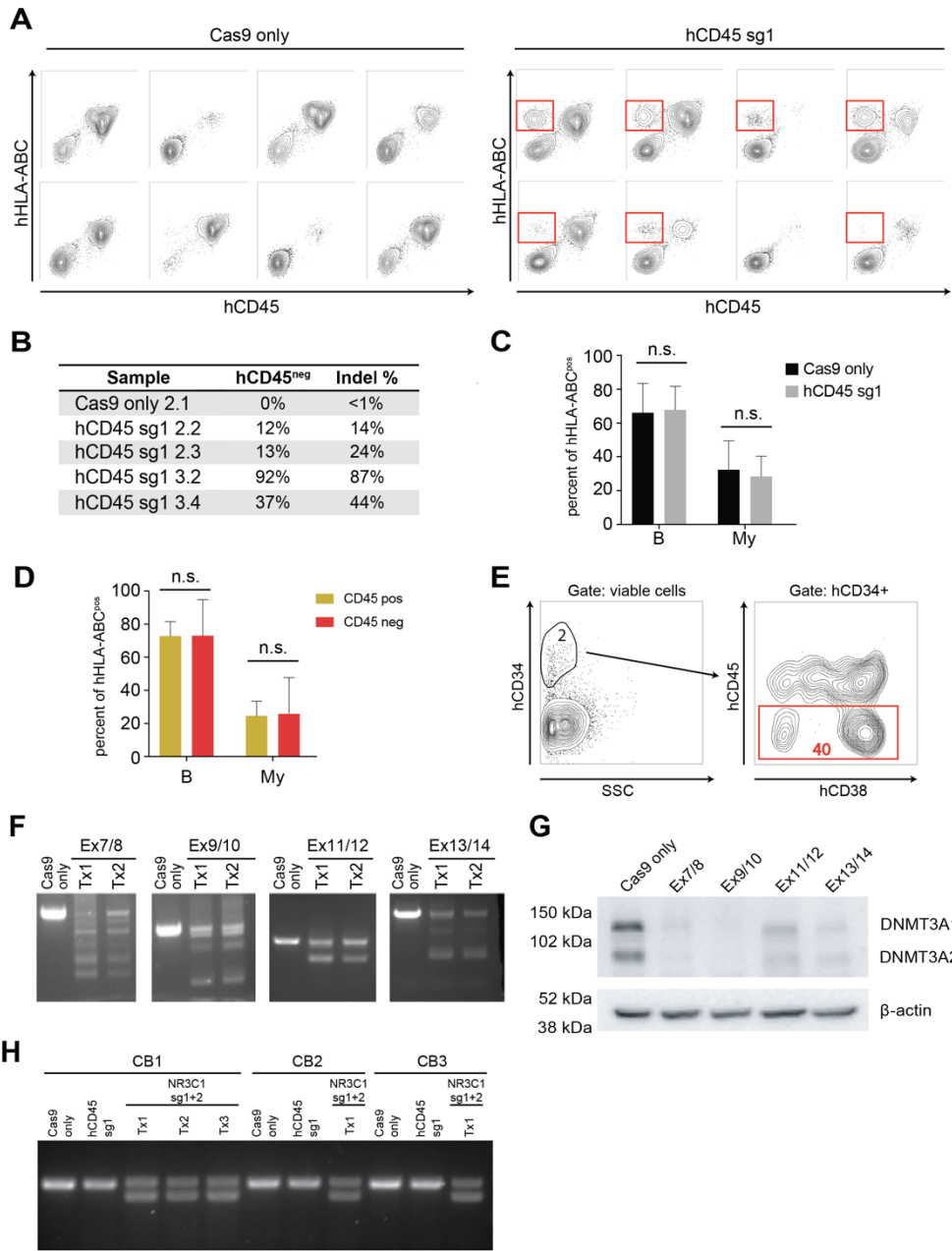

E

F

G

H

Figure S4. CRISPR-Cas9 toolbox applications in human primary CD34$^+$ cells (related to Figure 4).

(**A**) Flow cytometry analysis of bone marrows and spleens from NSG mice transplanted with either Cas9 only (left panels) or Cas9/hCD45-sg1 RNP (right panels) treated CD34$^+$ cells. hCD45 negative cells (gated in red) were detected only in mice transplanted with Cas9/hCD45-sg1 RNP electroporated human HSPCs. (**B**) Table showing the percentages of hCD45 negative cells paired with the indel frequencies detected at the targeted locus in engrafted human cells in one Cas9 only control (corresponding to the top left plot of Cas9 only controls on Fig S4A) and four Cas9/hCD45-sg1 RNP electroporated (corresponding to the top four plots of hCD45-sg1 samples on Fig S4A) xenografts. As expected, indel frequencies calculated by high-throughput sequencing are slightly higher than CD45^{neg} cells detected by flow cytometry because populations with two-fold differences in cell surface expression (WT vs heterozygous) are difficult to discriminate by flow cytometry and some of the indels may produce undetectable outcomes at protein level. (**C**) B-cell and myeloid percentages of human cells in Cas9 only (n=8) and in Cas9/hCD45-sg1 RNP (n=8) engrafted mice analyzed two months after transplantation. (**D**) B-cell and myeloid percentages of engrafted human CD45 positive and CD45 negative cells in five mice transplanted with Cas9/hCD45-sg1 CD34+ cells and analyzed two months after transplantation. No differences were detected in terms of lineage differentiation, comparing CD45 positive and CD45 negative human cells. (**E**) Flow cytometry analysis showing engrafted human CD34$^+$ cells in one representative NSG mouse bone marrow two months after transplantation (left panel). 40% of CD34$^+$ cells were hCD45 negative (right panel). hCD45 negative cells were detectable in both CD34$^+$CD38$^+$ and CD34$^+$CD38$^-$ populations. (**F**) Agarose gel electrophoresis images of amplified DNA from DNMT3A exons 7-14 in HL-60 cells treated with multiple guides targeting each exon. The multiple bands in each lane represent deletions between two guides. (**G**) Western blot analysis of DNMT3A expression in HL-60 cells 96hrs after electroporation with Cas9 only, Cas9/*DNMT3A* exon 7/8-sg (4 sgRNAs) RNP, Cas9/*DNMT3A* exon 9/10-sg (4 sgRNAs) RNP, Cas9/*DNMT3A* exon 11/12-sg (2 sgRNAs) RNP or Cas9/*DNMT3A* exon 13/14-sg (4 sgRNAs) RNP. (**H**) Agarose gel electrophoresis of amplified DNA from NRC31 exon 3 in human CD34$^+$ cells in Cas9 only controls, Cas9/hCD45-sg1 controls and Cas9/NR3C1 sg1 + sg2 replicates (Tx). CB1, CB2 and CB3 indicate cord blood cells from three different donors (biological replicates). Tx1, Tx2 and Tx3 indicate three technical replicates.

Table S1. Primer and oligo sequences (Related to Figures 1, 2, 3 and 4)

Oligo name	Sequence	Description
sgRNA common reverse primer (overlap PCR)	AAAAGCACCGACTCGGTGCCACTTTTTCAAGTTGATAACGGACTAGCCTTA TTTTAACTTGCTATTTCTAGCTCTAAAAC	sgRNA production
sgRNA common reverse primer (regular PCR)	AGCACCGACTCGGTGCCACT	sgRNA production
R26 sg	gaaattaatacgactcactataGGGGTCGGCCTCTGGCGGGGgttttagagctagaaatagc	sgRNA
GFP sg1	gaaattaatacgactcactataGGGCGAGGAGCTGTTCACCGgttttagagctagaaatagc	sgRNA
GFP sg1(i)	ttaatacgactcactataGGGCGAGGAGCTGTTCACCGgtttaagagctatgctggaaacagc	sgRNA
GFP sg2(i)	ttaatacgactcactataGGAGGAGCTGTTCACCGGGGgtttaagagctatgctggaaacagc	sgRNA
GFP sg3(i)	ttaatacgactcactataGGCGAGGGCGATGCCACCTAgtttaagagctatgctggaaacagc	sgRNA
mCD45 sg1	ttaatacgactcactataGGAGAGGGCGTCTGCGAGTCgtttaagagctatgctggaaacagc	sgRNA
mCD45 sg2	ttaatacgactcactataGGGAGTCAGGCTGTGGGGACgtttaagagctatgctggaaacagc	sgRNA
mCD45 sg3	ttaatacgactcactataGGTGCTGGTGTTGGGCGTACgtttaagagctatgctggaaacagc	sgRNA
Eed sg	gaaattaatacgactcactataGATGCTTGCATTGGGCAATCgttttagagctagaaatagc	sgRNA
Suz12 sg	gaaattaatacgactcactataGATTGAAGATGAACCTGCTGgttttagagctagaaatagc	sgRNA
hCD45 sg1	ttaatacgactcactataGGTGCTGGTGTTGGGCGCACgttttagagctagaaatagc	sgRNA
hCD45 sg2	ttaatacgactcactataGGGAGCAAGTGAGGATCCTCgttttagagctagaaatagc	sgRNA
hCD45 sg3	ttaatacgactcactataGGGATGCTTGTTCCCTTCAGgttttagagctagaaatagc	sgRNA
DNMT3A ex7 sg1	ttaatacgactcactataGGGGCCCGGGGAGTCTCAGAgttttagagctagaaatagc	sgRNA
DNMT3A ex7 sg2	ttaatacgactcactataGGCCGTGGGGTCCGATGCTGgttttagagctagaaatagc	sgRNA
DNMT3A ex8 sg1	ttaatacgactcactataGGGCCGGGGCTTTGGCATTGgttttagagctagaaatagc	sgRNA
DNMT3A ex8 sg2	ttaatacgactcactataGGGGTCATGTGGTTCGGAGAgttttagagctagaaatagc	sgRNA
DNMT3A ex9 sg1	ttaatacgactcactataGGACTGCAAAACGAGCTCAGgttttagagctagaaatagc	sgRNA
DNMT3A ex9 sg2	ttaatacgactcactataGGTTGTTGTACGTGGCCTGGgttttagagctagaaatagc	sgRNA
DNMT3A ex10 sg1	ttaatacgactcactataGGACACTGCCAAGGCCGTGGgttttagagctagaaatagc	sgRNA
DNMT3A ex10 sg2	ttaatacgactcactataGGGTGGCCAGCAGCCGCGCGgttttagagctagaaatagc	sgRNA
DNMT3A ex11 sg	ttaatacgactcactataGGTGCGTAGGCAGCTGCCTCgttttagagctagaaatagc	sgRNA
DNMT3A ex12 sg	ttaatacgactcactataGGCAGAGCGGCTGGTGTACGgttttagagctagaaatagc	sgRNA
DNMT3A ex13 sg1	ttaatacgactcactataGGGCTCCTACCTTGCAGTTTgttttagagctagaaatagc	sgRNA
DNMT3A ex13 sg2	ttaatacgactcactataGGTAACATTGAGGCTCCCACgttttagagctagaaatagc	sgRNA
DNMT3A ex14 sg1	ttaatacgactcactataGGGTACCAGTACGACGACGAgttttagagctagaaatagc	sgRNA
DNMT3A ex14 sg2	ttaatacgactcactataGGCCGTGAGGTGCTCATGTGgttttagagctagaaatagc	sgRNA
NR3C1 ex3 sg1	ttaatacgactcactataGGTGCTGTTGAGGAGCTGGAgttttagagctagaaatagc	sgRNA
NR3C1 ex3 sg2	ttaatacgactcactataGGAGCACACCAGGCAGAGTTgttttagagctagaaatagc	sgRNA
Cas9-GFP F	GGGGATGTCGAAGAGAATCC	T7E1/Seq
Ubc-GFP F	GGGTTGGCGAGTGTGTTTT	T7E1/Seq

GFP R	GAACTTCAGGGTCAGCTTGC	T7E1/Seq
Eed F	CCTTAGAGCCTGGTGCTCTGT	T7E1/Seq
Eed R	GGATGGCATAAGAAAGCTACAA	T7E1/Seq
Suz12 F	GTGCACTCTGAACTGCCGTA	T7E1/Seq
Suz12 R	CCACTGTAACCTGGGCAGA	T7E1/Seq
mCD45 1F	CTGTGGCACCTTTGTGTCAT	primer
mCD45 1R	TTGGCTGCTGAATGTCTGAG	primer
mCD45 2F	GGTTCCTTCACCCACTGAGA	primer
mCD45 2R	GACACCTCTGTCGCCTTAGC	primer
EGFP F	TTGAAACAAGCAGGGGATGT	primer
EGFP R	GAACTTCAGGGTCAGCTTGC	primer
hCD45 ex24-25 F	AGTACATGCAAGTCCTGCACAATATC	primer
hCD45 ex24-25 R	TTTGTGGTCATCTTTCTTCCACAGT	primer
hCD45 ex25 F	CACACCTGACAGCTTTTCCATGA	primer
hCD45 ex25 R	CATCCACTTTGTTCTCGGCTTCC	primer
DNMT3A ex7 F	TTTCACGGCAAGGCAGCTGGTTG	primer
DNMT3A ex7 R	AGAGGAGAGCAGGACGGGAGGAG	primer
DNMT3A ex8 F	GATCAGGGTGGCAGGGCCTCGT	primer
DNMT3A ex8 R	CACCACAGGCAGAGTAGGGGTGA	primer
DNMT3A ex9 F	GCCAGTTGCAAGGCATGGGGTG	primer
DNMT3A ex10 R	TTGCCTGTGCCACCCTCACTACTC	primer
DNMT3A ex11 F	TACTCTGCCCCATGCCACACTA	primer
DNMT3A ex12 R	ACCCCACTGTAAGGAGGGTGGG	primer
DNMT3A ex13 F	GGAGAGGCCCTTCGGTGGTACT	primer
DNMT3A ex14 R	GAGGCCAAGGTGTGCTACCTGGA	primer
NR3C1 ex3 F	GCCCCAGCATGAGACCAGAT	primer
NR3C1 ex3 R	CACACACTACCTTCCACTGCTCT	primer
hCD45 symmetric HDR template	TCGCCTTAGCTTGACAACATAACCATAAACATCCACTTTGTTCTCGGCTTCC AGGCCTTCTAGCATGGCATCAATTCCGATATAGGTTGCCGTACGACCAACA CCAGCACTGGCAAACCAAGCAAAAAAAAGCAGAGGCATGATCATGGAAAA GCTGTCAGGTGTGAAGCCAATATAAGAATCTAAG	ssODN
hCD45 asymmetric HDR template	TCGCCTTAGCTTGACAACATAACCATAAACATCCACTTTGTTCTCGGCTTCC AGGCCTTCTAGCATGGCATCAATTCCGATATAGGTTGCCGTACGACCAACA CCAGCACTGGCAAACCAAGCAAAAAAAAGCAG	ssODN

Table S2. Most commonly observed indels and large deletions in mouse and human HSPCs (Related to Figures 1, 3 and 4)

Supplementary Experimental Procedures

Mice

The mice used in this study were C57BL/6, Cas9 knock-in (Platt et al., 2014) and Vav-iCre (de Boer et al., 2003) mice. NOD/SCID/IL2Rγ-/- (NSG) mice (The Jackson Laboratory) were fed autoclaved food and water. Mice were housed in AAALAC-accredited, specific-pathogen-free animal care facilities at Baylor College of Medicine (BCM). All procedures were approved by BCM Institutional Animal Care and Use Committees.

Production of CRISPR sgRNA

Protospacer sequences for each target gene were identified using the CRISPRscan algorithm (www.crisprscan.org) (Moreno-Mateos et al., 2015). DNA templates for sgRNAs were made using the protocol described by Li et al (Li et al., 2013). In brief, primers containing a T7 promoter, the protospacer sequence, and a 21-nt sequence corresponding to the 5' end of the sgRNA scaffold sequence were obtained from Integrated DNA Technologies (IDT). Full-length DNA templates were then produced by amplifying the sgRNA scaffold off of the PX458 plasmid (Addgene #48138) using each custom forward primer and a universal reverse primer (see primers list) specific for the 3' end of the sgRNA scaffold. The PCR products were purified and in vitro transcribed with the HiScribe T7 High Yield RNA Synthesis Kit (NEB) following manufacturer instructions. In vitro transcription products were purified using RNA Clean & Concentrator-25 (Zymo Research) and eluted in nuclease-free water. To generate sgRNA containing the improved scaffold sequences, a forward primer containing a T7 promoter, a reverse primer specific for the 3' end of the improved scaffold, and pKLV-U6gRNA-EF(BbsI)-PGKpuro2ABFP plasmid (Addgene # 62348) were used in a PCR reaction.

Murine cell isolation, culture and transfection

Murine bone marrow cells were isolated by flushing tibias and femurs in HBSS supplemented with 2% heat-inactivated bovine serum (Gibco, Grand Island, NY). To isolate c-kit$^+$ cells, bone marrow cells were stained with biotin conjugated c-kit antibodies followed by anti-biotin microbeads (Miltenyl Biotec) and separated using autoMACS (Miltenyl Biotec). Cells were cultured in either

Supplemental Materials   10

X-Vivo 15 media (Lonza) supplemented with 2% FBS, 50 ng/ml SCF, 50 ng/ml TPO, 10 ng/ml IL-3, and 10 ng/ml IL-6, or StemPro-34 Serum Free media (Thermo Fisher Scientific) supplemented with L-Glutamine (2 mM), SCF (10 ng/mL), and TPO (100 ng/mL) with similar results. Cytokines were purchased from Peprotech or Miltenyi Biotec.

For experiments using Cas9-expressing mice, cells were either electroporated directly or after culturing for the indicated time. 1 x 10^5 cells were resuspended into 10 µl of Buffer T (Invitrogen), mixed with sgRNA and electroporated using the Neon transfection system (Thermo Fisher Scientific). For experiments using sgRNAs pre-complexed with Cas9 protein, 200 ng to 1 µg of sgRNA was incubated with 1 µg Cas9 protein (PNA Bio, 1 µg/µL in Buffer T or PBS) for 10-15 minutes at room temperature in a final volume of 2 µl. 1 x 10^5 cells cultured for 1-3 hours were resuspended in 10 µl of Buffer T and added to the Cas9-sgRNA RNP for a total volume of 12 µl. After optimizing the electroporation conditions as shown in Figure S1A, we used the optimal condition, which is 1700V, 20ms, 1 pulse for all other murine experiments. Electroporated cells were either directly used to sort HSCs, plated on Methocult M3434 (Stem Cell Technologies), or incubated in StemPro-34 with cytokines for 16-20 hours before plating in Methocult M3434 media.

Murine HSPC culture

To examine the serial replating capacity of HSPCs after gene editing, 5,000 cells were plated into Methocult M3434 (StemCell Technologies) after electroporation. Colony counting and replating were performed every 7 days. Media with colonies were resuspended in PBS and cells were counted to replate 5,000 cells into fresh media. Single colonies were picked and sequenced by Sanger sequencing.

To examine the clonality of murine HSPCs after electroporation, HSPCs were precultured for 1 hour and then either left without manipulation or electroporated with the components shown in Figure 2D. Cells were then stained with antibodies to identify HSCs (see "Flow cytometry" below) and sorted. Clonality was calculated based on the numbers of colonies formed 10-12 days after plating and the numbers of HSCs sorted. To examine GFP disruption in HSCs, cells were electroporated and stained as above, and single HSCs were sorted individually into a well of a 96-well plate. Colonies were individually resuspended in PBS 10-12 days later and analyzed by flow cytometry to examine GFP expression.

T7E1 and TIDE assays
Supplemental Materials   11

PCR amplicon spanning the Cas9-sgRNA cleavage site was diluted 1:4 in 1x Buffer 2 (NEB) and hybridized slowly in a thermal cycler. Hybridized fragments were then digested with 1.25 U of T7 endonuclease I (NEB) for 10 minutes at 37°C. Digested fragments were separated by polyacrylamide gel electrophoresis. Band intensities were analyzed using imageJ software by plotting band intensities of each lane. % cleavage was calculated by the ratio of the intensities of the cleaved bands to uncleaved bands. TIDE assays were performed as described previously (Brinkman et al., 2014).

Human cell culture, and transfection

Human acute myeloid leukemia (AML) cell lines (HL60, Kasumi and OCI-AML2) were obtained from ATCC and cultured in RPMI-1640 medium supplemented with 10% fetal bovine serum and 2% L-glutamine (cRPMI) (Thermo Fisher Scientific). Human cord blood and peripheral blood mononuclear cells (PBMCs) were processed by Ficoll gradient (Lymphoprep, StemCell Technologies). Human primary T- cells were selected and activated by culturing PBMCs from individual donors on anti-CD3/CD28 coated plates in RPMI/Click's 1:1 Medium supplemented with 10 ng/ml IL-7 and 5 ng/ml IL-15 for four days prior to electroporation. CD34$^+$ cord blood cells from individual donors were enriched from mononuclear cells using CD34 microbeads and Auto-MACS Pro (Miltenyi Biotec) following manufacturer's instructions. Purity of sorted human cord blood CD34$^+$ cells was assessed in each sample immediately after sorting. Sorted CD34$^+$ cells were cultured in StemSpan SFEM II (Stem Cell Technologies) supplemented with 100ng/ml FLT3L, 100ng/ml thrombopoietin and 100ng/ml stem cell factor (Peprotech) for a maximum of 48 hours prior to electroporation.

Incubation of Cas9 with sgRNAs was performed as described for mouse cells, except AML cell lines were electroporated in Buffer R (Invitrogen). In each replicate 150,000-250,000 cells were electroporated. Experiments with multiple guides in the same reaction had a total of 1 µg sgRNA (e.g. 500 ng of each sgRNAs when 2 guides were tested). Electroporation was performed using the Neon Transfection System (Thermo Fisher Scientific). Electroporation conditions used for AML cell lines were based on manufacturer instructions (1350V, 35ms, 1pulse). T cells were electroporated as previously described by Schumann et al (Schumann et al., 2015) (i.e. 1600V, 10ms, 3 pulses). For the human HSPCs electroporation optimization, cord blood derived CD34+ cells were expanded for 96 hours prior to electroporation. Following conditions were tested: 1) 1700V, 20ms, 1pulse; 2) 1400V, 30ms, 1pulse; 3)

1200V, 40ms, 1pulse; 4) 1200V, 20ms, 2pulses; 5) 1400V, 20ms, 2pulses; 6) 1150V, 30ms, 2pulses; 7) 1400V, 10ms, 3pulses, 8) 1500V, 10ms, 3pulses; 9) 1600V, 10ms, 3pulses. Condition 9 was used for all further experiments.

GFP-NPM1 construct was kindly provided by B. Falini (University of Perugia, Italy). GFP-NPM1 coding sequence was cloned adjacent to the T7 promoter contained in the pcDNA 3.1 plasmid (Invitrogen). GFP-NPM1 mRNA was in vitro transcribed using the T7 ARCA mRNA kit (NEB) and 1.2 µg mRNA were transfected in CD34$^+$ cells at different culture times (0, 24, and 48 hours of culture) using the previously described optimized conditions.

For knock-in experiments, ssODN templates oriented in an anti-sense direction relative to the target locus were ordered from IDT. The symmetric ssODN template (S) contained 90bp homology arms distal and proximal to the PAM sequence. The asymmetric ssODN template (A) contained a 36bp homology arm on the PAM distal side and a 90bp homology arm on the PAM proximal side (Richardson et al., 2016). Either 10 pmol or 30 pmol of ssODN templates (1 µl volume) were added to the Cas9-sgRNA RNP mixture (11.5 µl volume) immediately prior to electroporation.

In vivo transplantation of CD34$^+$ cord blood cells

Adult (6-8 weeks of age) NSG mice were conditioned with sub-lethal (2.5 Gy) total-body irradiation. The conditioned recipients were transplanted with 150,000-250,000 CD34$^+$ cord blood cells. Cells were isolated from individual cord blood donors, expanded for 48 hours and split into one Cas9 only and one Cas9/hCD45 sgRNA1 RNP electroporated aliquot. Each aliquot was injected into recipients 6 hours post electroporation for a total time of culture of 54 hours. At 2 months post-transplantation, the mice were euthanized and bone marrow and spleen were collected for identification of hematopoietic cell chimerism by flow cytometry. To confirm the engraftment of knock-out cells at genomic level, human CD45 exon 25 was amplified by PCR from harvested bone marrow cells and sequenced for analysis of indels at the targeted CD45 locus.

Flow cytometry

Murine GFP expression levels were measured 24 to 48 hours after electroporation. To sort murine HSCs after electroporation of c-kit$^+$ HSPCs, we stained electroporated cells with CD150-PE-Cy5 (Biolegend), CD48-PE-Cy7, Sca-1-APC, Streptavidin-APC-Cy7 (to label Biotin-conjugated c-kit antibody used to enrich HSPCs), and PE-conjugated lineage antibodies (B220, CD2, CD3, CD8, Gr-1,

Ter119). All murine antibodies were from eBioscience unless otherwise noted. To measure human CD45 expression in AML cell lines and primary cells, transfected cells were cultured for 4 days and stained with FITC-conjugated anti-human CD45 antibody (BD Biosciences). Sorting of CD45^{neg}, CD45^{dim}, CD45^{mid}, CD45^{bright} activated T-cells was performed four days after electroporation. Purity of sorted human cord blood CD34^{+} cells was assessed in each sample using PE-conjugated anti-CD34 antibody (BD Biosciences). Engraftment of human cells in NSG mice was evaluated in bone marrows and spleens using a specific PE-conjugated anti-human HLA-ABC antibody (BD Biosciences). Bone marrow cells were also stained with FITC-conjugated anti-human CD45, PerCP-Cy5.5 conjugated anti-human CD19 and APC conjugated anti-human CD3 antibodies (BD Biosciences).

For human xenograft lineage assessment B cells were gated as hHLA-ABC^{+}hCD19^{+}, T cells as hHLA-ABC^{+}hCD3^{+} and myeloid cells as hHLA-ABC^{+}hCD19^{-}hCD3^{-} viable events. Staining of engrafted HSPCs was performed using a combination of anti human CD45-FITC, anti human CD34-PE and anti human CD38-PE (BD Biosciences). In all experiments viable cells were selected applying a first gate on scatter parameters and a second gate on DAPI or propidium iodide negative cells. Flow cytometry was performed with FACSAria II, LSR II, or LSRFortessa flow-cytometers (BD Biosciences).

Western Blotting

5×10^{5} cells were dissolved directly in 50 µl of 1x Laemmli sample buffer and boiled at 95°C for 5 minutes. 15 µl of lysates were separated by SDS-polyacrylamide gel electrophoresis (SDS-PAGE) on 4-20% gradient gels (BioRad) and transferred onto PVDF membranes (GE Healthcare). Membranes were incubated with primary rabbit anti-DNMT3A (H-295, Santa Cruz) followed by horseradish peroxidase-conjugated secondary antibody (Santa Cruz).

High throughput sequencing

Sequencing libraries were prepared using Illumina Nextera XT Kit (Illumina) and sequenced with the Illumina MiSeq or NextSeq instruments (Illumina). Indel frequencies were computed by using a custom aligner/script.

Identification of off-target sites

Supplemental Materials   14

CRISPRscan (Moreno-Mateos et al., 2015) was used to predict possible off-target sites for hCD45-sg1. Three candidate loci were indentified:

- OT1: chr7:98949525 (TRAPP gene, exon 34)

- OT2: chr8:144448491 (intergenic)

- OT3: chr2:28427248 (intergenic)

Indel frequencies at predicted loci were calculated through high-throughput sequencing of amplicons spanning the off-target sites in T-cells and CD34+ cells targeted with Cas9/hCD45-sg1 RNP.

Supplementary References

Brinkman, E.K., Chen, T., Amendola, M., and van Steensel, B. (2014). Easy quantitative assessment of genome editing by sequence trace decomposition. Nucleic Acids Res *42*, e168.

Chen, B., Gilbert, L.A., Cimini, B.A., Schnitzbauer, J., Zhang, W., Li, G.W., Park, J., Blackburn, E.H., Weissman, J.S., Qi, L.S., *et al.* (2013). Dynamic imaging of genomic loci in living human cells by an optimized CRISPR/Cas system. Cell *155*, 1479-1491.

de Boer, J., Williams, A., Skavdis, G., Harker, N., Coles, M., Tolaini, M., Norton, T., Williams, K., Roderick, K., Potocnik, A.J., *et al.* (2003). Transgenic mice with hematopoietic and lymphoid specific expression of Cre. European journal of immunology *33*, 314-325.

Li, D., Qiu, Z., Shao, Y., Chen, Y., Guan, Y., Liu, M., Li, Y., Gao, N., Wang, L., Lu, X., *et al.* (2013). Heritable gene targeting in the mouse and rat using a CRISPR-Cas system. Nat Biotechnol *31*, 681-683.

Moreno-Mateos, M.A., Vejnar, C.E., Beaudoin, J.D., Fernandez, J.P., Mis, E.K., Khokha, M.K., and Giraldez, A.J. (2015). CRISPRscan: designing highly efficient sgRNAs for CRISPR-Cas9 targeting in vivo. Nat Methods *12*, 982-988.

Platt, R.J., Chen, S., Zhou, Y., Yim, M.J., Swiech, L., Kempton, H.R., Dahlman, J.E., Parnas, O., Eisenhaure, T.M., Jovanovic, M., *et al.* (2014). CRISPR-Cas9 Knockin Mice for Genome Editing and Cancer Modeling. Cell *159*, 440-455.

Richardson, C.D., Ray, G.J., DeWitt, M.A., Curie, G.L., and Corn, J.E. (2016). Enhancing homology-directed genome editing by catalytically active and inactive CRISPR-Cas9 using asymmetric donor DNA. Nat Biotechnol *34*, 339-344.

Schumann, K., Lin, S., Boyer, E., Simeonov, D.R., Subramaniam, M., Gate, R.E., Haliburton, G.E., Ye, C.J., Bluestone, J.A., Doudna, J.A., *et al.* (2015). Generation of knock-in primary human T cells using Cas9 ribonucleoproteins. Proc Natl Acad Sci U S A *112*, 10437-10442.

Supplemental Materials   15

3. Auszug Journal Summary List für Zeitschrift „Nature Medicine"

	InCites Journal Citation Reports		Clarivate Analytics

Journal Data Filtered By: Selected JCR Year: 2016 Selected Editions: SCIE Selected Categories: 'MEDICINE, RESEARCH & EXPERIMENTAL' Selected Category Scheme: WoS

Rank	Full Journal Title	Total Cites	Journal Impact Factor	Eigenfactor Score
1	NATURE MEDICINE	70,491	29.886	0.178470
2	Science Translational Medicine	22,073	16.761	0.125580
3	Annual Review of Medicine	5,974	13.609	0.012480
4	JOURNAL OF CLINICAL INVESTIGATION	105,106	12.784	0.183780
5	JOURNAL OF EXPERIMENTAL MEDICINE	63,434	11.991	0.099180
6	TRENDS IN MOLECULAR MEDICINE	8,371	10.732	0.019430
7	EMBO Molecular Medicine	5,352	9.249	0.024220
8	Theranostics	4,091	8.766	0.012640
9	MOLECULAR THERAPY	15,093	6.688	0.032360
10	Molecular Therapy-Nucleic Acids	1,490	6.392	0.006870
11	Nanomedicine-Nanotechnology Biology and Medicine	7,861	5.720	0.015180
12	MOLECULAR ASPECTS OF MEDICINE	4,657	5.686	0.009750
13	EXPERIMENTAL AND MOLECULAR MEDICINE	2,941	5.063	0.006530
14	CLINICAL SCIENCE	9,350	4.936	0.013790
15	mAbs	3,154	4.881	0.009550
16	LABORATORY INVESTIGATION	10,533	4.857	0.011990
17	Wiley Interdisciplinary Reviews-Nanomedicine and Nanobiotechnology	1,615	4.761	0.003240
18	JOURNAL OF MOLECULAR MEDICINE-JMM	6,738	4.686	0.011980
19	Translational Research	2,992	4.652	0.008550
20	JOURNAL OF CELLULAR AND MOLECULAR MEDICINE	10,258	4.499	0.017860

4. Publikation Wagner et al. 2019 Nature Medicine

High prevalence of *Streptococcus pyogenes* Cas9-reactive T cells within the adult human population

Dimitrios L. Wagner [1,2,3], Leila Amini [1,2], Desiree J. Wendering [1,2], Lisa-Marie Burkhardt [1], Levent Akyüz[1], Petra Reinke[2,4], Hans-Dieter Volk [1,2,4,5] and Michael Schmueck-Henneresse[1,2,4,5]*

The discovery of the highly efficient site-specific nuclease system CRISPR–Cas9 from *Streptococcus pyogenes* has galvanized the field of gene therapy[1,2]. The immunogenicity of Cas9 nuclease has been demonstrated in mice[3,4]. Preexisting immunity against therapeutic gene vectors or their cargo can decrease the efficacy of a potentially curative treatment and may pose significant safety issues[3-6]. *S. pyogenes* is a common cause for infectious diseases in humans, but it remains unclear whether it induces a T cell memory against the Cas9 nuclease[7,8]. Here, we show the presence of a preexisting ubiquitous effector T cell response directed toward the most widely used Cas9 homolog from *S. pyogenes* (SpCas9) within healthy humans. We characterize SpCas9-reactive T cells within the CD4/CD8 compartments for multi-effector potency, cytotoxicity, and lineage determination. In-depth analysis of SpCas9-reactive T cells reveals a high frequency of SpCas9-reactive regulatory T cells that can mitigate SpCas9-reactive effector T cell proliferation and function in vitro. Our results shed light on T cell–mediated immunity toward CRISPR-associated nucleases and offer a possible solution to overcome the problem of preexisting immunity.

[1]Institute for Medical Immunology, Charité – Universitätsmedizin Berlin, Berlin, Germany. [2]Berlin-Brandenburg Center for Regenerative Therapies (BCRT), Charité – Universitätsmedizin Berlin, Berlin, Germany. [3]Berlin Institute of Health (BIH), Berlin, Germany. [4]Berlin Center for Advanced Therapies (BeCAT), Charité – Universitätsmedizin Berlin, Berlin, Germany. [5]These authors jointly directed this study: Hans-Dieter Volk, Michael Schmueck-Henneresse.
*e-mail: michael.schmueck-henneresse@charite.de

High prevalence of *Streptococcus pyogenes* Cas9-reactive T cells within the adult human population

Dimitrios L. Wagner [1,2,3], Leila Amini [1,2], Desiree J. Wendering [1,2], Lisa-Marie Burkhardt [1],
Levent Akyüz [1], Petra Reinke [2,4], Hans-Dieter Volk [1,2,4,5] and Michael Schmueck-Henneresse [1,2,4,5]*

[1]Institute for Medical Immunology, Charité – Universitätsmedizin Berlin, Berlin, Germany. [2]Berlin-Brandenburg Center for Regenerative Therapies (BCRT),
Charité – Universitätsmedizin Berlin, Berlin, Germany. [3]Berlin Institute of Health (BIH), Berlin, Germany. [4]Berlin Center for Advanced Therapies (BeCAT),
Charité – Universitätsmedizin Berlin, Berlin, Germany. [5]These authors jointly directed this study: Hans-Dieter Volk, Michael Schmueck-Henneresse.
*e-mail: michael.schmueck-henneresse@charite.de

5. Auszug Journal Summary List für Zeitschrift „Leukemia"

InCites Journal Citation Reports

Clarivate
Analytics

Journal Data Filtered By: Selected JCR Year: 2018 Selected Editions: SCIE Selected Categories: 'HEMATOLOGY' Selected Category Scheme: WoS

Rank	Full Journal Title	Total Cites	Journal Impact Factor	Eigenfactor Score
1	BLOOD	161,908	16.601	0.241110
2	CIRCULATION RESEARCH	52,988	15.862	0.072270
3	Lancet Haematology	1,934	11.990	0.010550
4	LEUKEMIA	24,555	9.944	0.054750
5	Journal of Hematology & Oncology	5,366	8.731	0.013620
6	Blood Cancer Journal	2,247	7.895	0.009060
7	HAEMATOLOGICA	16,255	7.570	0.037650
8	ARTERIOSCLEROSIS THROMBOSIS AND VASCULAR BIOLOGY	33,223	6.618	0.036010
9	AMERICAN JOURNAL OF HEMATOLOGY	10,375	6.137	0.022930
10	BLOOD REVIEWS	2,889	6.125	0.005970
11	JOURNAL OF CEREBRAL BLOOD FLOW AND METABOLISM	19,766	6.040	0.028040
12	STEM CELLS	21,467	5.614	0.030290
13	BRITISH JOURNAL OF HAEMATOLOGY	23,963	5.206	0.037720
14	CRITICAL REVIEWS IN ONCOLOGY HEMATOLOGY	7,401	5.012	0.012890
15	THROMBOSIS AND HAEMOSTASIS	16,590	4.733	0.022810
16	BONE MARROW TRANSPLANTATION	12,031	4.674	0.020690
17	JOURNAL OF THROMBOSIS AND HAEMOSTASIS	18,886	4.662	0.028240
18	CYTOTHERAPY	5,969	4.297	0.009690
19	JOURNAL OF LEUKOCYTE BIOLOGY	16,921	4.012	0.019560
20	SEMINARS IN HEMATOLOGY	2,157	3.738	0.003950

6. Publikation Fousek et al. 2020 Leukemia

ARTICLE

Acute lymphoblastic leukemia

CAR T-cells that target acute B-lineage leukemia irrespective of CD19 expression

Kristen Fousek [1,2,3,4] · Junji Watanabe[5] · Sujith K. Joseph[2,3,4] · Ann George[5] · Xingyue An[6] · Tiara T. Byrd[1,2,3,4] · Jessica S. Morris[1,2,3,4] · Annie Luong[5,7] · Melisa A. Martínez-Paniagua[6] · Khaled Sanber[2,3,4] · Shoba A. Navai [2,3,4] · Ahmed Z. Gad [1,2,3,4] · Vita S. Salsman[2,3,4] · Pretty R. Mathew[2,3,4] · Hye Na Kim[5,7] · Dimitrios L. Wagner [2,8,9] · Lorenzo Brunetti[2] · Albert Jang[2] · Matthew L. Baker[10] · Navin Varadarajan[6] · Meenakshi Hegde[2,3,4] · Yong-Mi Kim[5,7] · Nora Heisterkamp[5,7,11] · Hisham Abdel-Azim[5,7] · Nabil Ahmed[1,2,3,4]

Abstract

Chimeric antigen receptor (CAR) T-cells targeting CD19 demonstrate remarkable efficacy in treating B-lineage acute lymphoblastic leukemia (BL-ALL), yet up to 39% of treated patients relapse with CD19(−) disease. We report that CD19(−) escape is associated with downregulation, but preservation, of targetable expression of CD20 and CD22. Accordingly, we reasoned that broadening the spectrum of CD19CAR T-cells to include both CD20 and CD22 would enable them to target CD19(−) escape BL-ALL while preserving their upfront efficacy. We created a CD19/20/22-targeting CAR T-cell by coexpressing individual CAR molecules on a single T-cell using one tricistronic transgene. CD19/20/22CAR T-cells killed CD19(−) blasts from patients who relapsed after CD19CAR T-cell therapy and CRISPR/Cas9 CD19 knockout primary BL-ALL both in vitro and in an animal model, while CD19CAR T-cells were ineffective. At the subcellular level, CD19/20/22CAR T-cells formed dense immune synapses with target cells that mediated effective cytolytic complex formation, were efficient serial killers in single-cell tracking studies, and were as efficacious as CD19CAR T-cells against primary CD19(+) disease. In conclusion, independent of CD19 expression, CD19/20/22CAR T-cells could be used as salvage or front-line CAR therapy for patients with recalcitrant disease.

These authors contributed equally: Hisham Abdel-Azim, Nabil Ahmed

✉ Hisham Abdel-Azim
   habdelazim@chla.usc.edu

✉ Nabil Ahmed
   nahmed@bcm.edu

1 Interdepartmental Program in Translational Biology and Molecular Medicine, Baylor College of Medicine, Houston, TX, USA

2 Center for Cell and Gene Therapy, Texas Children's Hospital, Houston Methodist Hospital, Baylor College of Medicine, Houston, TX, USA

3 Texas Children's Cancer and Hematology Centers, Texas Children's Hospital, Baylor College of Medicine, Houston, TX, USA

4 Department of Pediatrics, Baylor College of Medicine, Houston, TX, USA

5 Division of Hematology, Oncology and Bone Marrow Transplantation, Children's Hospital Los Angeles, Los Angeles, CA, United States

6 Department of Chemical and Biomolecular Engineering, University of Houston, Houston, TX, USA

7 University of Southern California Keck School of Medicine, Los Angeles, CA, USA

8 Institute of Medical Immunology, Campus Virchow Klinikum, Charité—Universitätsmedizin Berlin, Berlin, Germany

9 Berlin Institute of Health—Center for Regenerative Therapies (B-CRT), Charité—Universitätsmedizin Berlin, Berlin, Germany

10 National Center for Macromolecular Imaging and Verna and Marrs McLean Department of Biochemistry and Molecular Biology, Baylor College of Medicine, Houston, TX, USA

11 Department of Systems Biology, Beckman Research Institute City of Hope, Duarte, CA, United States

Introduction

The treatment of B-precursor lymphoid malignancies with chimeric antigen receptor (CAR) T-cells targeting the pan-B

cell marker CD19 remains the most impactful application of CAR therapy [1–5]. A substantial number of patients who have failed standard-of-care and salvage therapies, including hematopoietic stem cell transplantation, have achieved durable complete remission using this approach [1–5]. However, as more patients receive CD19CAR T-cells or CD19/CD3 bi-specific T-cell engagers and as long-term follow-up data become available, a high incidence of relapse with CD19(−) disease has been observed [2, 6–8]. It is estimated that this immune evasion mechanism occurs in up to 39% of patients after CD19-directed therapy [3, 7, 9–11].

In order to overcome this limitation, we revisited the exclusivity of CD19 as the sole optimal target antigen for B-lineage acute lymphoblastic leukemia (BL-ALL). We reasoned that other B-lineage markers, such as CD20 or CD22, should be considered as candidate targets. Whereas CD19 is generally ubiquitously expressed, CD20 is expressed in ~50% of cases, and CD22 is expressed in 80–90% [12]. Combinatorial CAR T-cell therapies have shown a clear advantage in preclinical studies of both solid and liquid tumors [13–15]. For example, the bivalent targeting of CD19/CD20 or CD19/CD22 in lymphoma and BL-ALL mitigated antigen escape in murine models [16–19]. Interestingly, we and others have observed that both monovalent and bivalent CD19-specific therapies result in off-target on-tumor antigen modulation, namely partial downregulation of CD20 and CD22 [20]. In addition, a recent clinical trial reported that while 73% of patients with relapsed BL-ALL achieve complete remission after higher dose levels of CD22CAR T-cells, those who relapse do so with CD22(−) or -dim disease [16]. Moreover, paralleling this observation, patients treated with the anti-CD22 antibody drug conjugate inotuzumab ozogamicin have relapsed with CD22-negative disease [21].

In two recent single-patient reports, "sequential loss" of tumor antigen expression has been observed. In diffuse large B-cell lymphoma, one case demonstrated differential loss of CD20, CD30, and CD19 [22] while another showed loss of CD19 and CD22 [23] following immune-based therapies [22, 23]. Furthermore, whereas CD20 expression is often low in BL-ALL, it is expressed by 40–50% of patients with more mature B-lymphoid neoplasms and is associated with poorer prognosis [24, 25]. Specifically, CD20 expression at diagnosis predicts relapse in adult patients, such that CD20-directed antibody therapy is now being incorporated into front-line therapy for adult BL-ALL [25, 26].

Based on these observations, we hypothesized that simultaneous targeting of CD20 and CD22 could confer a therapeutic advantage either as salvage or as upfront CAR therapy [16, 19, 27]. Accordingly, we created a CD19/20/22-targeting CAR T-cell, and we report on its antitumor

activity against primary relapsed CD19(+) and CD19(−) escape BL-ALL.

Materials and methods

Leukemia samples, blood donors, and cell lines

Primary human samples collection was approved by Institutional Review Boards (IRBs) in accordance with the Declaration of Helsinki. Informed consent was obtained as required by IRBs regulations. UPN01-3 are patient-derived BL-ALL cells, passaged through NOD/SCIDγc−/− (NSG) mice (approved by Institutional Animal Care and Use Committees) and cultured on OP9 cells, as described [28]. Other lines were purchased from American Type Culture Collection (ATCC, Manassas, VA). T-cells were maintained in T-cell media with IL-7/IL-15 as described [29]. BL-ALL were cultured in Alpha MEM, Raji in RPMI, and Daoy and HEK293T in DMEM all supplemented with 1% Glutamax and 10–20% FBS.

Computational modeling

Individual CAR and antigen models were first generated from amino acid sequences via Swiss-Model Webserver. Initial dockings were done by Patchdock/Firedock (CD19 and CD22CAR/antigen pairs) or based on GA101/CD20 structure (CD20CAR/antigen pair), then refined with Rosetta Dock as described [30].

Construction of DNA transgenes

Sequences encoding CD19, CD20, and CD22 were obtained from the Research Collaboratory of Structural Bioinformatics Protein Data Base. The CD19-specific single-chain variable fragment (scFv) FMC63 [31] and CD22-specific scFv m971 [32] were previously described. The CD20-scFv was derived from C2B8 and retained part of the constant region, C_L and C_{H1} [33]. CAR exodomain sequences were assembled in-frame with a CD8α-hinge and transmembrane domain and 4–1BB and CD3ζ endodomains in Clone-Manager (Sci-Ed, Denver, CO). The CARs were separated by retroviral 2A sequences. DNA sequences were codon-optimized, synthesized by GeneArt (ThermoFisher, Regensburg, Germany), cloned into SFG [34], and verified by pyrosequencing (Epoch, Missouri City, TX).

Retroviral transduction of cells

T-cells, Daoy, Raji, or UPN03 were transduced with CAR, target, or eGFP.FFLuciferase-encoding transgenes as described [29, 35, 36].

Flow cytometry and sorting

Accuri-C6, FACSCanto-II, Aria (BD, San Jose, CA), or Gallios (Beckman-Coulter [BC], Brea, CA), were used. Surface staining was performed as described [29]. Data were analyzed using FlowJo software (FlowJo, Ashland, OR). CAR expression was evaluated with CD19CAR FMC63-antibody as described [37]. We used anti-Rituximab (Bio-Rad, Hercules, CA) to detect the CD20CAR, and Fc-conjugated recombinant huCD22 protein (R&D, Minneapolis, MN) (primary) followed by goat anti-human-Fc (Thermo-Fisher, Waltham, MA) (secondary) to assess the surface expression of the CD22CAR. Proliferation was assessed using eFluor670 (eBiosciences, San Diego, CA). Antigens were assessed with CD19, CD20, and CD22 antibodies (BD).

CRISPR-edited knock-out

CD19 was disrupted in UPN02 and Raji cells by the CRISPR-Cas9 endonuclease system, as described [38]. The primers to generate CD19-specific single-guide RNA were kindly provided by Dr. Lorenzo Brunetti. Three huCD19-specific sgRNAs were produced and electroporation of primary BL-ALL was done as described [38].

Impedance-based tumor cell killing assay (xCELLigence)

The xCELLigence (ACEA, San Diego, CA) long-term tumor cell killing was used over 100–160 h. Tumor cells were expanded for 18–24 h before T-cells were added. The cell index was monitored every 15-min. A decreasing cell index indicated tumor lysis.

Cytotoxicity assay

^{51}Cr-release assays were previously described [39]. The average lysis of triplicate wells = (test release—spontaneous release)/(max release—spontaneous release) ×100. CAR T-cells were normalized for percentage of transduction.

Intracellular cytokine staining

BL-ALL and CAR T-cells were cocultured in the presence of Brefeldin A (eBioscience) at 37 °C for 4 h. Cells were fixed (BD Cytofix), permeabilized (BD Perm II), and immunostained for CD45, CD3, CD4, CD8, CD19, IFNγ, and TNFα (BD).

Imaging flow cytometry

BL-ALL and CAR T-cells were cocultured at 37 °C for 1 h, fixed, permeabilized, then immunostained with CD3, phalloidin, and 7-AAD (Thermo). 1×10^5 events were collected, and samples were analyzed using ImageStream MKII (Luminex, Austin, TX). Acquisition and data analysis were performed using ISX and IDEAS, respectively (Luminex).

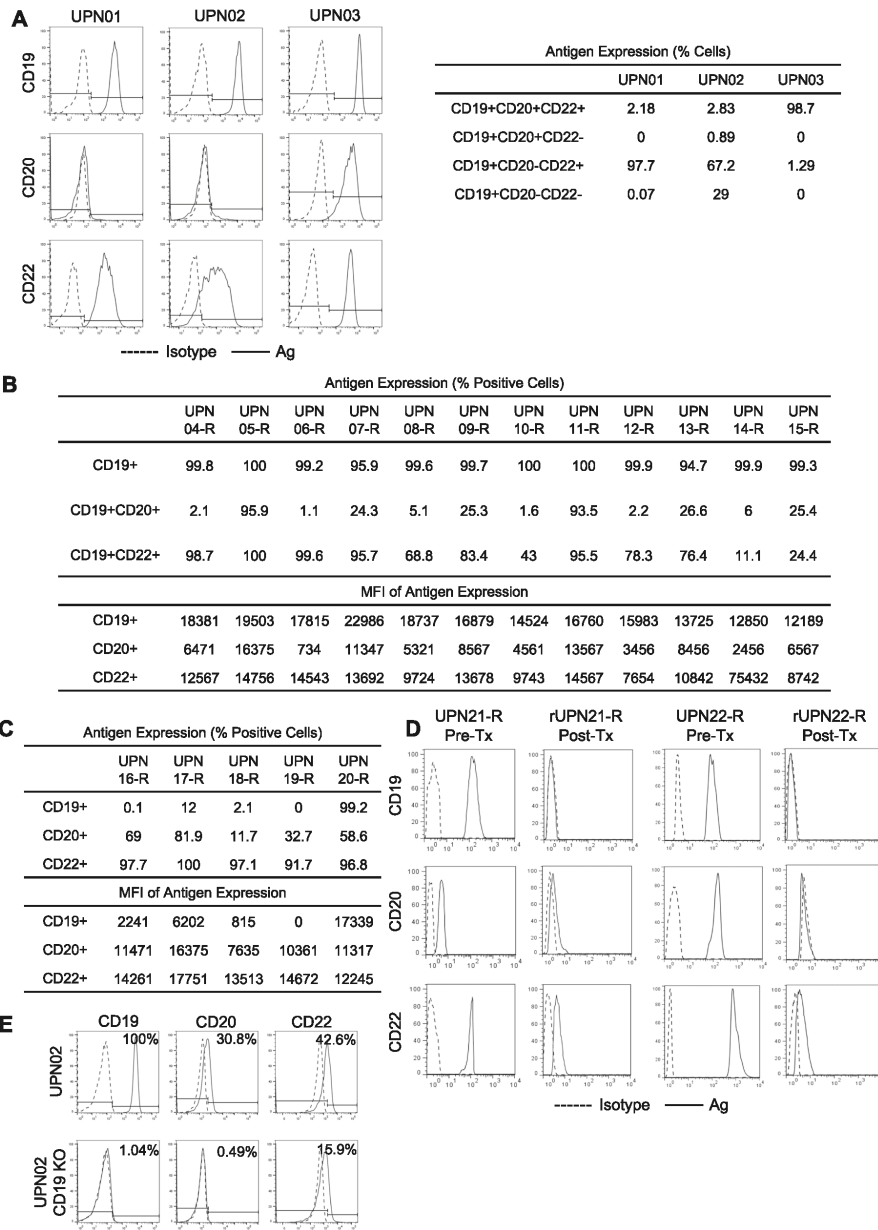## Time-lapse imaging microscopy in nanowell grids (TIMING)

The nanowell manufacture and testing were described previously [40–42]. CAR T-cells and targets were labeled with fluorescent dyes, loaded onto arrays, incubated in media + Annexin V (Invitrogen, Carlsbad, CA), and monitored using a Carl Zeiss Axio Observer (Dublin, CA) fitted with a Hamamatsu (Bridgewater, NJ) Orca-Flash sCMOS camera using a 20×0.8 NA objective for 6 h at 5-min intervals. Images were collected and processed for ≥500 wells using an in-house algorithm for cell tracking and segmentation [43].

CAR-T-cell polyfunctionality evaluation in response to BL-ALL associated antigens by single-cell cytokine profiling

Viable CD8+T-cell subsets were isolated from CAR T-cell products with anti-CD8 microbeads (Miltenyi) and cocultured with Raji cells, Raji-CD19-KO, K562 cells transduced to express CD19 (K562-CD19), or Daoy cells transduced to express either single or combinations of CD19, CD20, and CD22 antigens. The nontransduced CD8+T-cells subjected to the same stimulation were used as a negative control. Subsequent processing, culture conditions, 32-plex antibody barcoded chip analysis, and polyfunctional profiling with determination of polyfunctionality strength index (PSI) and polyfunctional activated topology principal component analysis (PAT PCA) were performed as described [44, 45].

Animal studies and bioluminescence imaging (BLI)

NSG mice were purchased from The Jackson Laboratory (Bar Harbor, Maine). Sample size not estimated a priori, and experimental arms were unblinded. Mice were ranked based on leukemia engraftment by BLI into high and intermediate, then mice were evenly randomized among all tested groups before T-cell injections. *Raji.CD19KO.eGFP. FFLuc Xenograft:* Raji cells were modified to lose CD19 expression and express eGFP. Firefly luciferase as described above. Cells were sorted on CD19(−)GFP(+) and expanded; 2.5×10^5 tumor cells were tail-vein administered. Engrafted animals were randomly assigned a T-cell group ($n = 6$ each). On day 3, 10×10^6 T-cells were tail-vein injected and tumor burden was tracked by BLI [35]. *rUPN21-R Patient-Derived-Xenograft:* 2×10^5 rUPN21-R

A

Antigen Expression (% Cells)			
	UPN01	UPN02	UPN03
CD19+CD20+CD22+	2.18	2.83	98.7
CD19+CD20+CD22-	0	0.89	0
CD19+CD20-CD22+	97.7	67.2	1.29
CD19+CD20-CD22-	0.07	29	0

------ Isotype ——— Ag

B

Antigen Expression (% Positive Cells)

	UPN 04-R	UPN 05-R	UPN 06-R	UPN 07-R	UPN 08-R	UPN 09-R	UPN 10-R	UPN 11-R	UPN 12-R	UPN 13-R	UPN 14-R	UPN 15-R
CD19+	99.8	100	99.2	95.9	99.6	99.7	100	100	99.9	94.7	99.9	99.3
CD19+CD20+	2.1	95.9	1.1	24.3	5.1	25.3	1.6	93.5	2.2	26.6	6	25.4
CD19+CD22+	98.7	100	99.6	95.7	68.8	83.4	43	95.5	78.3	76.4	11.1	24.4

MFI of Antigen Expression

CD19+	18381	19503	17815	22986	18737	16879	14524	16760	15983	13725	12850	12189
CD20+	6471	16375	734	11347	5321	8567	4561	13567	3456	8456	2456	6567
CD22+	12567	14756	14543	13692	9724	13678	9743	14567	7654	10842	75432	8742

C

Antigen Expression (% Positive Cells)

	UPN 16-R	UPN 17-R	UPN 18-R	UPN 19-R	UPN 20-R
CD19+	0.1	12	2.1	0	99.2
CD20+	69	81.9	11.7	32.7	58.6
CD22+	97.7	100	97.1	91.7	96.8

MFI of Antigen Expression

CD19+	2241	6202	815	0	17339
CD20+	11471	16375	7635	10361	11317
CD22+	14261	17751	13513	14672	12245

D

------ Isotype ——— Ag

E

primary relapse BL-ALL cells were injected into mice. Animals were randomized into Non-transduced (NT) ($n = 6$), CD19CAR ($n = 10$), and CD19/20/22CAR ($n = 10$) groups; on days 3 and 7 each mouse received 3×10^{6} T-cells. Mice were monitored for overall health, and weight was assessed twice/week. Signs of overall decline in health,

◀ **Fig. 1 B-lineage ALL expresses variable yet targetable levels of alternative antigens, CD20 and CD22.** Flow cytometry was done on ≥30,000 B-lineage BL-ALL cells to assess the expression of CD19 (FITC), CD20 (PE), and CD22 (APC) in each BL-ALL sample. Histograms displayed are representative data. ($n = 3$). **a** Samples from three patients (UPN01, UPN02, and UPN03) were cultured in vitro and assessed for their antigen expression profile. Dotted histogram, isotype; solid line, target antibody. Table displays quantification of antigen expression. **b** Antigen expression in BL-ALL blasts from 12 patients (UPN04-R to UPN15-R) who relapsed after chemotherapy. Quantification of the percentage of antigen-positive cells and the density using mean fluorescence intensity (MFI) are shown in the table. **c** Quantification of CD19, CD20, and CD22 on BL-ALL samples from five patients who relapsed after CD19-directed immune therapy (UPN16-R to UPN20-R). **(d)** B-lineage BL-ALL phenotype before (UPN21-R and UPN22-R) and after CD19CAR T-cell therapy (rUPN21-R and rUPN22-R). **(e)** CD19, CD20, and CD22 expression in UPN02 BL-ALL cells, after CD19 was knocked out using CRISPR/Cas9 technology.

hind-limb paralysis, and 20% weight loss were used as criteria for euthanasia. *UPN03 Xenograft:* UPN03 primary cells (5×10^5) expressing eGFP. Firefly luciferase were administered intravenously, and all engrafted mice were randomized into treatment groups ($n = 4$–5 per group). On day 9, 5×10^6 T-cells were injected via the tail-vein, and the tumor was quantified over time by BLI.

Statistical analysis

BL-ALL data were analyzed in Prism v7 software (GraphPad, La Jolla, CA). Data are presented as mean ± standard deviation unless annotated otherwise in figure legends. Variances observed were similar across experimental groups in the results reported. P value of <0.05 was considered significant, and the threshold of significance is denoted by *$p < 0.05$, **$p < 0.01$, ***$p < 0.001$, ****$p < 0.0001$.

Results

CD20 and CD22 are heterogeneously expressed in primary BL-ALL and are downregulated in CD19(−) escape

CD19 is near-uniformly expressed on BL-ALL [12]. We examined the antigen expression of three primary BL-ALL cell lines: two Philadelphia (Ph) negative, UPN01 and UPN02, and one Ph + UPN03 (Fig. 1a). All three lines uniformly expressed CD19 but expressed variable levels of CD20 and CD22. In addition, we observed remarkable heterogeneity within each sample with single-, double-, and triple- antigen-positive populations. Similarly, in contrast to uniform CD19 expression, we observed heterogeneity in both percentage and density of CD20 and CD22 in a cohort

of 12 patients with BL-ALL who relapsed after chemotherapy (Fig. 1b). Subsequently, we studied samples from five patients who relapsed after CD19-directed immunotherapy and observed loss of CD19 in 4/5, with two (UPN16-R and UPN19-R) exhibiting complete absence of this target antigen while retaining CD20 and CD22 expression (Fig. 1c). In two additional patient samples, we evaluated antigen expression before CD19CAR T-cell therapy (UPN21-R and UPN22-R) and after the emergence of relapse with CD19(−) escape (rUPN21-R and rUPN22-R; Fig. 1d). UPN21-R and UPN22-R expressed high levels of CD19, CD20, and CD22 with varying densities. Upon relapse, rUPN21-R and rUPN22-R lost CD19 expression but preserved CD22 albeit at considerably lower levels. To confirm this observation experimentally, we knocked out CD19 using CRISPR/Cas9 in UPN02 BL-ALL (UPN02 CD19-KO) and confirmed the absence of CD19 from the cell surface using flow cytometry (Fig. 1e). Interestingly, we similarly saw concomitant downregulation but not complete loss of CD20 and CD22. Based on these findings, we reasoned that CD19(−) recalcitrant disease could be controlled by extending the specificity of therapeutic T-cells to target both CD20 and CD22 simultaneously.

Generation of a CAR T-cell to cotarget CD19, CD20, and CD22

We engineered a T-cell capable of targeting CD19, CD20, and CD22, using three individual CAR molecules specific for these proteins. As prior literature has demonstrated that the choice of scFv influences CAR functionality [32], we individually modeled the docking of each scFv with its target antigen in silico. CD19/FMC63, CD20/C2B8, and CD22/m971 exhibited favorable electrostatic interaction energies, with minimal adverse cross-reactivity (Table S1; Fig. S1A). To achieve proportionate expression of each CAR on T-cells, we created a single tricistronic transgene encoding the three CAR molecules joined in tandem by 2A-sequences (Fig. 2a). Each CAR exodomain was fused to a hinge and CD8α transmembrane domain followed by a 4–1BB and the T-cell receptor ζ-chain 2nd generation signaling endo-domain (Fig. 2b). To avoid homologous recombination of recurring DNA sequences and secondary RNA structure formation which can lead to poor gene expression [46], we wobbled all similar sequences ≥20 bases (Fig. 2c). The transgene was delivered to donor T-cells using a MoMuLv-based retroviral system, and the surface expression of each CAR exodomain was confirmed by flow cytometry utilizing three distinct scFv-specific methods (Figs. 2d; S1B, C). NT and CD19CAR T-cells served as controls. The CAR T-cell products consisted of a majority (78–86%) of CD8 (+) T-cells (Fig. S1D). To test
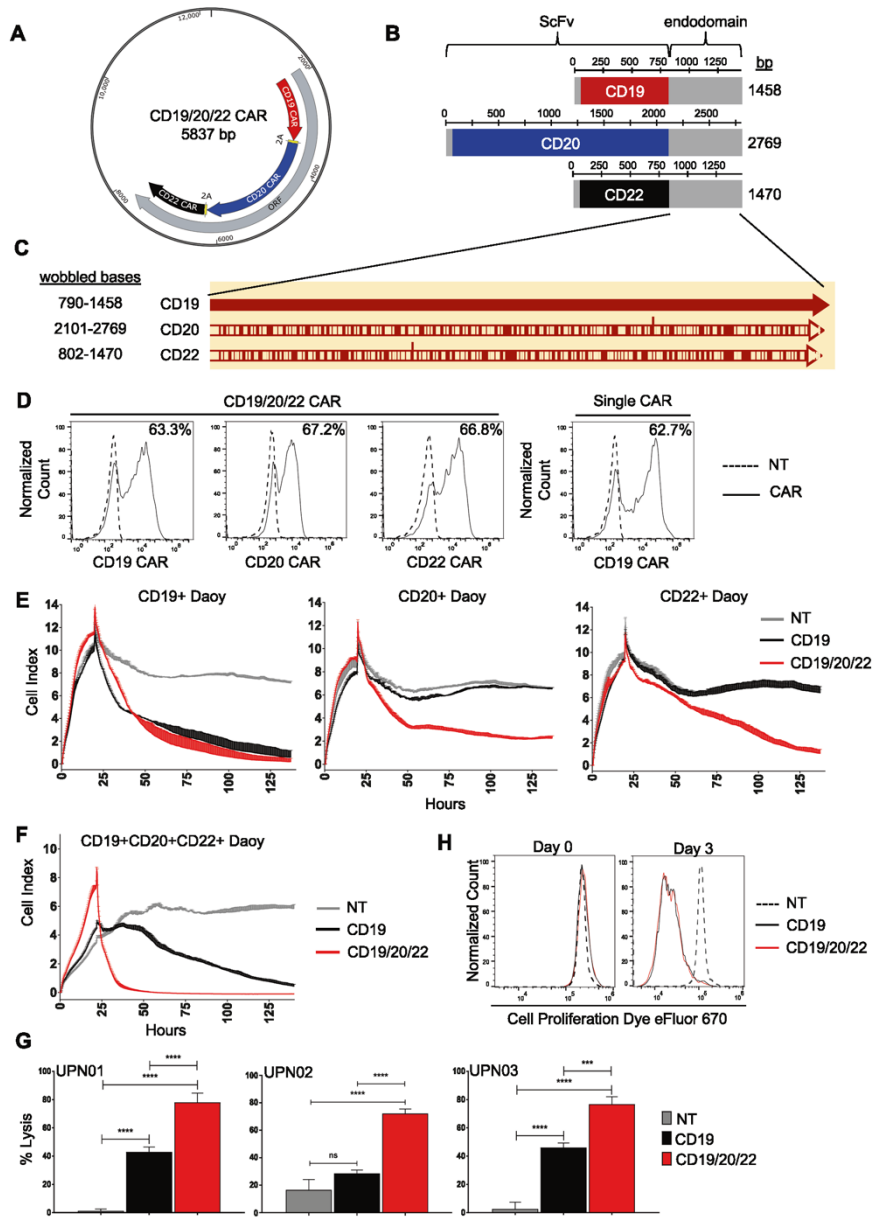
the ability of CD19/20/22CAR T-cells to distinctly target CD19, CD20, and CD22, we force-expressed these molecules individually on Daoy medulloblastoma cells, which

are null for all three antigens (Fig. S2A). Both Daoy and its derivative lines expressed similar levels of immune stimulatory and inhibitory molecules after interferon-γ

CAR T-cells that target acute B-lineage leukemia irrespective of CD19 expression

◀ **Fig. 2 Design of CD19/20/22CAR T-cells. a** A tricistronic vector was designed with self-cleaving 2A peptides, enabling trivalent protein expression of CD19/20/22-directed CARs on T-cells. **b** Design of CAR transgenes. Each CAR endo-domain contains a CD8α hinge and transmembrane region followed by downstream 4-1BB and CD3ζ intracellular signaling domains. **c** Diagram of DNA wobbling of CAR endo-domain transgenes. Common segments of DNA were wobbled so that no more than 20 consecutive base pairs are the same in any of the three transgenes. Using the CD19CAR sequence as a reference, red bars on the CD20 and CD22 CARs indicate the positions of DNA wobbling. **d** Flow cytometry was performed on T-cells ~1 week after retroviral CAR transduction. Results demonstrate specific binding to each individual scFv region with detection methods unique to each CAR (Fig. S1B). Histograms shown are representative data. Long-term impedance-based xCELLigence killing assay targeting Daoy tumor cells (Fig. S2A, B) expressing each target antigen singly ($n = 2$) (**e**) or all three antigens simultaneously ($n = 2$) (**f**). Tumor cells adhered and expanded for 24 h before CAR T-cells were added in a 1:3 E:T ratio. NT T-cells serve as a negative control. A decreasing cell index indicates tumor lysis. **g** Four hours ^{51}Cr release assay targeting B-lineage BL-ALL cells, UPN01, UPN02, and UPN03, at an E:T ratio of 3:1 ($n = 3$). NT T-cells serve as a negative control. Data represent the mean of triplicate samples +SD; $*p < 0.05$, $***p < 0.001$, $****p < 0.0001$, one-way ANOVA with Tukey's multiple comparison post-test. **h** NT, CD19CAR, and CD19/20/22CAR T-cells were stained with eFluor 670 proliferation dye, and proliferation capacity of CAR-expressing T-cells was assessed over 72 h of exposure to BL-ALL cells ($n = 2$).

conditioning (to simulate T-cell activation) and exhibited similar growth dynamics and doubling times (Fig. S3). A long-term killing assay (xCELLIGENCE) demonstrated that while CD19CAR T-cells could kill CD19(+)Daoy but not CD20(+)Daoy or CD22(+)Daoy, CD19/20/22CAR T-cells killed all three lines, confirming their distinct trivalency (Fig. 2e).

We then force-expressed CD19, CD20, and CD22 together on Daoy cells and tested the efficacy of CD19/20/22CAR T-cells, CD19CAR T-cells, and NT in a long-term killing assay. CD19/20/22CAR T-cells eliminated target cells more promptly and sustained this effect over 5 days of testing (Fig. 2f). Next, we tested the cytolytic activity of CD19/20/22CAR, CD19CAR, and NT T-cells against patient-derived BL-ALL: UPN01, UPN02, and UPN03, which have variable expression of the target antigens (see Fig. 1a). CD19/20/22CAR T-cells killed BL-ALL targets better than CD19CAR and NT T-cells (Fig. 2g), yet this enhanced killing capacity was not associated with a more proliferative T-cell phenotype (Fig. 2h).

## CD19/20/22CAR T-cells form a highly functional immune synapse and are more avid serial killers

CD19/20/22CAR T-cells exhibited superior in vitro cytolysis, though not due to a higher proliferative capacity. We therefore investigated whether this advantage could be attributed to more favorable tumor engagement dynamics at the individual T-cell level.

First, we examined the T-cell/tumor cell interface using high-throughput imaging flow cytometry (ImageStream) to study indices of the CAR Immunological Synapses (CARIS; Fig. 3a) [47]. We probed for actin using phalloidin to quantify the effective CARIS area (CARIS^{area}) and intensity (CARIS^{intensity}) and the effector/target internuclear distance to assess the tensile properties of the CARIS (CARIS^{tension}; Fig. 3a). Our analysis gated on cell doublets of T-cells (CD19/20/22CAR, CD19CAR, or NT) and BL-ALL cells (Fig. 3b). We found that CD19/20/22CAR T-cells engaged BL-ALL cells in CARIS of similar areas (CARIS^{area}; Fig. 3c) but of significantly more actin micro-cluster density (CARIS^{density}; Fig. 3d), when compared with CD19CAR or NT T-cells. The distance between the CD19/20/22CAR T-cell nucleus and that of its target were significantly shorter, indicating higher CARIS^{tension} (Fig. 3e). The observed differences in CARIS properties suggest that CD19/20/22CAR T-cells exhibit favorable CARIS cytoskeletal properties, which could enhance their immunoactivity upon engaging BL-ALL cells.

Next, we investigated whether this favorable initial cell interaction leads to superior killing dynamics of individual T-cells. We used high-throughput time-lapse imaging microscopy in nanowell grids (TIMING) assays, which evaluate CAR T-cell engagement and killing dynamics at a single-cell level at various effector to target (E:T) ratios, as previously described [40]. We measured the time T-cells seek BL-ALL cells (T^{seek}), the duration in contact (T^{contact}), and the time to target death once effector-target conjugation is initiated (T^{death}) (Fig. 3f, g and Video S1). CD19/20/22CAR T-cells took significantly longer time to seek target cells and kill their first target compared with CD19CAR T-cells. Thereafter, T^{contact} and T^{death} were significantly shorter with subsequent targets, as CD19/20/22CAR T-cells were able to initiate apoptosis of the BL-ALL cells more efficiently (Fig. 3h–j). Collectively, we observed a higher frequency of second and third (Fig. 3k) serial target killing by a single CD19/20/22CAR T-cell, a higher overall total number of targets killed, and a significantly lower failure rate compared with CD19CAR T-cells. The superiority of CD19/20/22CAR T-cells observed in population-based killing assays could thus be attributable to more efficient anti-leukemic activity of individual CAR T-cells.

Polyfunctional CD19/20/22CAR T-cells effectively target CD19(−) escape BL-ALL

First, we confirmed that that CD19/20/22CAR T-cells could readily mediate a CARIS formation with both CD19(+) and CD19(−) BL-ALL cells (Fig. 4a). As expected, CD19CAR T-cells failed to mediate such a synapse with CD19(−) BL-ALL cells.
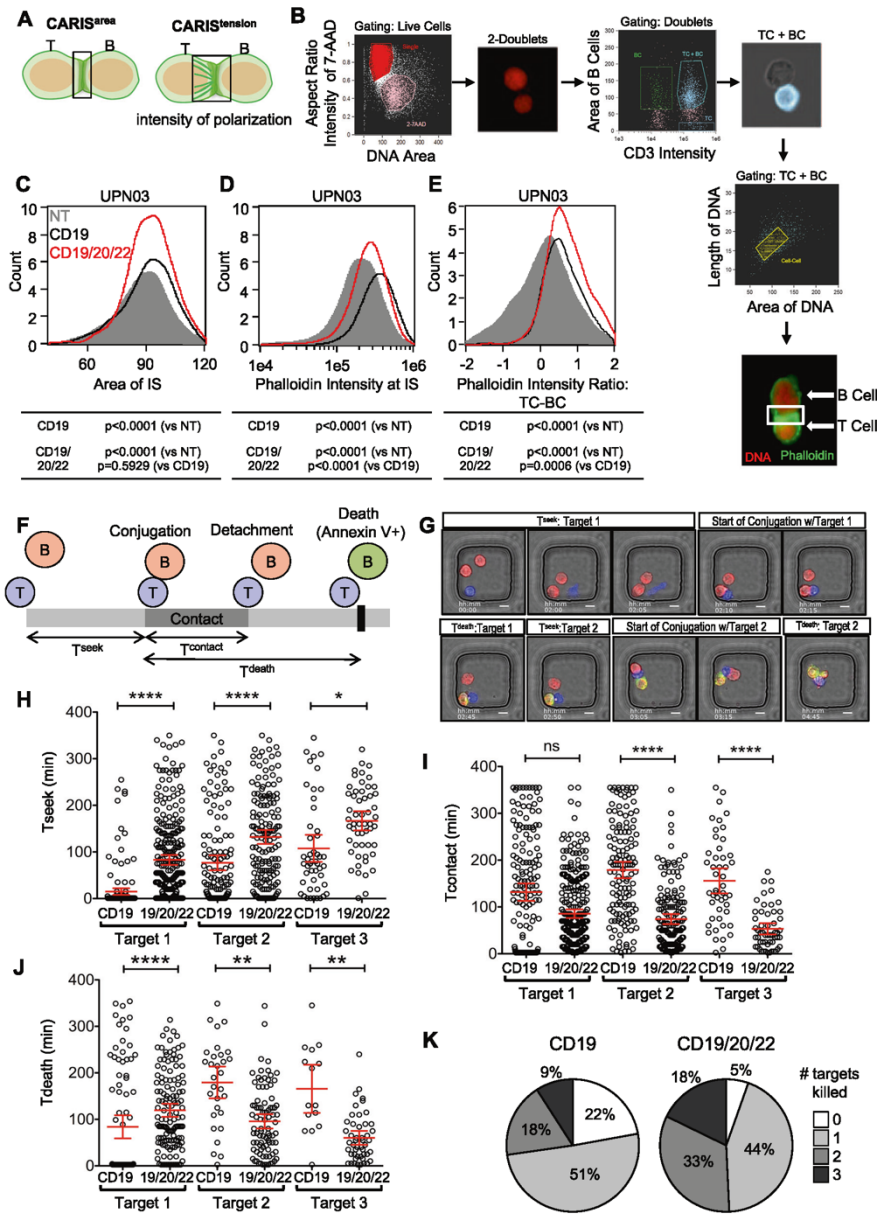
To model the scenario of CD20 and CD22 expression in the absence of CD19, we force-expressed CD20, CD22, and/or CD19 on Daoy and sorted distinct populations based on antigen expression (Fig. S2B). We then tested the cytolytic activity of CD19/20/22CAR, CD19CAR, and NT T-cells against CD19+CD20+CD22+ and CD19-CD20+

◀ **Fig. 3 CD19/20/22CAR T cells have increased immunoactivity and serial killing activity at the single-cell level. a** Schematic illustrating the parameters assessed in the chimeric antigen receptor immune synapse (CARIS). **b** UPN03 cells were cocultured with NT, CD19CAR, or CD19/20/22CAR T-cells at a ratio of 1:1 for 1 h. After incubation, cells were analyzed for expression of CD3 (BV450), phalloidin (FITC), and 7-AAD using ImageStream. ($n = 3$) Duplex cells were separated from single cells by DNA contents and aspect ratio of 7-AAD. Intact T and B (BL-ALL) cells were identified by CD3 intensity and area of CD3(−), respectively. Duplex cells containing both T and B cells were selected for further analysis. Formation of immune synapses between T and B cells were defined by length and area of two DNA clusters between duplex cells. The final image exemplifies the characterization of a CARIS. The DNA is shown as red and F-actin (phalloidin staining) as green. The area boxed in white is the immune synapse (IS) area that is quantified in the analysis. Quantification of (**c**) the area encompassed by the IS (CARIS^{area}), (**d**) the intensity of F-actin (phalloidin) at the CARIS (CARIS^{density}), and (**e**) the ratio of intensity of phalloidin between T-cells to B-cells (BL-ALL) (CARIS^{tension}). The frequency of each parameter for NT (gray), CD19CAR (black), and CD19/20/22CAR (red) T-cells is shown in a histogram. 1×10^5 events were assessed; two-way ANOVA was performed for statistical analysis, and $p < 0.05$ was considered significant. (**f–k**) CD19CAR or CD19/20/22CAR T-cells were incubated with UPN02 cells at an E:T ratio of 1:3 to assess their cytolysis activity at the single-cell level using a TIMING nanowell assay. (**f**) Schematic depicting measurements quantified by TIMING assay. (**g**) Microscopy images representing T^{seek}, T^{contact}, and T^{death} parameters. Scale bars represent 10 μm. (**h–j**): Quantification of the time spent (**h**) searching for target by T-cells (T^{seek}), (**i**) the duration of contact maintained between an individual CAR T-cell and their first, second, and third target (T^{contact}), and (**j**) the time to apoptosis of individual target cells since the start of conjugation (T^{death}) at an E:T ratio of 1:3. Each data point represents a single effector cell. $****p < 0.0001$, $**p < 0.01$, $*p < 0.05$, ns = > 0.05; Kruskall–Wallis test with Dunn's multiple correction. Data are presented as mean ± 95% confidence interval. (**k**) Pie chart comparing proportion of CD19CAR and CD19/20/22CAR T-cells able to kill multiple targets when plated at an E:T ratio of 1:3. >165 individual wells were analyzed for each effector cell type.

CD22+targets. CD19/20/22CAR T-cells were significantly better killers of CD19- targets, both in short- (Fig. 4b) and long-term (Fig. 4c) assays compared with CD19CAR T-cells. We then used primary patient leukemia, UPN02, UPN02 CD19-KO, and two post-CD19CAR T-cell escape relapsed BM samples, rUPN21-R and rUPN22-R, as targets and observed that CD19/20/22CAR T-cells induced significantly higher lysis (Fig. 4d) and produced significantly higher levels of the T$_H$1 cytokines TNF-α (Fig. 4e) and IFN-γ (Fig. 4f).

Next, we performed single-cell cytokine profiling on the CAR and NT T-cells in the presence and absence of CD19 expression on the target cell, using polyfunctionality in response to BL-ALL associated antigens as a readout. Polyfunctionality is defined as the ability of such T cells to secrete ≥2 cytokines. Individual CD19/20/22CAR T-cells showed greater antigen-specific polyfunctionality upon stimulation with CD19+ (Raji) and CD19− (Raji.CD19KO) targets (Fig. S2C), compared with CD19CAR and NT T-cells (Fig. 4g [left panel] and S4). PAT PCA was used to group

polyfunctional cell subsets based on common protein combinations. The common expression of Granzyme B, IFN-γ, MIP-1α, MIP-1β, sCD137 components defined a deeply effector-skewed polyfunctional subset, which drove polyfunctional heterogeneity and was predominately upregulated in CD19/20/22CAR (Fig. S5) compared with CD19CAR and NT T-cells. The PSI, a measure for potency, was significantly higher in CD19/20/22CAR T-cells compared with CD19CAR and NT T-cells (Fig. 4g [Right panel]). The enhanced PSI of the CD19/20/22CAR T-cells was primarily composed of secreted effector proteins. We then tested the single-cell polyfunctional activity of CD19/20/22CAR, CD19CAR, and NT T-cells against single or various combinations of CD19, CD20, and CD22 targets. As shown in Fig. 4h, single-cell functionality profiling showed that CD19/20/22CAR T-cells had increased polyfunctionality compared with CD19CAR or NT T-cells.

These results demonstrate that CD19/20/22CAR T-cells can mediate an effective CARIS with CD19(−) BL-ALL targets and can exhibit robust antitumor immune reactivity and retain considerable polyfunctionality in the face of CD19 loss.

CD19/20/22 CAR T-cells demonstrate anti-leukemic activity in vivo against CD19(−) and CD19(+) BL-ALL

We next evaluated the antitumor efficacy of CD19/20/22CAR T-cells against CD19(−) escape in two models of CD19(−) BL-ALL. First, we modified Raji cells using CRISPR/Cas9 to knockout CD19 and subsequently expressed an eGFP-firefly luciferase (eGFP.FFLuc) reporter gene by retroviral transduction. Cells were sorted based on CD19(−)GFP(+) status (Raji CD19-KO) (Fig. S2C) then engrafted into NSG mice. Mice were treated with CD19/20/22CAR, CD19CAR, or NT T-cells, and bioluminescence imaging (BLI) was used to monitor the tumor burden over time. Only CD19/20/22CAR T-cells mediated an antitumor response, inducing a rapid initial decrease in tumor burden followed by delayed progression (Fig. 5a). All mice treated with CD19CAR and NT T-cells progressed steadily. CD19/20/22CAR T-cells induced a significant delay in tumor progression (Fig. 5b). In addition, we tested CD19/20/22CAR T-cells in mice transplanted with rUPN21-R, a primary B-lineage BL-ALL exhibiting CD19-escape after CD19CAR T-cell therapy. Significant weight loss and hindlimb paralysis were used as signs of progression and as indications for euthanasia. At 45 days, all CD19/20/22CAR mice were alive, whereas 50% of CD19CAR and NT T-cell treated mice had succumbed to disease (Fig. 5c).

Finally, we assess the in vivo efficacy of CD19/20/22CAR T-cells against CD19+ disease compared with CD19CAR T-cells. NSG mice were engrafted with CD19+CD20+CD22+
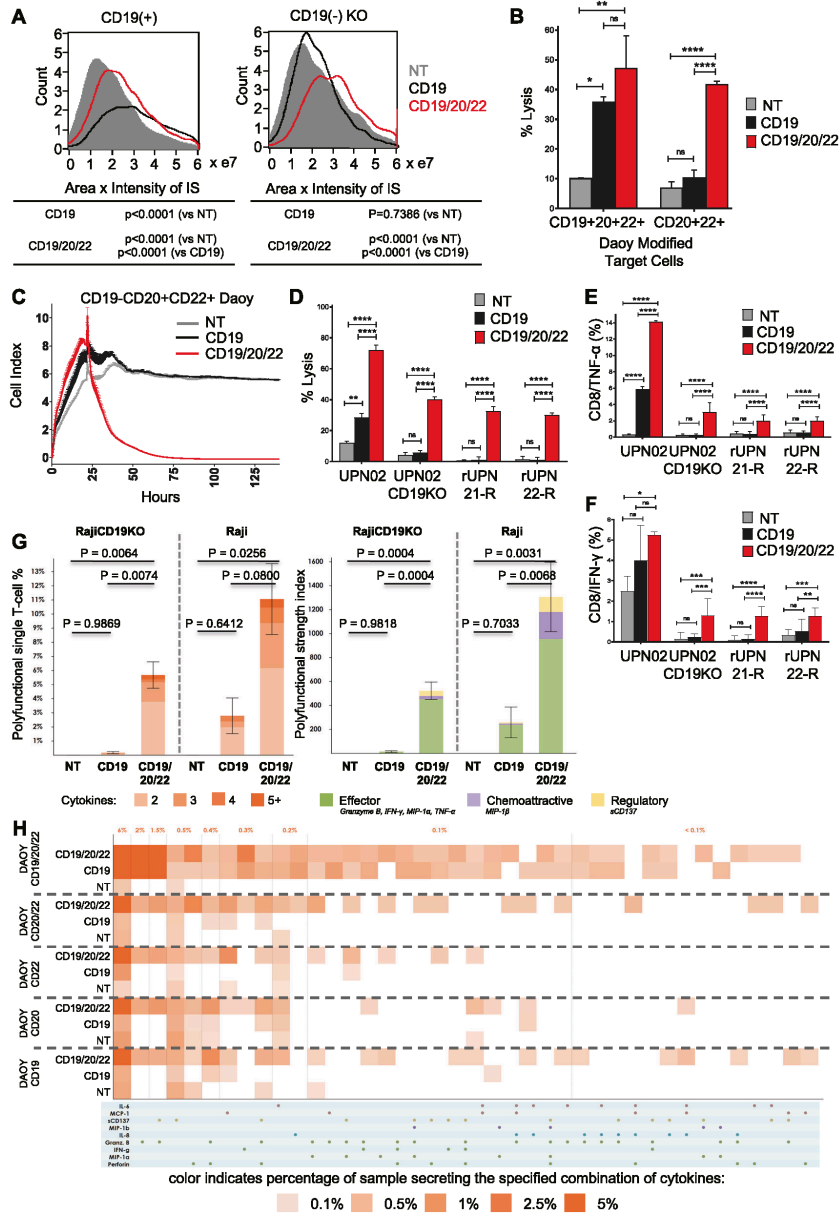
UPN03 cells transduced with an eGFP-firefly luciferase (eGFP.FFLuc) reporter gene and treated with CD19/20/22CAR, CD19CAR, or NT T-cells. The tumor burden was assessed over time using BLI. The tumors were controlled equally well by CD19/20/22CAR T-cells as by CD19CAR T-cells while NT T-cells failed to exhibit measurable antitumor

CAR T-cells that target acute B-lineage leukemia irrespective of CD19 expression

◀ **Fig. 4 Trivalent CAR T-cells overcome CD19(−) antigen escape in primary BL-ALL. a** Image stream analysis was performed as described in Fig. 3. The area × intensity of phalloidin in the CARIS is quantified for NT, CD19CAR, and CD19/20/22CAR T-cells in their interaction with CD19-expressing and CD19 KO target cells. **b** Eight hours ^{51}Cr release assay targeting cells over-expressing CD19, CD20, and CD22 (triple positive) or CD20 and CD22 (double positive) cells at an E:T ratio of 5:1 ($n = 2$). **c** Long-term impedance-based xCEL-Ligence killing assay targeting double positive (CD20+CD22+) but CD19- cells that are described in Fig. S2B. Target cells were cultured for ~24 h before NT, CD19CAR, or CD19/20/22CAR T-cells were added in a 1:3 E:T ratio. Tumor cell lysis, represented by a decrease in cell index, was measured over time ($n = 2$). **d** Target BL-ALL cells (UPN02, UPN02 CD19KO, rUPN21-R, rUPN22-R) were cocultured with NT or CAR T-cells at an E:T ratio of 3:1 for 4 h and cell lysis was determined by ^{51}Cr assay (data shown are representative data, $n = 3$). **$p < 0.01$, ****$p < 0.0001$, one-way ANOVA with Tukey's multiple comparison post-test. BL-ALL target cells (UPN02, UPN02 CD19KO, rUPN21-R, rUPN22-R) were cocultured with T-cells in the presence of brefeldin A at an E:T ratio of 10:1 for 4 h. Cells were stained to determine levels of intracellular **(e)** TNF-α + CD8 + T-cells or **(f)** IFN-γ + CD8+T-cells. NT T-cells serve as a negative control in all experiments ($n = 3$). **$p < 0.01$, ***$p \leq 0.001$, ****$p < 0.0001$, one-way ANOVA with Tukey's multiple comparison post-test. **(g–h)** CD19+ and CD19- target cells were cocultured with CD8+ isolated CD19/20/22CAR, CD19CAR, and NT T-cells, and single-cell polyfunctionality assessed via a 32-plex antibody barcoded chip analysis. **(g)** Polyfunctionality evaluation of the number and subset classification of cytokines produced by single cells in response to antigen-specific stimulation **(h)** Single-cell functional heatmap demonstrates proportions of polyfunctional subsets of T-cells in response to Daoy cells transduced with various combinations of tumor antigens. Each column corresponds to a specific cytokine or combination of cytokines, and the orange squares represent the frequency at which the cytokine set was secreted by the corresponding sample. The cytokine groups are ordered by overall frequency across all samples.

efficacy (Fig. 5d). CD19/20/22CAR and CD19CAR T-cells also comparably improved the time to progression probability of the treated mice (Fig. 5e). Altogether, these results demonstrate that CD19/20/22CAR T-cells are as effective against CD19-expressing BL-ALL as CD19CAR T-cells but only CD19/20/22CAR T-cells are able to provide tumor control against CD19(−) escape disease.

Discussion

In general, CD19 is ubiquitously expressed on primary pre-B ALL, and approximately half of cases express CD20, with CD22 high expression on about 80–90% of cases [12]. However, the emerging problem of CD19(−) escape after CD19-directed immunotherapies [2, 3, 6–11] compromises the success of these breakthrough approaches. Similarly, even CD22(−) escape was reported in a phase 1 clinical trial of CD22CAR T-cells [16]. Here, we found that following CD19CAR T-cell therapy, expression of CD19 varied from ubiquitous (e.g., UPN20-R) to, more commonly, less than 10% of cells. On the other hand, CD22 and

CD20 were expressed at varying percentages in samples from both diagnosis and relapse, as reported by others [20]. Thus, CD19(−) escape variants downregulate but not altogether eliminate CD20 and CD22 cell surface expression. We conclude that CD19, CD22, or CD20 target densities are unpredictable and likely to vary in relapsed patients. This raises the question if a minimum antigen threshold exists to provoke a productive CAR T-cell response. Although a signal threshold does appear to exist for T-cell receptor-mediated signaling, much less is known regarding T-cells expressing a CAR. One study reported that the combination of CAR density and tumor antigen density regulated T-cell potency in mouse models [48] but overall little is known. Hamieh et al. [49]. more recently addressed this important point in depth by comparing CAR T-cell activities against NALM6 cells with mono- or biallelic knockout of CD19, finding that the configuration of the intracellular CAR domain [-BBζ vs −28ζ] together with the target density of CD19 determined the threshold efficacy for CAR T-cell activation and target cell lysis. Interestingly, the authors also showed that a combination of CD19CAR-28ζ with CD22CAR-BBζ CARs expressed in the same T cell provided a significant benefit in mouse models with low Nalm6 CD19 and CD22 target densities. These results concur with our studies and suggest that the addition of CD20 in our product is likely to further mitigate the deleterious effects of low target densities on the target cell. Taking these findings into account we used a variety of primary BL-ALL samples and models with differential CD19, CD20, and CD22 expression profiles as observed in patients and generated a trivalent CAR T-cell targeting all three antigens.

Our CAR T-cell design incorporated a number of features to support high CAR expression. First, we used in silico modeling that relies on analysis of the stereo-electric coaptation of the three CAR recognition exodomains to avoid detrimental conformations in this complex biologic as used here. One potential confounding factor was that we needed to include three CAR endodomains in a single DNA construct. As previously described, homologous recombination between the repeated sequences and increased RNA secondary structure formation may be problematic with this approach [46]. Thus, to optimize the production of the three identical CAR endodomains we "wobbled" –namely, used alternative DNA coding sequences that transcribe into the same amino acid sequence [46]. This strategy optimizes protein production and increases the effective surface expression of each distinct CAR. Indeed, the three CARs were expressed at similarly high levels (63–67%) on the surface and were comparable to the expression of the single CD19CAR. Finally, to facilitate clinical translation, we used a single transgene to express the three CAR molecules, which theoretically decreases the risk of insertional
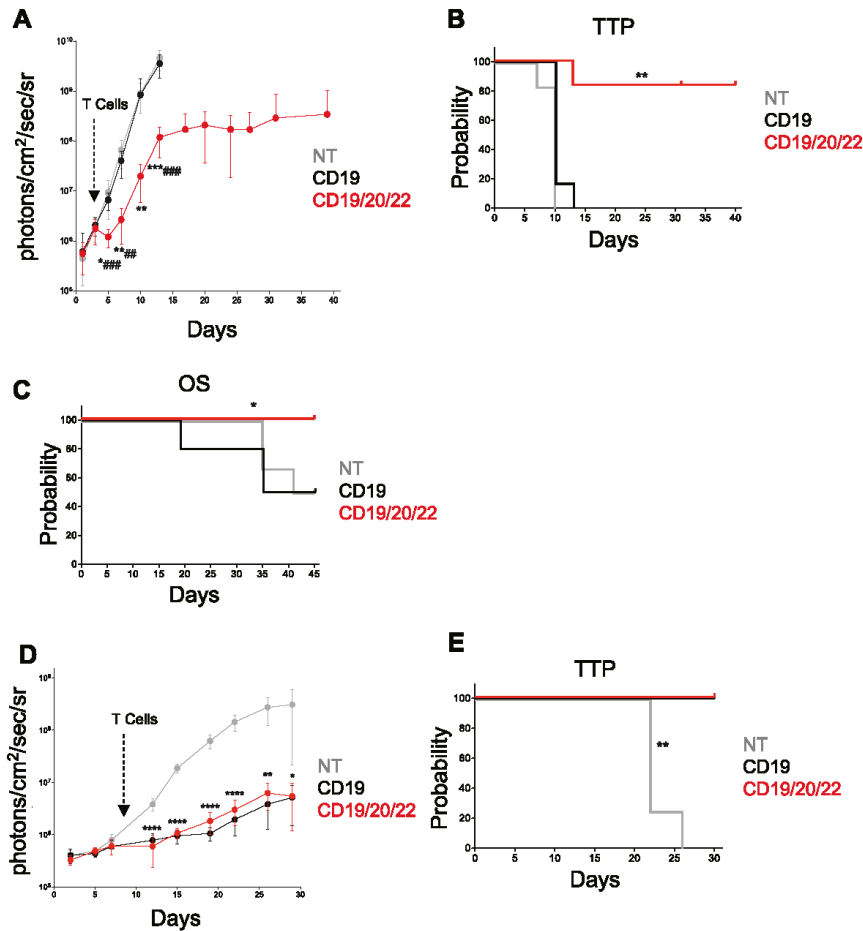
Fig. 5 CD19/20/22CAR T-cell efficacy in xenograft models of CD19(−) disease. a, b Mice were administered Raji.CD19KO.GFP. FFLuc cells (Fig. S2C) on day 0 followed by NT, CD19CAR, or CD19/20/22CAR T-cells on day 3 ($n = 6$ mice per group). Biolumi-nescent signal was tracked and quantified over the course of 40 days. a The average BLI ± SD for each group is displayed. (*denotes comparisons between NT and CD19/20/22CAR, # denotes CD19CAR vs CD19/20/22CAR; *$p < 0.05$, **$p < 0.01$, ***$p < 0.001$; ## $p < 0.01$, ### $p \leq 0.001$, one-way ANOVA with Tukey's post-test). b Time to progression (TTP) represented as Kaplan–Meier estimate (tumor bur-den of 1×10^8 photons/cm²/sec/sr considered as disease progression); **$p = 0.0013$ NT vs CD19/20/22CAR, $p = 0.0017$ CD19 vs CD19/20/22CAR, Gehan-Breslow-Wilcoxon test. c Overall survival in mice transplanted with rUPN21-R, a primary BL-ALL exhibiting CD19-escape after CD19CAR T-cell therapy. Injection with rUPN21-R cells

on day 0 followed by T-cells on days 3 and 7: NT ($n = 6$ mice), CD19CAR ($n = 10$ mice), or CD19/20/22CAR ($n = 10$ mice). Mice were monitored for signs of disease, weight loss, and general well-being, and overall survival was quantified after 45 days. (*$p = 0.0015$ NT vs CD19/20/22CAR, $p = 0.0126$ CD19 vs CD19/20/22CAR, Gehan-Breslow-Wilcoxon test). d, e Mice were administered UPN03. GFP.FFLuc cells on day 0 followed by NT ($n = 4$ mice), CD19CAR ($n = 5$ mice), or CD19/20/22CAR ($n = 4$ mice) T-cells on day 9. d Bioluminescent signal (BLI) was recorded and average BLI ± SD quantified over 30 days (*$p < 0.05$, **$p < 0.01$, ****$p < 0.0001$; NT vs CD19 or CD19/20/22CAR; one-way ANOVA with Tukey's post-test) (E) Time to tumor progression (tumor burden of 1×10^8 photons/cm²/sec/sr considered as disease progression) represented as Kaplan–Meier estimate; **$p = 0.0047$ NT vs CD19CAR and NT vs CD19/20/22CAR, Gehan-Breslow-Wilcoxon Test.

mutagenesis compared with repeated, separate integrations of multiple genes and associated promoters into the T-cell genome.

When we compared the CD19/20/22CAR to the CD19 single CAR using in vitro functional testing against target cells, CD19/20/22CAR T-cells exhibited superior

SPRINGER NATURE

cytolytic activity compared with CD19CAR T-cells, both against modified Daoy cells and against three primary BL-ALLs with differential expression of CD20 and CD22. We observed differences in the kinetics of CAR T-cell interactions with BL-ALL cells that could explain the superior killing activity of CD19/20/22CAR T-cells, and indeed they were significantly better serial killers. Specifically, as the CARIS and its important structural component F-actin are critical for target killing [47], we quantitated F-actin in the IS and the intensity of cell polarization. The CD19/20/22CAR CARIS contained more F-actin, and the nuclei of target and T-cells reached closer proximity compared with target and CD19CAR T-cell nuclei. We speculate that this could be a reason why CD19/20/22CAR T-cells needed more time to repolarize, engage and form a CARIS, and also disassemble and reassemble the structures needed to support target cell lysis and switch to the migratory program, resulting in a longer T_{seek} time than CD19CAR T-cells. These combined properties of CD19/20/22CAR T-cells, which form a synapse that is stronger but has a shorter span of existence, suggest that some T-cells can integrate the strength of the CARIS with the contact time to produce a uniform cytotoxic response. The latter could explain the performance of individual CAR T-cells upon polyfunctional profiling. When evaluated on the single-cell level, CD19/20/22CAR T-cells had significantly higher polyfunctionality, as measured by PSI, against CD19+ and CD19− targets than CD19CAR T-cells. In previous studies, higher PSI values were associated with higher effector cell potency in in vivo preclinical models [50], revealed differences in CAR T-cell product optimization [51], and predicted patient response to CAR T-cell therapy [44]. Together, the CARIS and PSI findings support a potential advantage of CD19/20/22CAR in clinical applications.

On a functional level, the assessment of T-cell activation upon target encounter collectively showed that CD19/20/22CAR T-cells are adaptively more activated upon encounter of their target(s). We evaluated their phenotypic activation/exhaustion profile and observed that CD19/20/22CAR T-cells are more activated upon encounter of either CD19+ or CD19+CD22+CD22+ when compared with CD19CAR T-cells (Fig. S6A, B). The expression levels of PD-1 and LAG-3 on CD19/20/22CAR T-cells upon encounter of CD19+ targets were comparable to CD19CAR T-cells, yet they exhibited more PD-1 and LAG-3 only upon encounter of CD19+CD20+CD22+targets (Fig. S6C, D). Interestingly, we observed precipitous CD19CAR downregulation in both CD19/20/22CAR T-cells and CD19CAR T-cells upon encounter of CD19+ targets. Only CD19/20/22CAR T-cells maintained CD20 and CD22 CAR expression and consequently their activity against these target molecules (Fig. S7). The expression of activation/exhaustion molecules has traditionally been used

to describe a phenotype of immune cells, yet the functional indices of activation (cytokine, killing, multiplex cytokine) and sustenance of functionality in the face of exhaustion (individual cell serial killing, xCelligence, and animal experiments) should be considered for a more complete functionality profile.

To confirm the advantages observed in our in vitro findings, we tested the activity of the CD19/20/22CAR T-cells in vivo. We found that in NSG xenograft models, the CD19/20/22CAR T-cells were able to overcome the inability of CD19CAR T-cells to control growth of CD19(−) leukemia cells from patients who failed CD19CAR T-cell therapy, as well as of the genetically-modeled CD19(−) escape variants (Raji.CD19KO). Importantly, CD19/20/22CAR T-cells were as efficacious as CD19CAR T-cells against primary relapse CD19(+) BL-ALL. Simultaneous targeting of CD19 and CD22 reduced the risk of CD19-relapse compared with "single targeting" in a human study reported by Wang et al. [52]. In this work studying the efficacy and safety of CAR19/22 T-cell cocktail therapy in patients with refractory/relapsed B-cell malignancies, only one of 89 patients (1.1%) relapsed with CD19 negative disease with a median follow-up of 14.4 months (range, 0.4–27.4). This is in sharp contrast to the reports of CD19 negative relapse (18–25%) from various clinical trials infusing CD19CAR T-cells [53]. To rigorously test whether the CD19/20/22CAR T-cell would reduce the upfront chance of CD19-/lo relapse, a similarly designed human trial would be warranted.

CAR T-cells that target multiple tumor antigens were shown in our previous work to overcome low levels of tumor antigen expression [29]. For the specific treatment of BL-ALL, we have increased the activity and broadened the spectrum of CD19CAR T-cells by targeting two additional antigens and extended the therapeutic reach of the T-cell product to other CD20-expressing lympho-reticular malignancies. Thus, a single CAR T-cell product targeting all three antigens provides the advantage of applicability to a broader population of patients with BL-ALL and to a more comprehensive range of other B-lineage malignancies, which routinely express higher levels of CD20 [54]. We note that although the target density of CD19, CD20, and CD22 antigens on individual diagnosis and relapsed patient cells is unpredictable, and the degree to which CD19, CD20, or CD22 are targeted individually cannot be deduced from our data, our results suggest these may not be key factors relevant for effective cell killing by our trivalent CAR T-cells. Thus, although the toxicity of our CAR T-cell product will need to be assessed in carefully designed human trials, the effectiveness of CD19/20/22CAR T-cells against CD19(−) escape BL-ALL and CD19(+) BL-ALL alike compares very favorably to that of the benchmark CD19CAR T-cells.

Compliance with ethical standards

Publisher's note Springer Nature remains neutral with regard to jurisdictional claims in published maps and institutional affiliations.

References

1. Davila ML, Riviere I, Wang X, Bartido S, Park J, Curran K, et al. Efficacy and toxicity management of 19-28z CAR T cell therapy in B cell acute lymphoblastic leukemia. Sci Transl Med. 2014;6:224ra25.
2. Grupp SA, Kalos M, Barrett D, Aplenc R, Porter DL, Rheingold SR, et al. Chimeric antigen receptor-modified T cells for acute lymphoid leukemia. N Engl J Med 2013;368:1509–18.
3. Lee DW, Kochenderfer JN, Stetler-Stevenson M, Cui YK, Delbrook C, Feldman SA, et al. T cells expressing CD19 chimeric antigen receptors for acute lymphoblastic leukaemia in children and young adults: a phase 1 dose-escalation trial. Lancet. 2015;385:517–28.
4. Maude SL, Frey N, Shaw PA, Aplenc R, Barrett DM, Bunin NJ, et al. Chimeric antigen receptor T cells for sustained remissions in leukemia. N Engl J Med. 2014;371:1507–17.
5. Turtle CJ, Hanafi LA, Berger C, Gooley TA, Cherian S, Hudecek M, et al. CD19 CAR-T cells of defined CD4+:CD8+ composition in adult B cell ALL patients. J Clin Invest. 2016;126:2123–38.
6. Braig F, Brandt A, Goebeler M, Tony HP, Kurze AK, Nollau P, et al. Resistance to anti-CD19/CD3 BiTE in acute lymphoblastic leukemia may be mediated by disrupted CD19 membrane trafficking. Blood. 2017;129:100–4.
7. Grupp SA, Maude SL, Shaw PA, Aplenc R, Barrett DM, Callahan C, et al. Durable remissions in children with relapsed/refractory ALL treated with T cells engineered with a CD19-targeted chimeric antigen receptor (CTL019). Blood. 2015;126:681.
8. Topp MS, Gokbuget N, Zugmaier G, Degenhard E, Goebeler ME, Klinger M, et al. Long-term follow-up of hematologic relapse-free survival in a phase 2 study of blinatumomab in patients with MRD in B-lineage ALL. Blood. 2012;120:5185–7.
9. Sotillo E, Barrett DM, Black KL, Bagashev A, Oldridge D, Wu G, et al. Convergence of acquired mutations and alternative splicing of CD19 enables resistance to CART-19 immunotherapy. Cancer Discov. 2015;5:1282–95.
10. Gardner R, Wu D, Cherian S, Fang M, Hanafi LA, Finney O, et al. Acquisition of a CD19-negative myeloid phenotype allows immune escape of MLL-rearranged B-ALL from CD19 CAR-T-cell therapy. Blood. 2016;127:2406–10.
11. Nagel I, Bartels M, Duell J, Oberg HH, Ussat S, Bruckmueller H, et al. Hematopoietic stem cell involvement in BCR-ABL1-positive ALL as a potential mechanism of resistance to blinatumomab therapy. Blood. 2017;130:2027–31.
12. Zhou Y, You MJ, Young KH, Lin P, Lu G, Medeiros LJ, et al. Advances in the molecular pathobiology of B-lymphoblastic leukemia. Hum Pathol. 2012;43:1347–62.
13. Bielamowicz K, Fousek K, Byrd TT, Samaha H, Mukherjee M, Aware N, et al. Trivalent CAR T cells overcome interpatient antigenic variability in glioblastoma. Neuro-Oncol. 2018;20: 506–18.
14. Hegde M, Corder A, Chow KK, Mukherjee M, Ashoori A, Kew Y, et al. Combinational targeting offsets antigen escape and enhances effector functions of adoptively transferred T cells in glioblastoma. Mol Ther J Am Soc Gene Ther. 2013;21: 2087–101.
15. Ruella M, Maus MV. Catch me if you can: leukemia escape after CD19-directed T cell immunotherapies. Comput Struct Biotechnol J. 2016;14:357–62.
16. Fry TJ, Shah NN, Orentas RJ, Stetler-Stevenson M, Yuan CM, Ramakrishna S, et al. CD22-targeted CAR T cells induce remission in B-ALL that is naive or resistant to CD19-targeted CAR immunotherapy. Nat Med. 2018;24:20–8.
17. Martyniszyn A, Krahl AC, Andre MC, Hombach AA, Abken H. CD20-CD19 bispecific CAR T cells for the treatment of B-cell malignancies. Hum Gene Ther. 2017;28:1147–57.
18. Qin H, Ramakrishna S, Nguyen S, Fountaine TJ, Ponduri A, Stetler-Stevenson M, et al. Preclinical development of bivalent chimeric antigen receptors targeting both CD19 and CD22. Mol Ther Oncolytics. 2018;11:127–37.
19. Zah E, Lin MY, Silva-Benedict A, Jensen MC, Chen YY. T cells expressing CD19/CD20 bispecific chimeric antigen receptors prevent antigen escape by malignant B cells. Cancer Immunol Res. 2016;4:498–508.
20. Schneider D, Xiong Y, Wu D, Nlle V, Schmitz S, Haso W, et al. A tandem CD19/CD20 CAR lentiviral vector drives on-target and off-target antigen modulation in leukemia cell lines. J Immunother Cancer. 2017;5:42.
21. Bhojwani D, Sposto R, Shah NN, Rodriguez V, Yuan C, Stetler-Stevenson M, et al. Inotuzumab ozogamicin in pediatric patients

CAR T-cells that target acute B-lineage leukemia irrespective of CD19 expression

with relapsed/refractory acute lymphoblastic leukemia. Leukemia. 2019;33:884–92.

22. Shalabi H, Kraft IL, Wang HW, Yuan CM, Yates B, Delbrook C, et al. Sequential loss of tumor surface antigens following chimeric antigen receptor T-cell therapies in diffuse large B-cell lymphoma. Haematologica. 2018;103:e215–e8.

23. Yu H, Sotillo E, Harrington C, Wertheim G, Paessler M, Maude SL, et al. Repeated loss of target surface antigen after immunotherapy in primary mediastinal large B cell lymphoma. Am J Hematol. 2017;92:E11–E13.

24. Maury S, Huguet F, Leguay T, Lacombe F, Maynadie M, Girard S, et al. Adverse prognostic significance of CD20 expression in adults with Philadelphia chromosome-negative B-cell precursor acute lymphoblastic leukemia. Haematologica 2010;95:324–8.

25. Thomas DA, O'Brien S, Jorgensen JL, Cortes J, Faderl S, Garcia-Manero G, et al. Prognostic significance of CD20 expression in adults with de novo precursor B-lineage acute lymphoblastic leukemia. Blood. 2009;113:6330–7.

26. Maury S, Chevret S, Thomas X, Heim D, Leguay T, Huguet F, et al. Rituximab in B-lineage adult acute lymphoblastic leukemia. N Engl J Med. 2016;375:1044–53.

27. Ruella M, Barrett DM, Kenderian SS, Shestova O, Hofmann TJ, Perazzelli J, et al. Dual CD19 and CD123 targeting prevents antigen-loss relapses after CD19-directed immunotherapies. J Clin Invest. 2016;126:3814–26.

28. George AA, Paz H, Fei F, Kirzner J, Kim YM, Heisterkamp N, et al. Phosphoflow-based evaluation of Mek inhibitors as small-molecule therapeutics for B-cell precursor acute lymphoblastic leukemia. PLoS ONE. 2015;10:e0137917.

29. Hegde M, Mukherjee M, Grada Z, Pignata A, Landi D, Navai SA, et al. Tandem CAR T cells targeting HER2 and IL13Ralpha2 mitigate tumor antigen escape. J Clin Invest. 2016;126:3036–52.

30. DiMaio F, Tyka MD, Baker ML, Chiu W, Baker D. Refinement of protein structures into low-resolution density maps using rosetta. J Mol Biol. 2009;392:181–90.

31. Nicholson IC, Lenton KA, Little DJ, Decorso T, Lee FT, Scott AM, et al. Construction and characterisation of a functional CD19 specific single chain Fv fragment for immunotherapy of B lineage leukaemia and lymphoma. Mol Immunol. 1997;34:1157–65.

32. Haso W, Lee DW, Shah NN, Stetler-Stevenson M, Yuan CM, Pastan IH, et al. Anti-CD22-chimeric antigen receptors targeting B-cell precursor acute lymphoblastic leukemia. Blood. 2013;121:1165–74.

33. Weiner GJ. Rituximab: mechanism of action. Semin Hematol. 2010;47:115–23.

34. Riviere I, Brose K, Mulligan RC. Effects of retroviral vector design on expression of human adenosine deaminase in murine bone marrow transplant recipients engrafted with genetically modified cells. Proc Natl Acad Sci USA. 1995;92:6733–7.

35. Ahmed N, Salsman VS, Kew Y, Shaffer D, Powell S, Zhang YJ, et al. HER2-specific T cells target primary glioblastoma stem cells and induce regression of autologous experimental tumors. Clin Cancer Res. 2010;16:474–85.

36. Cornetta K, Pollok KE, Miller AD. Transduction of cell lines by retroviral vectors. CSH Protoc. 2008;2008:pdb prot4883.

37. Jena B, Maiti S, Huls H, Singh H, Lee DA, Champlin RE, et al. Chimeric antigen receptor (CAR)-specific monoclonal antibody to detect CD19-specific T cells in clinical trials. PLoS ONE. 2013;8: e57838.

38. Gundry MC, Brunetti L, Lin A, Mayle AE, Kitano A, Wagner D, et al. Highly efficient genome editing of murine and human

39. hematopoietic progenitor cells by CRISPR/Cas9. Cell Rep. 2016;17:1453–61.

39. Gottschalk S, Edwards OL, Sili U, Huls MH, Goltsova T, Davis AR, et al. Generating CTLs against the subdominant Epstein-Barr virus LMP1 antigen for the adoptive immunotherapy of EBV-associated malignancies. Blood. 2003;101:1905–12.

40. Liadi I, Singh H, Romain G, Rey-Villamizar N, Merouane A, Adolacion JR, et al. Individual motile CD4(+) T cells can participate in efficient multikilling through conjugation to multiple tumor cells. Cancer Immunol Res. 2015;3:473–82.

41. Romain G, Senyukov V, Rey-Villamizar N, Merouane A, Kelton W, Liadi I, et al. Antibody Fc engineering improves frequency and promotes kinetic boosting of serial killing mediated by NK cells. Blood. 2014;124:3241–9.

42. An X, Sendra VG, Liadi I, Ramesh B, Romain G, Haymaker C, et al. Single-cell profiling of dynamic cytokine secretion and the phenotype of immune cells. PLoS ONE. 2017;12:e0181904.

43. Merouane A, Rey-Villamizar N, Lu Y, Liadi I, Romain G, Lu J, et al. Automated profiling of individual cell-cell interactions from high-throughput time-lapse imaging microscopy in nanowell grids (TIMING). Bioinformatics. 2015;31:3189–97.

44. Rossi J, Paczkowski P, Shen YW, Morse K, Flynn B, Kaiser A, et al. Preinfusion polyfunctional anti-CD19 chimeric antigen receptor T cells are associated with clinical outcomes in NHL. Blood. 2018;132:804–14.

45. Xue Q, Bettini E, Paczkowski P, Ng C, Kaiser A, McConnell T, et al. Single-cell multiplexed cytokine profiling of CD19 CAR-T cells reveals a diverse landscape of polyfunctional antigen-specific response. J Immunother Cancer. 2017;5:85.

46. Demidenko AA, Blattman JN, Blattman NN, Greenberg PD, Nibert ML. Engineering recombinant reoviruses with tandem repeats and a tetravirus 2A-like element for exogenous polypeptide expression. Proc Natl Acad Sci USA. 2013;110:E1867–76.

47. Mukherjee M, Mace EM, Carisey AF, Ahmed N, Orange JS. Quantitative imaging approaches to study the CAR immunological synapse. Mol Ther: J Am Soc Gene Ther. 2017;25:1757–68.

48. Walker AJ, Majzner RG, Zhang L, Wanhainen K, Long AH, Nguyen SM, et al. Tumor antigen and receptor densities regulate efficacy of a chimeric antigen receptor targeting anaplastic lymphoma kinase. Mol Ther. 2017;25:2189–201.

49. Hamieh M, Dobrin A, Cabriolu A, van der Stegen SJC, Giavridis T, Mansilla-Soto J, et al. CAR T cell trogocytosis and cooperative killing regulate tumour antigen escape. Nature. 2019;568:112–6.

50. Klapper JA, Downey SG, Smith FO, Yang JC, Hughes MS, Kammula US, et al. High-dose interleukin-2 for the treatment of metastatic renal cell carcinoma: a retrospective analysis of response and survival in patients treated in the surgery branch at the National Cancer Institute between 1986 and 2006. Cancer. 2008;113:293–301.

51. Srivastava SK, Panch SR, Jin J, Shalabi H, Shah NN, Highfill SL, et al. Abbreviated T-cell activation on the automated clinimacs prodigy device enhances bispecific CD19/22 chimeric antigen receptor T-cell viability and fold expansion, reducing total culture duration. Blood. 2018;132(Suppl 1):4551. (abstract 711).

52. Wang Z, Wu Z, Liu Y, Han W. New development in CAR-T cell therapy. J Hematol Oncol. 2017;10:53.

53. Majzner RG, Mackall CL. Tumor antigen escape from CAR T-cell therapy. Cancer Discov. 2018;8:1219–26.

54. Ginaldi L, De Martinis M, Matutes E, Farahat N, Morilla R, Catovsky D. Levels of expression of CD19 and CD20 in chronic B cell leukaemias. J Clin Pathol. 1998;51:364–9.

10. Curriculum Vitae

Mein Lebenslauf wird aus datenschutzrechtlichen Gründen in der elektronischer Version meiner Arbeit nicht veröffentlicht.

11. Publikationsliste (peer-reviewed)

Central memory phenotype drives success of checkpoint inhibition in combination with CAR T cells
Toews K, Grunewald L, Schwiebert S, Klaus A, Winkler A, Ali S, Zirngibl F, Astrahantseff K, Wagner DL, Henssen AG, Deubzer HE, Schulte JH, Ochsenreither S, Eggert A, Künkele A.
Molecular Carcinogenesis 2020

CAR T-cells that target acute B-lineage leukemia irrespective of CD19 expression
Fousek K, Watanabe J, Joseph SK, George A, An X, Byrd TT, Morris JS, Luong A, Martínez-Paniagua MA, Sanber K, Navai SA, Gad AZ, Salsman VS, Mathew PR, Kim HN, Wagner DL, Brunetti L, Jang A, Baker ML, Varadarajan N, Hegde M, Kim Y-M, Heisterkamp N, Abdel-Azim, Ahmed N.
Leukemia 2020

Homozygous PAX5 sequence mutations define a novel subtype of B cell precursor acute lymphoblastic leukemia
Bastian L, Schroeder MP, Eckert E, Schlee C, Ortiz Tanchez J, Kämpf S, Wagner DL, Schulze V, Isaakidis K, James AR, Burmeister T, Schwartz S, Vosberg S, Krebs S, Blum H, Hecht J, Greif PA, Rieger MA, Brüggemann M, Gökbuget N, Müller-Tidow C, Serve H, Neumann M, Baldus CD.
Leukemia 2019

High prevalence of *Streptococcus pyogenes* Cas9-reactive T cells within the adult human population
Wagner DL, Amini L, Wendering DJ, Burkhardt L-M, Akyüz L, Reinke P, Volk HD, Schmueck-Henneresse M.
Nature Medicine 2019 (prelim. Version available on biorxiv.org: https://doi.org/10.1101/295139)

Constitutive signaling from an engineered IL-7 receptor promotes durable tumor elimination by tumor redirected T-cells.
Shum T, Omer B, Tashiro H, Kruse RK, Wagner DL, Parikh K, Yi Z, Sauer T, Liu D, Parihar R, Castillo P, Liu H, Brenner MK, Metelitsa LS, Gottschalk S, Rooney CM.
Cancer Discovery 2017

CD7-edited T cells expressing a CD7-specific CAR for the therapy of T-cell malignancies
Gomes-Silva D, Srinivasan M, Sharma S, Lee CM, Wagner DL, Davis TH, Rouce RH, Bao G, Brenner MK, Mamonkin M.
Blood 2017

Highly Efficient Genome Editing of Murine and Human Hematopoietic Progenitor Cells by CRISPR/Cas9.
Gundry MC, Brunetti L, Lin A, Mayle AE, Kitano A, Wagner D, Hsu JI, Hoegenauer KA, Rooney CM, Goodell MA, Nakada D.
Cell Reports 2016

12. Danksagung

Here, I would like to mention some of the most important human beings
that guided, helped and carried me along the way to this thesis.

Thank you / Vielen Dank

Berlin

Hans-Dieter Volk: für dein Vertrauen, deine stetige Unterstützung sowie deine Begeisterung und Visionen, die eine Inspiration für mich sind.

Petra Reinke: für deinen kontinuierlichen Beistand, deine Zuversicht und den mutigen, gemeinsamen Blick nach vorn.

Uwe Kornak, Claire Schlack, Björn Fischer-Zirnsak, Leila Amini, Denise Jahn: Bei und von euch lernte ich, was es heißt im Labor zu arbeiten. Angefangen von Pipettieren, über Klonieren, dem Versorgen von T-Zellkulturen bis hin zur eigenverantwortlichen Arbeit.

Michael Schmück-Henneresse: Für deine starke Unterstützung, die zahlreichen Stunden gemeinsamer harter Arbeit, inklusive der Lacher zwischendurch, und die Hoffnung gemeinsam etwas Besonderes zu erreichen.

Houston

Cliona M Rooney: for your trust, support and time. You gave me a unique opportunity to experience, learn and live science with you and your (extended) family which starts from great morning seminars to lovely Christmas dinners.

Michael Gundry and Lorenzo Brunetti: for your friendship and teaching me CRISPR.

Max Mamonkin, Thomas Shum, Haruko Tashiro: I learned from you and I laughed with you.

Luiz Miguel De Oliveira Martins: my handyman, my nurse and my brother in a foreign place.

Siobhan Norton and Ciaran Lee: for music, for science and a second home.

Überall

Meine Eltern Yvonne und Johannes: Für das „Immer-Da-Sein" und das Vertrauen, dass ich mit euch im Rücken meinen Träumen folgen kann.

Frieda: Für deine ansteckende Freude, deine Unterstützung und Geduld mit mir.

Cornelius, Carl, Lennard: Ihr seid dabei gewesen und ihr werdet immer da sein.

Stefan Mundlos: Für deinen Rat und Tat, die mich in die Wissenschaft führten und hoffentlich weiter begleiten werden.